

INORGANIC AND ORGANIC ANALYSIS BY INFRARED SPECTROMETRY IN COAL PROBLEMS

R. A. Friedel and J. A. Queiser

U.S. Department of the Interior, Bureau of Mines,
Pittsburgh Coal Research Center, Pittsburgh, Pa.

SUMMARY

A group of problems are discussed. In Inorganic work the identification of mineral absorption bands in infrared spectra has been carried out by a combination of spectrometry and coal petrography. The absorption bands of the whole coal that are found to decrease significantly with the removal of mineral matter are easily identified by this means.

An important safety problem in coal mines has been substantially helped by infrared analysis of minerals. The content of rock dust found in the float dust of return airways of coal mines is important and preferably should be determined with speed. The usual procedure is to wait for dust to settle sufficiently to collect 100 mg of sample for chemical analyses. By the application of infrared spectrometry to this problem it is possible to carry out a complete analysis for rock dust content on as little as 2 mg sample. Greater speed is achieved.

In organic work, attenuated total reflectance of shock-heated coal has shown that considerable infrared fine structure is developed relative to the original coal (Spectra by Barnes Engineering Co.). The spectra obtained are, however, not representative of the whole coals. More volatile portions of the coal are found to leave the coal first as expected and to collect first on the ATR prism. Because of the very slight optical penetration of the sample by the spectral beam the spectrometer sees only the initial volatile parts of the coal. This method is therefore very good for concentration of and study of the volatile portions of the coal. A principle use of ATR at the Bureau has been in the study of spectra of sorbates added to coals.

Infrared spectral changes with acid-base interactions (charge-transfer complexes) have been studied by the ATR method. With coal as the acid (acceptor) and pyridine as the base (donor) the same changes in the pyridine spectrum are found as in other charge-transfer complexations involving pyridine.

INTRODUCTION

The application of infrared spectrometry to chemical substances represents the largest use in science of any spectral method. These applications are overwhelmingly in the field of organic chemistry. But infrared spectrometry is also used for analysis of inorganics. In addition to qualitative information it is possible to obtain quantitative information as well. As in organic infrared a straight line relationship usually exists between the concentration of each component in a mixture and the spectral absorption of that component. This paper will treat a few applications of infrared spectrometry to both organic and inorganic problems. In most cases other available spectral methods (mass spectrometry, ultra-violet-visible, nuclear magnetic resonance, electron paramagnetic resonance) are used in conjunction with infrared, but only infrared is discussed here.

INORGANIC APPLICATIONS

Inorganic materials which possess anions of oxygenated systems, namely, carbonates, chlorates, sulfates, silicates, etc., usually possess in their infrared spectra distinct, intense spectral bands. Such substances are amenable to analysis by infrared spectroscopy. One distinct difference between organic and inorganic substances is that inorganics have fewer spectral absorption bands than organics. With fewer bands to work with, analyses of complex mixtures are limited. This is one major reason why infrared analyses of inorganics have not been as popular as analyses of organics. Organic molecules produce profuse spectra because of the large number of atoms involved, and because many of these atoms are usually hydrogens which are responsible for many of the intense bands in the spectra of organic compounds. When hydrogens are present in inorganic compounds, these too show a greater profusion of spectral bands; the bicarbonates are an example.

It is interesting to note that one of the earliest and best text books on infrared, written by German spectroscopists Schaeffer and Matossi^{1/} 36 years ago, discussed the inorganic applications at length, almost to the exclusion of organic applications. It was soon after this period that the greater applicability to organic structures aroused so much activity that it practically swept aside the inorganic applications of infrared. A considerable impetus was given to infrared analysis of inorganics by Miller and Wilkins of Mellon Institute in their publication of a catalog of spectra of inorganic compounds,^{2/} and by Hunt et al. in a publication of infrared spectra of minerals.^{3/} This impetus was needed, although it did not produce any great activity in inorganic analysis until recent years--more than a decade after publication. A recurring difficulty with inorganics is that spectra of unknowns often differ significantly from the spectra of standards. This is a disturbing occurrence and makes difficult the assignment of spectra to specific structures. A list of possible reasons for spectral differences follows: (1) Infrared spectra often differ for different crystal structures of a substance. This is a factor in dealing with pure substances, and is an even bigger factor in the presence of impurities and in mixed salts. Epitaxy can produce differing crystal structures and infrared spectra. (2) Substrates can have a tremendous effect on the spectrum of an inorganic substance. Large spectral changes are well known in the case of organic materials studied *in situ* on catalysts. (3) Reaction may occur between the minute crystals of the sample and the KBr, or other halide, used for infrared pelleting.

In Bureau of Mines work infrared applications in inorganics occurred in connection with: (1) Our early work on coal spectra; unassigned bands thought to be due to ethers in bituminous coal spectra were reported in 1956 to be due to minerals, principally kaolinite;^{4/} (2) spectra of oil shales and other carbonaceous shale produced little information; (3) brief investigations of alkalinized alumina in 1963 gave limited information: the presence of sodium aluminate was indicated, which substantiated the X-ray indications of this group; the presence of sulfates (not definitely assignable) on alkalinized alumina exposed to sulfur oxides has been shown; (4) formation of inorganic carbonates in the pyrolysis of lignites and of peat at 400° C was shown; (5) recent examination of probe samples obtained in combustion experiments showed identifiable sulfates. Further work on (1) will be described.

1. Identification of Mineral Absorption Bands in Coal Spectra

The discovery of the correct assignment of certain absorption bands to minerals^{4/} came about through the observation in 1953 that the spectra of coals and their petrographic components differed considerably. As in other laboratories our suspicions were that these differences were attributable to differences in organic

structure between the coal and its petrographic constituents. But it became apparent that this could not be. A coal such as Pittsburgh seam is very largely vitrain. With only a few percent of the constituents removed from the major component, vitrain, it was not feasible that there should be differences in organic structure between coal and vitrain spectra as great as 5-fold in the intensities of some absorption bands. It eventually became evident that the constituents which were changed many fold in the isolation of vitrain were the mineral components. On comparison of these anomalous absorption bands with the spectra of the few minerals available at that time, it was found that most of the bands were assignable to kaolinite.^{4/} Thus these informative comparisons of spectra represented a very useful combination of spectral and petrographic methods.

Our published investigations on this subject were limited to the 5,000 - 650 wavenumber region.^{5,6,7/} With the advent of instruments for adequate operation below 650 cm^{-1} in the infrared (R. C. Lord has named this region the "middle infrared") it became possible to extend the study of mineral absorption bands through the combination of spectral and petrographic techniques. By a comparison of Pittsburgh coal and vitrain spectra the following bands due to minerals, principally kaolinite, have been observed in the middle infrared: 698, 543, 471, and 420 cm^{-1} . The strongest of these bands are those at 543 and 471. Both bands are attributable to kaolinite. As discussed above some of the intensity differences are extremely large and cannot possibly be attributed to differences in organic structure. For example, the strong band at 543 wave numbers in the coal is 10 times as great as the corresponding absorption intensity in the vitrain spectrum. Such radical differences can only be attributed to mineral absorption. Intensities of these absorption bands can be accurately calculated and used for quantitative determinations of minerals present.

Graphite has been examined in this region of the spectrum. Though strong absorption for graphite was detected out to 290 wave numbers no discrete absorption bands were found. Additional runs out to 100 cm^{-1} have been made by Dr. William Fateley, Mellon Institute, and no specific absorption bands occur.

2. Rock Dust in Float Dust

Infrared spectrometry has recently been applied to analysis of rock dust in float dusts from return airways of coal mines. Sample collection for the purpose of analyzing by wet chemical methods is a difficult problem usually because a considerable amount of dust, about 100 mg, must be collected. This requires more time than desirable; the element of safety is therefore involved. With the use of infrared spectrometry in such a problem only very small samples need be collected. Two mg are ample and collection is rapid.

The dust samples collected in the mine, mixtures of coal and rock dust, are prepared for infrared investigation by mixing 1 part of dust with 100 parts of potassium bromide which is pelleted by a standard technique. The infrared spectrum of the pellet is obtained. Advantageous absorption band or bands are chosen for analytical work. For quantitative analysis it is necessary to check the linearity of the concentration versus spectral absorption by preparing standard samples at various concentrations and measuring their absorption intensities at the appropriate absorption bands. After the linearity of the calibration curve is established, then unknown samples can be prepared in KBr pellets and their spectra obtained. Intensity of absorption at appropriate bands may then be applied to the calibration curve and the concentration of the desired component in the dust is obtained.

The rock dusts dealt with in this investigation were either calcite (CaCO_3) or dolomite, $\text{CaMg}(\text{CO}_3)_2$; calibration curves were obtained for each of the rock dusts plus coal. Though the rocks involved are both carbonates their absorption spectra differ slightly. This is an advantage, as each may be determined in the presence of the other if necessary. Coal also has an absorption spectrum and accordingly the coal dust collected in the mine will produce interfering absorption which must be corrected for. This is most simply done by choosing the calibration band for the carbonates if possible in regions of broad, non-specific absorption of the coal. Then from the spectrum of the mixture of coal and rock dust the absorption band of the rock dust will be superimposed on the broad background of the coal absorption. By drawing a baseline across the base of the absorption band it is possible to correct out the non-specific coal absorption.^{5,6/} The intensity of the rock dust absorption then is measured from this base line to the peak of the absorption band. In this way calibration curves were obtained.

For both calcite and dolomite two absorption bands were obtained for possible analysis. All four bands provided acceptable results, about + 10 percent of the amount present, in the desired range of about 20 to 80 percent rock dust. Results indicate that there is no preference between the two absorption bands studied for each dust. One other carbonate band, at about 7.0 microns, is available for analysis. With its greater intensity this band would be useful for analysis of traces of rock dust in coal dust. In the present problem analysis of traces is not required so the less intense, sharp bands used are preferred. It should be mentioned that only three carbonate bands are available for analysis; as stated earlier, organic materials usually have many bands that can be used. If differentiation between carbonates is required, then two bands only are available, for the strongest band at 7.0 microns is essentially identical in various carbonates.^{2,3/}

ORGANIC APPLICATIONS

1. Attenuated Total Reflectance Spectra. Shock-Carbonized Coals; Sorbates on Coal

Recent investigations on attenuated total reflectance (ATR) of coal were carried out by Bent and Ladner.^{8/} Their results demonstrated the difficulties of utilizing this technique on coals. Very close optical contact is difficult to achieve with the surface plateaus produced by conventional grinding and polishing of coal. These authors demonstrated that the method was more applicable to the spectral investigation of chloroform extracts of shock-carbonized coals.

Volatile products from shock-carbonizing of coals can be condensed directly on the ATR optical element to produce good spectra. However, this technique might be somewhat misleading; on shock carbonizing, the more volatile products and therefore the lower molecular weight products, would be expected to reach the ATR prism first. Because of the slight optical penetration of the sample by the infrared beam in the ATR technique, it is probable that only these most volatile products would be observed in the spectrum. The method is therefore very good for the concentration of and study of the volatile portions of the coal.

Spectra of the volatile products from four shock-carbonized vitrains were investigated by Barnes Engineering Company with an ATR crystal of thallium-bromide-iodide which provides 20 reflections within the crystal. The vitrains were shock-carbonized at 900° C; the volatilized material was collected on the ATR crystal and spectra were determined. Appreciable differences in the spectra of the products from three coal vitrains were observed in comparison with the spectra of the original coal vitrains; greater fine structure and new bands were produced. The fourth sample, shock-carbonized Beulah lignite vitrain showed no spectral changes other than quantitative changes. The spectral changes for the three coal

vitrains are indicated in Table 1. The formation of two doublets is interesting. The doublet at 1625-1600 in the spectra of shock-carbonized products may signify that the 1610 cm^{-1} band in coal is actually attributable to two different chemical species, as suggested by Fujii.^{9/} The doublet at 1440-1400 cm^{-1} is surprising. The origin of these bands is not known; the high temperature used undoubtedly produced considerable reaction.

Table 1.- Infrared spectral differences between ATR spectra of three coal vitrains and the corresponding shock-carbonized products.

Vitrain, coal seam	Infrared frequency, cm^{-1}			
Pittsburgh (hvab)	1610	1450	-	-
Pittsburgh, shock-carbonized	1625-1595 ^{a/}	1440-1402 ^{a/}	1250	1093
Pocahontas (lvb)	1610	1450	-	-
Pocahontas, shock-carbonized	1627-1600 ^{a/}	1443-1400 ^{a/}	1250	1093
Dorrance anthracite	1610	1450	-	-
Dorrance, shock-carbonized	1625-1595 ^{a/}	1440-1398 ^{a/}	1250	1093

a/ Doublets

Interest in attenuated total reflectance at the Bureau of Mines has been principally directed towards the study of sorbates on coals. Good spectra can be obtained when good optical contact is achieved. The interaction between sorbate and the substrate coal can be followed nicely by placing upon the ATR prism a slurry of coal and sorbate. Then the spectrum is scanned repeatedly as the sorbate is allowed to evaporate. If the sorbate is of low volatility a heat lamp can be used to increase the volatility.

Significant spectral changes have been observed for pyridine on coal. (see below.) Whether or not changes in the spectrum of the coal have occurred has not been ascertained because of the broadness of the coal bands and the interference of the intense, sharp, pyridine bands. Observations have also been made on benzene-coal and methanol-coal systems. No significant spectral changes have been seen for either the sorbate or the coal. Spectra of these systems can also be obtained by ordinary transmission spectral methods, but the ATR method provides better spectra, particularly for the sorbate.

2. Charge-Transfer Complexes

Charge-transfer complexes represent one type of weak acid-base interactions. The complexes are formed between electron-rich (donor) molecules and electron-poor (acceptor) molecules.^{10/} Redistribution of electron charge occurs so that the properties of the two moieties are changed; however, definite chemical reaction does not occur and the original moieties are nearly always recoverable by simple processes such as dissolution, or distillation, plus some method of separation. One of the changes experienced by both donor and acceptor molecules in a complex is a change in bond lengths, which produces changes in the vibration spectra; thus infrared spectra can indicate the formation of such complexes.

Observations of the infrared spectra of coal-pyridine systems have led to the belief that charge-complex formation occurs between pyridine (donor) and coal (acceptor). Examination of the pyridine-coal system by the ATR method (described above) provided interesting spectral changes as pyridine is allowed to evaporate. The principal spectral characteristics of the coal-pyridine system are those of pyridine itself with a background due to the coal extract. As evaporation of the pyridine progresses a new band shoulder is formed at about 1000 cm^{-1} and the neighboring band of pyridine at 990 cm^{-1} begins to disappear. As evaporation continues the pyridine band continues to decrease and finally disappears; meanwhile the new coal-pyridine band continues to shift slightly. The final location of the band is 1020 cm^{-1} ; at this point all the remaining pyridine molecules are apparently complexed with the coal extract. The interactions involved in this process are of interest. The results apparently are indicative of the formation of a charge-transfer molecular complex, as pyridine does indeed behave in this manner in the formation of charge-transfer complexes with many electron acceptors.^{10/} We have demonstrated that these same spectral changes occur as phenol is added to pyridine. It is logical to believe that the complexing of coal and pyridine involves the phenolic structures in the coal.

References

1. Schaeffer, C., and F. Matossi. "Das Ultrarote Spectrum," Springer Co., Berlin, 1930.
2. Miller, F. A., and C. H. Wilkins. Infrared Spectra and Characteristic Frequencies of Inorganic Ions. Anal. Chem., v. 24, 1952, pp. 1253-1294.
3. Hunt, J. M., M. F. Wisherd, and L. C. Bonham. Infrared Absorption Spectra of Minerals and Other Inorganic Compounds. Anal. Chem., v. 22, 1950, pp. 1478-1497.
4. Friedel, R. A., and J. A. Queiser. Infrared Analysis of Bituminous Coals and Other Carbonaceous Materials. Anal. Chem., v. 28, 1956, pp. 22-30.
5. Friedel, R. A. Infrared Spectra of Thin Sections of Coal Vitrains. Brennstoff-Chemie, v. 44, 1963, pp. 23-24.
6. Friedel, R. A. Infrared in Coal Structure Research. Ch. in "Applied Infrared Spectroscopy," ed. D. N. Kendall, Reinhold Pub. Co., New York, pp. 312-343.
7. Friedel, R. A. The Use of Infrared Spectra of Chars in Coal Structure Research. Applied Optics, v. 2, No. 11, Nov. 1963, pp. 1109-1111.
8. Bent, R., and W. R. Ladner. A Preliminary Investigation into the Use of Attenuated Total Reflectance for Obtaining the Infra-red Spectra of Coals. Fuel, v. 44, 1965, pp. 243-248.
9. Fujii, Shuya. Infrared Spectra of Coal: The Absorption Band at 1600 cm^{-1} . Fuel, v. 42, 1963, pp. 17-23.
10. Andrews, L. J., and R. M. Keefer. Molecular Complexes in Organic Chemistry. Holden-Day, Inc., 1964, San Francisco, Calif., p. 36.

MEASUREMENT OF THE SURFACE AREAS OF COALS FROM
THE DYNAMIC SORPTION OF CARBON DIOXIDE

Josephus Thomas, Jr., Gary S. Benson, and Gary M. Hieftje

Illinois State Geological Survey, Urbana, Illinois

INTRODUCTION

Dynamic-sorption apparatus has been described by Nelsen and Eggertsen¹ and refined by Daeschner and Stross² for use in the determination of the surface area of solids. The essentials of the apparatus have been incorporated in commercially available equipment (Perkin-Elmer's Sorptometer). With the apparatus, the volume of nitrogen sorbed by the sample from a nitrogen-helium gas stream is determined by thermal conductivity measurements. Other mixed-gas systems may be used for special studies. The surface area is calculated using the well-known theoretical principles of Brunauer, Emmett, and Teller³ (BET equation). Surface-area values are in close agreement with those obtained from the use of more conventional apparatus in which pressure-volume measurements are made in a static system. The dynamic-sorption apparatus, however, lends itself more readily to routine measurements, having the advantage over conventional apparatus in speed and simplicity of operation. In addition, the rate of sorption is recorded directly. This can be of value in revealing pore-size variations, particularly in microporous substances where equilibrium is slow in being reached.

It is well-recognized that nitrogen at 77° K. does not reach a large part of the internal surface of coals. This is attributable, for the most part, to activated diffusion^{4,5} although thermal contraction can not be completely ruled out as being responsible for some pore closure. Conversely, it has been concluded that carbon dioxide at 195° K. does reach most of the internal surface^{6,7,8}. Three recent papers^{9,10,11} are substantially in agreement as to the magnitude of the surface-area values obtained using carbon dioxide as the adsorbate. The values are appreciably greater than those obtainable from nitrogen adsorption and do not differ greatly from those obtained using heats of wetting in methyl alcohol^{12,13}.

The primary purposes of the work reported herein are (1) to demonstrate the applicability of continuous-flow measurements to internal surface studies of coals and (2) to report for comparative purposes the surface-area values obtained for the different coals studied. Of special significance are the values obtained for coals from the Illinois Basin. These coals are high volatile A, B, and C bituminous and, to the authors' knowledge, with the exception of the work reported by Machin, Staplin, and Deadmore¹⁴ in which nitrogen and water vapor were used as adsorbates, they have not been studied to any appreciable extent.

EXPERIMENTAL

Apparatus

The adsorption apparatus was quite similar in design and use to the original apparatus described in detail in the afore-mentioned references. Modifications included: (1) needle valves for controlling gas flow rates (2) a disc integrator (Disc Instruments, Inc., Santa Ana, California) attached to a Sargent Model MR recorder for integrating peak areas (3) a reversing switch in the bridge circuit to permit positive adsorption peaks to be recorded for integration as well as positive desorption peaks and (4) a Sorensen QB12-2 D.C. Power Supply (Raytheon Company, South Norwalk, Connecticut).

Samples

Coal samples used in the study and appropriate analytical data are given in Table I. The Illinois high volatile A, B, and C bituminous coals (3 for each rank) represent only a fraction of the total number of coals of similar rank that were studied and include those coals which yielded the extremes of the range of surface-area values found for each rank.

Samples of anatase, silica spheres, bone char, carbon black (Spheron 6), and a silica-alumina catalyst with known surface areas were used to establish the effective cross-sectional area for the carbon dioxide molecule under the given experimental conditions. These substances have been evaluated at several participating laboratories by the BET nitrogen adsorption method and are distributed by the Bone Char Research Project, Inc. (Revere Sugar Refinery, 333 Medford Street, Charlestown 29, Mass.).

Procedure

Operational details for the apparatus are clearly outlined in the work of Nelsen and Eggertsen, as is the transformation of experimental data into a surface-area determination. The conditions used for the coal studies reported here are summarized as follows: A 40 x 120-mesh sample of approximately 0.2 gram is weighed into the sample tube which is then attached to the apparatus, and the sample is outgassed at 90° C. for 1 hour under a flow of helium. A controlled gas mixture of carbon dioxide and helium is permitted to flow over the sample. A dry ice-absolute ethanol bath (approximately 195° K.) is raised into position around the sample tube and adsorption is continued for 16 hours. (The adsorption step for a few samples was conducted for 30 minutes, 2 hours, and 24 hours for comparison purposes.)

After the adsorption step is completed, the gas is desorbed from the sample by removing the dry ice-ethanol bath and quickly replacing it with another bath (glycerol here) at 150° C. The volume of desorbed gas is determined from a calibration curve (detector response versus known volumes of carbon dioxide) and it is this volume that is used for determining the surface area. The relatively high desorption temperature is necessary to remove virtually all the adsorbed carbon dioxide (less than 0.5% of the original volume is retained at this temperature) and it helps provide a sharper, symmetrical desorption peak that is more comparable with calibration data. Thus, errors which may arise from badly tailing peaks are minimized.

From the familiar BET equation, which is assumed to be applicable, a single-point plot using P/P_0 as the abscissa and $P/V(P_0 - P)$ as the ordinate, and with the intercept at 0, yields $V_m = 1/\text{slope}$. The saturation vapor pressure (P_0) used in the calculations was 1450 mm. which allows for a very slightly higher temperature than the value (1.86 atm. at 195° K.) given by Bridgeman.¹⁵ Surface area then is readily determined from V_m , from the area occupied by a carbon dioxide molecule, and from the sample weight which is more carefully determined on the dry sample after the desorption step.

Multipoint plots were used for three coal samples and for all the substances involved in the determination of the effective area occupied by the carbon dioxide molecule. The constant C of the BET equation is large for carbon dioxide as the adsorbate on coal and a multipoint plot passes practically through the origin of coordinates. This enables one to use the single-point method on a more-or-less routine basis, particularly in view of the inherent uncertainties of the BET method with coals and the necessary long adsorption periods.

TABLE I

Selected Analyses of Coals Studied

No.	Sample	Proximate Analysis				Dry, Mm-Free		Heating Value	
		Moisture, %	Moist, Mm-Free Matter, %	Volatile Matter, %	Fixed Carbon, %	Fixed Carbon, %	Moist, Mm-Free Btu per pound		
<u>Illinois hvCb</u>									
1	Madison Co. (#6 coal)	17.6	35.5	46.9	57.0	11,700			
2	Kankakee Co. (#2 coal)	15.2	41.2	43.6	51.4	12,300			
3	Vermillion Co. (#7 coal)	13.1	42.6	44.3	50.8	12,700			
<u>Illinois hvBb</u>									
4	Franklin Co. (#6 coal)	11.2	33.8	55.0	62.0	13,000			
5	Williamson Co. (#6 coal)	7.9	39.1	53.0	57.5	13,700			
6	Saline Co. (#6 coal)	7.6	37.6	54.8	59.3	13,600			
<u>Illinois hvAb</u>									
7	Gallatin Co. (#5 coal)	5.9	39.4	54.7	58.2	14,100			
8	Gallatin Co. (Lower Willis)	2.3	36.9	60.8	62.2	14,900			
9	Gallatin Co. (#6 coal)	3.2	41.7	55.1	56.8	14,600			
10	West Virginia (Pittsburgh seam)	1.7	42.7	55.6	56.6	15,200			
11	West Virginia (Sewell seam)	2.1	29.9	68.0	69.5	- - -			
12	West Virginia (Bakerstown)	2.3	17.9	79.8	81.6	- - -			
13	Utah	5.7	45.0	49.3	52.3	13,700			
14	Kentucky (#5 coal)	2.6	39.1	58.3	59.8	14,700			
15	Arkansas (Hartshorne)	1.6	17.8	80.6	81.9	- - -			
16	Pennsylvania anthracite	2.1	5.1	92.7	94.8	- - -			
17	Meta-anthracite (Leoben, Austria)	0.1	1.8 (d.a.f.)	-	98.2 (d.a.f.)	- - -			
18	Borneo (Silantek)	0.8	25.3	73.9	74.5	- - -			

RESULTS AND DISCUSSION

Molecular Area of Carbon Dioxide

Table II gives the results from which the effective cross-sectional area of the carbon dioxide molecule used as the adsorbate in the studies was established. The cross-sectional area of the nitrogen molecule was taken as 16.3 \AA^2 . The assumption is made that carbon dioxide at 195° K . should give the same surface area as N_2 at 77° K . It is seen that the values are in satisfactory agreement with the exception of that obtained for the carbon black. Slight differences are to be expected, of course, owing to the wide differences in the chemical compositions of the substances used. It would appear that the large difference is due to the presence of a micro-pore system - similar perhaps to that which exists in coals - that also is not permeated during nitrogen adsorption at 77° K .

Excluding the value obtained for the carbon black, the average effective molecular area of carbon dioxide is 22.1 \AA^2 . Calculated from this value, the surface area for Spheron 6 should be about $150\text{-}155 \text{ m}^2/\text{g}$.

Adsorption-Desorption Characteristics

The desorption curve and the portion of the adsorption curve shown in Figure 1 are typical for carbon dioxide adsorbed on coals. During adsorption, a rather sudden uptake of the gas extending over a period of 2-3 minutes is followed by very slow diffusion that may extend over a period of 16 hours. As much as one third of the total adsorption volume is adsorbed by certain high-volatile C bituminous coals during the first 2-3 minutes.

Table III gives some comparative data for various periods of adsorption. Although the table includes only a small sampling of coals, the data clearly show that adsorption is far from complete at 2 hours but also indicate that it is essentially complete somewhere between 2 and 16 hours. The 16-hour period was selected as it was found convenient to conduct adsorption overnight.

Adsorption is much too slow to enable one to use the adsorption curve for the gas-volume determination since calibration curves are practically impossible to construct for the extended removal or addition of a gas introduced at a variable rate into the mixed-gas stream. Fortunately, however, for analysis purposes, desorption is rapid and essentially complete within the first 2-3 minutes of its initiation.

Surface Areas of Coals

Table IV lists the surface-area values for the coals studied. As indicated earlier, a larger number of Illinois coals than shown were investigated and a range of intermediate values was found within the extremes shown here for each rank. Some overlap of values is present between the ranks of Illinois coals as would be anticipated. The range of values from the work of Machin et al. by classical nitrogen adsorption methods is shown for comparative and supplemental purposes.

It is seen that the values from carbon dioxide adsorption are of the same order of magnitude as values obtained from heats of wetting and, thus, also are in agreement with the more recent studies in which carbon dioxide was used as the adsorbate in static systems and to which references have been made. Values for the hvAb coals are the lowest reported thus far from carbon dioxide adsorption on coals, with the exception of meta-anthracite, but they are not any lower than values that have been obtained from heats-of-wetting methods.

Maximal and minimal values among all the coals studied are found essentially within the ranks of Illinois coals. Since the Illinois coals comprise such a narrow

TABLE II

Determination of the Effective Cross Sectional Area of the Carbon
Dioxide Molecule

Adsorbent	S.A., m ² /g*		N ₂ S.A. CO ₂ S.A.	Effective Molecular Area of CO ₂ , A ²
	(N ₂ ads.)	(CO ₂ ads.)		
Anatase	10.3	7.9	1.30	22.1
Silica spheres	24.3	18.6	1.31	22.3
Bone char	69	52	1.33	22.6
Carbon black(Spheron 6)	110	117	0.94	16.0
Silica-Alumina catalyst	550	436	1.26	21.4

*Mean of accepted values from several participating laboratories.

**Assuming a cross sectional area of 17.0 A² for the carbon dioxide molecule.

TABLE III

Adsorption of Carbon Dioxide on Coals for Different Adsorption Times

Coal	Volume Adsorbed Per Gram of Sample (ml.)*			
	0.5 hour	2 hours	16 hours	24 hours
Sample 4	27.1	35.1	42.2	42.3
Sample 7	3.3	5.8	10.2	- -
Utah	14.1	17.7	28.3	28.4
Borneo	29.9	38.0	38.4	38.4

*P/P₀ differed slightly among the coals used but was the same for each coal for the different adsorption periods.

TABLE IV

Surface Areas of Coals

No.	Sample	Surface Area, m ² /g		No.	Sample	Surface Area, m ² /g	
		CO ₂ ads.	N ₂ ads.*			CO ₂ ads.	N ₂ ads.*
	<u>Illinois hvCb</u>		46.8-91.8	10	W. Virginia (Pitts. seam)		43
1	Madison Co. (#6 coal)	292		11	W. Virginia (Sewell seam)		197
2	Kankakee Co. (#2 coal)	248		12	W. Virginia (Bakerstown)		128
3	Vermilion Co. (#7 coal)	184					
	<u>Illinois hvBb</u>		7.2-16.3	13	Utah		145
4	Franklin Co. (#6 coal)	205		14	Kentucky (#5 coal)		66
5	Williamson Co. (#6 coal)	115		15	Arkansas (Hartshorne)		182
6	Saline Co. (#6 coal)	83					
	<u>Illinois hvAb</u>		1.8-4.5	16	Pennsylvania anthracite		262
7	Gallatin Co. (#5 coal)	86		17	Meta-anthracite (Leoben, Austria)		6.0
8	Gallatin Co. (Lower Willis)	57		18	Borneo (Silantek)		290
9	Gallatin Co. (#6 coal)	46					

*From work by Machin, Staplin, and Deadmore.

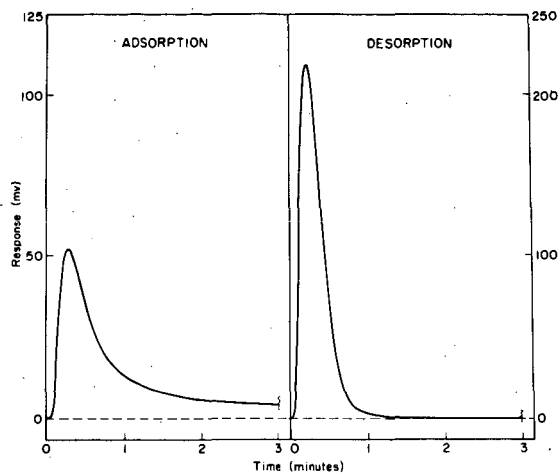


Figure 1. Typical carbon dioxide adsorption and desorption curves for coals (without integrator record)

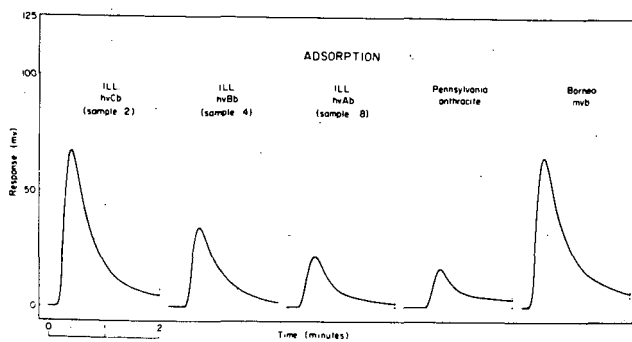


Figure 2. Initial portions of adsorption curves for 0.2-gram samples of various coals (without integrator record)

portion of the overall degree of metamorphism among coals, and since the values for the higher rank coals examined do not change in an orderly manner with increase in rank, there appears to be little basis for attempts to construct a curve relating rank and surface area.

Implications from Initial Adsorption Rates

It is significant that surface-area values for Illinois hvCb coals from nitrogen adsorption isotherms reported by Machin et al. are as high as $91 \text{ m}^2/\text{g}$. A search of the literature failed to uncover a report in which a coal sample produced a surface area this large by nitrogen adsorption. In some of our own studies using nitrogen as the adsorbate in the continuous-flow apparatus, values for sample numbers 2 and 3 were found to be 99 and $48 \text{ m}^2/\text{g}$, respectively. Indications are that a larger proportion of pores of greater diameter than a certain minimal size exists in the hvCb coals permitting greater quantities of nitrogen to permeate the structure at 77° K .

Further proof of this may be seen in a comparison of the initial adsorption rates for carbon dioxide on similar sample weights of several coals shown in Figure 2. All of the coals shown have surface-area values of over $200 \text{ m}^2/\text{g}$, with the exception of the hvAb which should not be used directly in this comparison. It is readily apparent that the rate of carbon dioxide taken up during the first 2-3 minutes differs markedly among the coals. It would appear that the greater rate of adsorption of carbon dioxide by the hvCb coal in comparison with the hvBb, hvAb, and anthracite coals coincides with a greater macropore volume of the coal and would tend to supplement the nitrogen adsorption data from this standpoint. It is tempting to say, without knowledge of the Borneo coal, that the macropore volume decreases with rank, and this appears to be true for the Illinois coals studied thus far. The large volume of carbon dioxide initially adsorbed by the Borneo coal (mvb), however, would tend to negate this concept, and yet nitrogen adsorption for this coal gives a surface-area value of only $0.8 \text{ m}^2/\text{g}$. Thus, it would appear that this coal has very little macropore volume available to nitrogen at 77° K ., and yet it has a large number of pores of sufficient size to permit carbon dioxide to permeate the structure rapidly at 195° K . making it different from anthracite or hvAb coals in this regard. This only serves to emphasize the danger in making generalities about coals from widely differing localities and perhaps formed in widely differing environments.

CONCLUSIONS

It is recognized that in the determination of the surface areas of coals no method reported thus far is completely free of criticism. In the work reported here it is assumed that the BET equation is applicable, and this in itself is subject to some criticism. The abbreviated single-point method used here, however, should be as good as any other method for obtaining useful relative data for practical comparative purposes. In addition, the ability to easily follow the initial adsorption rate should be of advantage in attempts to describe quantitatively the molecular sieve characteristics of various coals.

ACKNOWLEDGMENT

The authors wish to express their gratitude to H. D. Glass, H. J. Gluskoter, and J. H. Harrison for their assistance in procuring various samples, and to the staff of the Analytical Section of the Illinois Geological Survey for the coal analyses.

REFERENCES

- (1) Nelsen, F. M., and Eggertsen, F. T., *Anal. Chem.* 30, 1387 (1958).
- (2) Daeschner, H. W., and Stross, F. H., *Ibid.*, 34, 1150 (1962).
- (3) Brunauer, S., Emmett, P. H., and Teller, E., *J. Am. Chem. Soc.* 60, 309 (1938).
- (4) Zwietering, P., and van Krevelen, D. W., *Fuel, Lond.* 33, 331 (1954).
- (5) Zwietering, P., Overeem, J., and van Krevelen, D. W., *Ibid.*, 35, 66 (1956).
- (6) Kini, K. A., Reports of the 27th International Congress on Industrial Chemistry, Brussels, 20, 110 (1954).
- (7) Walker, Jr., P. L., and Geller, I., *Nature, Lond.* 178, 1001 (1956).
- (8) Anderson, R. B., Hofer, L. J. E., and Bayer, J., *Fuel, Lond.* 41, 559 (1962).
- (9) Marsh, H., and Siemieniowska, T., *Ibid.*, 44, 355 (1965).
- (10) Anderson, R. B., Bayer, J., and Hofer, L. J. E., *Ibid.*, 44, 443 (1965).
- (11) Walker Jr., P. L., and Kini, K. A., *Ibid.*, 44, 453 (1965).
- (12) Maggs, F. A. P., *J. Inst. Fuel*, 17, 49 (1943).
- (13) Griffith, M., and Hirst, W., *Proc. Conf. Ultrafine Structure of Coals and Cokes, Brit. Coal Util. Res. Assoc.*, 80 (1944).
- (14) Machin, J. S., Staplin, F., and Deadmore, D. L., *Illinois State Geological Survey Circular* 350 (1963).
- (15) Bridgeman, O. C., *J. Am. Chem. Soc.*, 49, 1174 (1927).

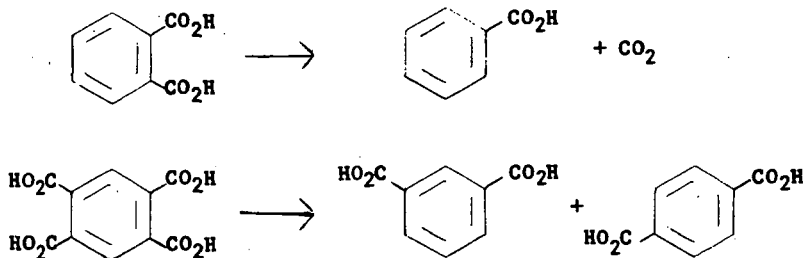
GAS CHROMATOGRAPHIC SEPARATIONS OF BENZENECARBOXYLIC ACIDS DERIVED FROM COAL

Marvin L. Kaufman, Sidney Friedman, and Irving Wender

U. S. Bureau of Mines, Pittsburgh Coal Research Center,
4800 Forbes Avenue, Pittsburgh, Pennsylvania 15213

INTRODUCTION

When benzenepolycarboxylic acids are treated with hydrogen and carbon monoxide at elevated temperatures and pressures in the presence of dicobalt octacarbonyl, a reductive decarboxylation reaction occurs^{2/}



The products of the reaction are carboxylic acids containing fewer carboxyl groups than are present in the starting acid. In most cases mixtures of benzenecarboxylic acids are obtained.

Alkaline oxidation of coal produces a mixture containing relatively large amounts of benzenecarboxylic acids.^{2,7/} If these "coal acids" can be decarboxylated by the above reaction, commercially useful products such as isophthalic and terephthalic acids might be obtained. In studying the feasibility of this decarboxylation reaction, it is necessary to have an analytical procedure by which the benzenecarboxylic acids can be separated and analyzed quantitatively. Several chromatographic procedures, including thin layer, column, and paper chromatography, for the separation of this type of acids appear in the literature.^{2,3,6/} All of these procedures, however, are deficient in some respects. The visualization and quantitative estimation of the separated acids is difficult. Moreover, the separation of isophthalic and terephthalic acids was not reported.

The free acids cannot be analyzed by gas liquid chromatography (g.l.c.) because they are not volatile enough and they tend to decarboxylate or form anhydrides at high temperatures. In order to chromatograph acids, derivatives are usually prepared; esters are the most common. Schnitzer and Desjardins^{8/} have described a g.l.c. procedure utilizing methyl esters to separate benzenecarboxylic acids. Complete esterification of all of the acids required the use of diazomethane, a reagent with some undesirable properties. In addition, isophthalic and terephthalic acids were not separated sufficiently for quantitative analysis and tailing of the peaks was noticeable. Trimethylsilyl esters of amino acids,^{1/} phosphonic acids^{5/} and carboxylic acids^{4/} have been prepared and analyzed by g.l.c. Symmetrical peaks are obtained and separations were usually adequate. The preparation of trimethylsilyl esters is also relatively simple experimentally. For these reasons, the preparation and gas chromatographic behavior of the trimethylsilyl esters of benzenecarboxylic acids was investigated and is the subject of this paper.

ACKNOWLEDGMENT

The authors wish to thank Mrs. Joan Gordon for her assistance in the experimental portion of this work. This work was also supported in part by the Union Carbide Corporation.

DISCUSSION

Several methods have been used for the preparation of trimethylsilyl derivatives.^{1,4,5/} All of the reagents investigated for the preparation of trimethylsilyl esters of benzenecarboxylic acids were successful in silylating the acids that contained up to four carboxyl groups. However, the esters of the pentacarboxylic acid and the hexacarboxylic (mellitic) acids either did not form or their formation was not reproducible. A procedure that was found to give consistent results was to reflux the acids with equal volumes of hexamethyldisilazane, trimethylchlorosilane and toluene until the resulting ammonium chloride sublimed and the acids were completely solubilized. This procedure was used to obtain the esters used in this paper.

To carry out a quantitative analysis on benzenecarboxylic acids and on the coal acids, flame ionization detector response factors for each of the acids were determined relative to *m*-toluic acid as a standard. Synthetic mixtures of ten benzenecarboxylic acids plus *m*-toluic acid were prepared, silylated and chromatographed. Figure 1 shows the separation of this synthetic mixture. Once the response factors were determined, other mixtures of the acids containing different weights of each acid were prepared and analyzed using the appropriate response factors. Table 1 compares the known and found values of a sample mixture and shows that the analysis can be made satisfactorily.

Table 1. Analysis of synthetic mixture of benzenecarboxylic acids

Component	Position of carboxyl groups	Composition, percent by weight	
		Known	Found
Benzoic	1	6.5	6.3
Phthalic	1,2	4.3	4.0
Isophthalic	1,3	8.4	8.6
Terephthalic	1,4	6.6	7.1
Hemimellitic	1,2,3	5.5	5.1
Trimellitic	1,2,4	14.2	15.8
Trimesic	1,3,5	12.8	13.4
Pyromellitic ^{1/}	1,2,4,5	20.5	21.4
Pentacarboxylic	1,2,3,4,5	8.6	6.3
Mellitic	1,2,3,4,5,6	12.6	12.0

^{1/} The other tetracarboxylic acids [prehnitic (1,2,3,5) and mellophanic (1,2,3,4)] were not available. From comparison between the chromatograms of the methyl and trimethylsilyl esters, the authors feel that these should also be separable as trimethylsilyl esters.

The newly developed analytical method was then used for determining the nature of the products from the decarboxylation of pure acids. It was found that polycarboxylic acids containing carboxyl groups ortho to each other decarboxylated giving mixtures of acids containing fewer carboxyl groups than were present in the original acid. For example, in aqueous dioxane, pyromellitic acid yields a 2:1 mixture of isophthalic and terephthalic acids while hemimellitic acid yields a 1:1 mixture of benzoic and isophthalic acids. In general, yields are 70 to 90%.

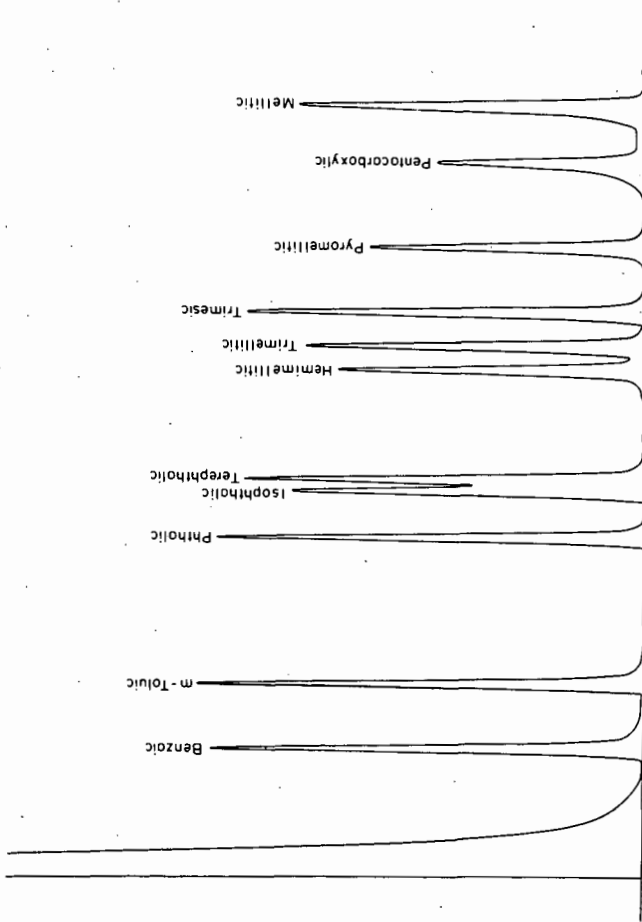


Figure 1. — Separation of benzenecarboxylic acid trimethylsilyl esters.

The coal acids, a mixture obtained from the Dow Chemical Company, and the decarboxylated acids containing a known amount of m-toluic acid were then silylated and chromatographed. Figures 2 and 3 show the type of chromatogram obtained. Using the correction factors which were determined previously, the analysis of the coal acids was carried out. Table 2 summarizes the results. It can be seen that the starting acids contain fairly large amounts of phthalic, hemimellitic, trimellitic, pyromellitic and pentacarboxylic acids. The decarboxylated acids contain large amounts of benzoic, isophthalic and terephthalic acids with only traces of higher acids. Thus it was shown that the decarboxylation reaction essentially converts almost all of the tri-, tetra-, and pentacarboxylic acids to iso- and terephthalic acids and that the benzoic acid results primarily from decarboxylation of phthalic acid. By use of the analytical method described, it was shown that the coal acids were upgraded and converted into valuable products, i.e., benzoic, isophthalic and terephthalic acids, upon undergoing the decarboxylation reaction.

Table 2. Analysis of coal acids

Component	Coal acids, weight percent	
	Before decarboxylation	After decarboxylation
Benzoic	-	4
Phthalic	3.3	Trace
Isophthalic	} 0.4	10
Terephthalic		3
Hemimellitic	2.8	-
Trimellitic	5.5	-
Trimesic	-	> 0.5
Pyromellitic	10.1	Trace
Mellophanic	-	1/
Prehnitic	-	1/
Pentacarboxylic	3.4	Trace
Mellitic	Trace	Trace
Total	25.5	17.5

1/ Traces possibly present; no standards available.

EXPERIMENTAL

Reductive Decarboxylation of Hemimellitic Acid. A solution of 3.1 g. hemimellitic acid (0.0187 mole) and 2.1 g. dicobalt octacarbonyl in 70 ml. dioxane and 15 ml. of water was placed in a 150 ml. Aminco rocking autoclave and pressured to 3500 p.s.i.g. with 1:1 synthesis gas ($H_2:CO$). The autoclave was heated to 200°C. for 5 hr. and allowed to cool overnight. The gases were vented and the reaction mixture taken to dryness under vacuum. The residue was refluxed with dilute hydrochloric acid and again taken to dryness. Most of the product was crystalline, but some gummy material was still present. The product was refluxed with water, cooled, and filtered to yield 3.0 g. of pale, purple solid. A further 0.54 g. of product was extracted from the filtrate with ether.

Gas Chromatographic Analyses. The gas chromatographic analyses were performed on a Micro Tek GC 2000R dual column, programmed-temperature chromatograph equipped with a dual hydrogen flame ionization detector. A 3 foot by 1/8 inch OD stainless steel column packed with 3% Apiezon L on 60 to 80 mesh AW-DMCS treated Chromosorb G was used. Helium at a flow rate of approximately 55 ml. per min. was the carrier gas. Runs were temperature programmed from 90° to 260° at a rate of 7.5° per min. The analysis takes less than one-half hr. under these conditions.

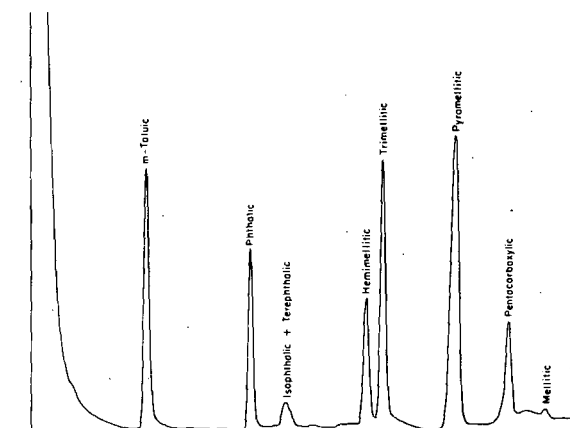


Figure 2 - Cool acids before decarboxylation.

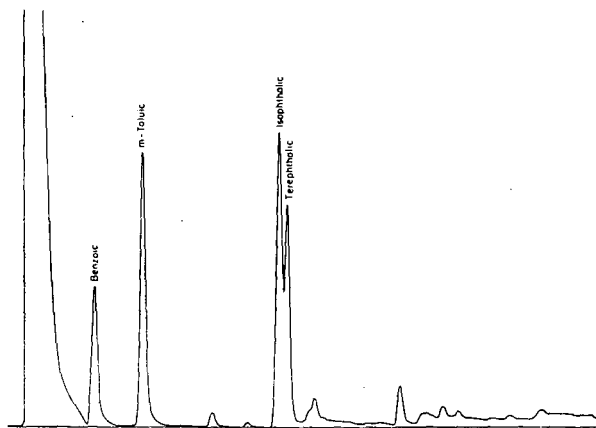


Figure 3 - Cool acids after decarboxylation.

The trimethylsilyl esters were prepared by refluxing the acids with a 1:1:1 mixture of hexamethyldisilazane:trimethylchlorosilane:toluene until the acids were completely solubilized and the resulting ammonium chloride had sublimed. This takes one to two hr. The reaction mixture is kept in a vial sealed with a serum cap to keep out moisture. The fact that the trimethylsilyl ester derivatives are readily hydrolyzable back to the original acid is a useful property of these esters. For example, upon elution from the chromatograph, the ester is trapped out in a capillary tube and exposed to the atmosphere for a short time to affect hydrolysis to the free acid. The infrared spectrum of the acid can then be obtained for positive identification. This has proved extremely helpful for identification since retention times are not reproducible to the degree necessary for identification.

CONCLUSION

By using a g.l.c. separation based on trimethylsilyl esters, it has been possible to rapidly analyze mixtures of carboxylic acids and show that benzenecarboxylic acids undergo a reductive decarboxylation in the presence of hydrogen and carbon monoxide at elevated temperatures and pressures with dicobalt octacarbonyl as a catalyst. The advantages of the trimethylsilyl esters over the methyl esters are that they are easily prepared, chromatograph without tailing, are better separated and are easily converted to the original acid for positive identification. Additionally, with the use of this procedure it has been shown that coal acids undergo this reaction and that valuable products are obtained.

REFERENCES

Manufacturers and products named only to identify the materials used; no endorsement by the Bureau of Mines is implied.

1. Birkofer, L. and Ritter, A. Silicon-Organic Compounds. IV. Silylation of Amino Acids. Chem. Ber., 93, 424 (1960).
2. Germain, J. E. and Valadon, F. Identification of Benzenepolycarboxylic Acids. Bull. soc. chim. France, 1415 (1958).
3. Germain, J. E. and Valadon, F. Study of the Oxidation of Coal. II. Analysis of Benzenepolycarboxylic Acids. Bull. soc. chim. France, 11 (1960).
4. Horii, Z., Makita, M., and Tamura, Y. Gas-Liquid Chromatographic Separation of Acids of Krebs Cycle as Trimethylsilyl Derivatives. Chem. and Ind. (London), 1494 (1965).
5. Kaufman, M. L. Ph.D. Dissertation, University of Pittsburgh, 1966.
6. Maximov, O. B. and Pantiukhina, L. S. Thin-Layer Partition Chromatography of Benzenecarboxylic and Hydroxybenzenecarboxylic Acids. J. Chromatog., 20, 160 (1965).
7. Ruof, C. H., Savich, T. R., and Howard, H. C. Nuclear Structure of the Water-Soluble Polycarboxylic Acids from Oxidation of Bituminous Coal. J. Am. Chem. Soc., 73, 3873 (1951).
8. Schnitzer, M. and Desjardins, J. G. Gas Chromatographic Separation of Benzene Carboxylic Acids. J. Gas Chromatog., 270 (1964).
9. Wender, I., Friedman, S., Steiner, W., and Anderson, R. B. Exchange of Carbonyl Groups in Anhydrides with Carbon Monoxide. Mechanism of Carbon Monoxide Transfer to Organic Molecules Via Transition Metals. Chem. and Ind. (London), 1694 (1958).

QUANTITATIVE ULTRAVIOLET ANALYSIS OF C₁₀-C₁₅
NAPHTHALENES IN HYDROCARBON OILSPatricia A. Estep, Edward E. Childers, John J. Kovach
and Clarence Karr, Jr.Morgantown Coal Research Center, Bureau of Mines,
U. S. Department of the Interior, Morgantown, W. Va.

INTRODUCTION

The characterization of neutral oils from low-temperature coal tars required the development of a quantitative determination of alkylnaphthalenes according to their degree of substitution.

The near ultraviolet spectrum of naphthalene consists of three principle regions of absorption which, according to Clar's classification (13), are called the β -, para-, and α -band systems and are related to the three band systems of benzene. The principle bands of these systems are located at 220.7, 275.5, and 311.5 m μ (log ϵ 5.08, 3.77, and 2.40, respectively). For the quantitative analysis of C₁₀-C₁₁ naphthalenes, the use of the α -bands has been reported by Neimark (31), Adams (2), and Coggeshall (15). An ASTM method (4) for total naphthalenes in jet fuels using the para bands has been adopted and the extent of interference of other aromatics pointed out. Snyder (34) has said that the ASTM procedure using the para bands for naphthalene determination is inapplicable in gasoline samples because of serious interference of monoaromatics. Mixtures of coal tar neutral oils analyzed in this laboratory (23) also prohibits the use of the para bands because of possible interference from other aromatics. Therefore, the present paper describes a method developed for the analysis of C₁₀-C₁₈ alkylnaphthalenes using the most intense β -band of naphthalenes, thereby improving sensitivity and increasing selectivity by reducing interference from other classes.

EXPERIMENTAL

As part of a recently developed low-temperature coal tar assay (23), total naphthalenes were isolated from a high-quality neutral oil using liquid chromatography on a gas chromatography analog. The detailed procedure for this chromatographic technique has been described (21, 22). For the separation, a weighed quantity close to 1 gram of the high-quality neutral oil was introduced to a 25-ft length of 3/8 in. tubing packed with 80-100 mesh F-20 alumina containing 4 weight-percent water and pretreated with spectral grade cyclohexane. The charge was eluted with cyclohexane under 75 psig nitrogen. Fractions of 14 ml each were collected, and elution of naphthalenes was followed by the automatic recording of a chromatogram with an ultraviolet absorption monitoring device. Ultraviolet spectra were obtained on the cyclohexane solutions from tubes corresponding to the chromatogram peaks, using a Perkin-Elmer 350 ultraviolet spectrophotometer and matched quartz absorption cells.

For the absorptivity data, pure samples of naphthalenes and all methyl- and ethylnaphthalenes C₁₀-C₁₂ were commercially available. Zone refined samples from James Hinton, 358 Chicago Ave., Valparaiso, Fla., were used when possible

and were found to be the highest purity available. Out of the 14 possible isomers of trimethylnaphthalenes, the only commercially available samples were the 1, 3, 7-, the 2, 3, 5-, and the 2, 3, 6- isomers. All samples were weighed on a microbalance for the absorptivity data. A study of the β -band for naphthalene and monomethylnaphthalenes showed that these classes behaved in accordance with the laws of Lambert and Beer and it was assumed that higher homologs also obeyed these laws in the concentrations used.

RESULTS AND DISCUSSION

Elution Chromatographic Separation. - Naphthalene and its alkyl derivatives emerged from the column relatively free from other classes of compounds, thus allowing the application of ultraviolet quantitative procedures. Aliphatic material, biphenyls, hydroaromatics, and monoaromatics were all eluted before naphthalenes, with only a small amount of overlapping. Three-ring compounds such as dibenzofurans, fluorenes, phenanthrenes, and anthracenes are eluted later and do not interfere seriously. Within naphthalenes as a class, the parameter which causes a pronounced change in adsorbability was the degree of substitution, while position-substitution effects and size-of-alkyl group effects were secondary. Thus, all isomers of mono-, di-, tri-, tetra-, and pentaalkylnaphthalenes were eluted as classes and were sufficiently separated from each other, as evidenced by marked changes in the ultraviolet spectra of successive fractions.

Figure 1 for a synthetic mixture of four pure naphthalenes shows that overlapping occurs more extensively in lower classes and that increased alkyl substitution is effective in enhancing class separation. Klemm (25) points out that methylation of naphthalene enhances adsorbability but increasing the bulkiness of the substituent group decreases adsorbability. Snyder's data on naphthalenes agrees with the increase of adsorbability with alkylation (35), but shows very little difference in adsorbability of 1-ethyl-, 1-n-butyl-, and 1-n-hexylnaphthalene (36). Ethyl groups were known to be present in the naphthalene mixtures analyzed; a detailed characterization of a bituminous coal tar (11) and recent gas chromatographic data on the naphthalene fractions isolated from 18 tars (23) showed that monoethylnaphthalenes comprised 16 percent of the total amount for monosubstituted naphthalenes and that ethylmethylnaphthalenes were 16 percent of the total amount for disubstituted naphthalenes.

Figure 2 shows that the wavelength of the β -band for naphthalenes containing alkyl groups other than methyl depends more on the number than on the size of the substituent. Hence, any marked change in adsorbability of an alkyl naphthalene from that of the correspondingly substituted methylnaphthalene would be readily detected by its β -band. Since such a change was not observed either in the elution of neutral oil mixtures or synthetic mixtures containing ethylnaphthalenes, it was assumed that naphthalenes containing ethyl groups are eluted with methylnaphthalenes with the same degree of substitution. Further, it is assumed that their amounts were accurately accounted for because their absorptivities were not significantly different from methylnaphthalenes with the same degree of substitution. Small differences in adsorbability among some of the various isomers in mono-, di-, and trimethylnaphthalenes were observed in pure compound elution runs.

Figure 3 shows the results for a neutral oil from a low-temperature tar produced from a Colorado subbituminous coal in a fluidized-bed with internal heating at 500° C.

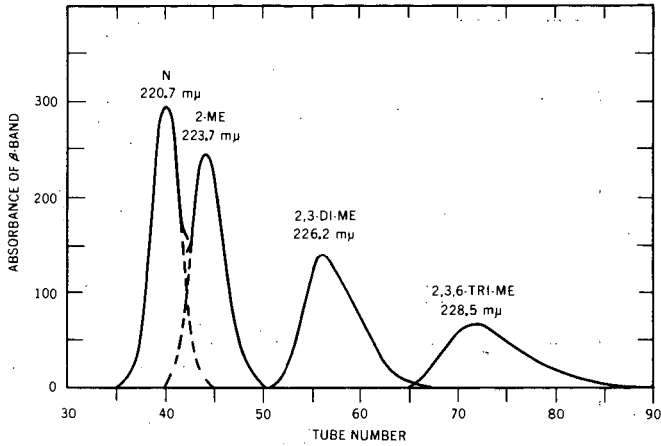


FIGURE 1. - Elution of a Synthetic Mixture of C₁₀-C₁₃ Naphthalenes.

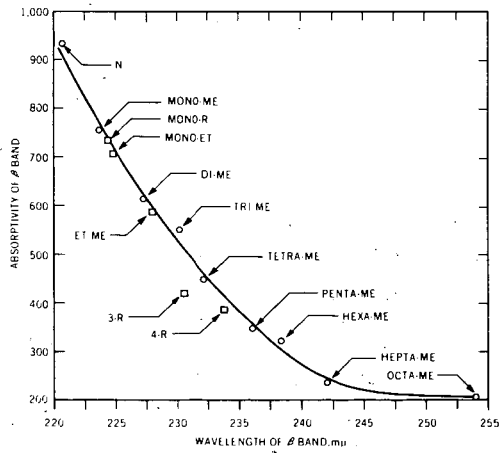


FIGURE 2. - Wavelength and Absorptivity Data for C₁₀-C₁₈ Alkyl naphthalenes.

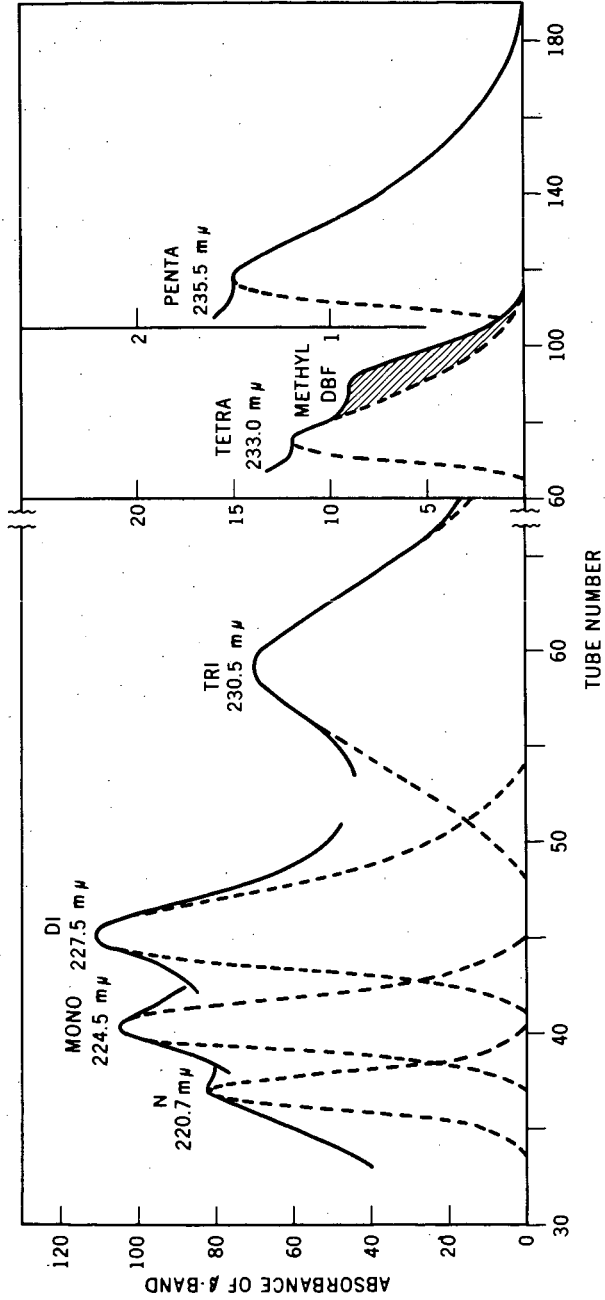


FIGURE 3. - Elution of a Neutral Oil, C₁₀-C₁₅ Naphthalenes.

Since tube number is arbitrary and columns gradually deactivate with extended use, the relative retention of each class to an internal standard can be utilized to aid in the determination of peak tubes, particularly in the broader bands of pentamethylnaphthalenes. For this purpose, 20 μ l of o-ethyltoluene was added to each sample. Since the synthetic mixture shown in Figure 1 and the neutral oil shown in Figure 3 were run several months apart, the peak tube numbers do not agree. However, their relative retentions are comparable. Figure 1 gives relative retentions of 1.5, 1.7, 2.2, and 2.8 for naphthalene and one isomer each of mono-, di-, and trimethylnaphthalene classes, relative to o-ethyltoluene in tube 26. Figure 3 gives relative retention values of 1.4, 1.5, 1.7, and 2.3, respectively, for natural, complex mixtures of these classes, relative to o-ethyltoluene in tube 26.

Determination of Ultraviolet Calibration Data. - It has been observed by Mosby (30) for ultraviolet spectra of C_{14} - C_{16} methylnaphthalenes that with increasing methylation there are bathochromic shifts relative to naphthalene. Dannenberg (16) has shown that for the β -band of naphthalenes there is a constant bathochromic shift of 3 $m\mu$ per alkyl substituent introduced to the ring, independent of its bulkiness and its position in the ring up to the octa-substituted compound. The data presented in Table 1 for C_{10} - C_{18} methylnaphthalenes support this wavelength correlation with the exception of octamethylnaphthalene. A study of both wavelengths and absorptivities was made on C_{10} - C_{18} alkylnaphthalenes, making extensive use of literature data. Ultraviolet spectral data have been reported on all of the 14 possible trimethylnaphthalenes (3, 5, 8, 9, 12, 14, 17, 18, 19, 24, 28, 32, 33), 8 of the tetramethylnaphthalenes (3, 6, 7, 8, 27, 30, 33, 37), 2 pentamethylnaphthalenes (1, 30), 4 hexamethylnaphthalenes (1, 10, 30), 1 heptamethylnaphthalene (1), and octamethylnaphthalene (1, 29). No solvent corrections were applied to the literature data, which are reported both in alcohol and hydrocarbon solvents. Mosby (30) reports that for a tetramethylnaphthalene the only observable difference in methanol and isooctane spectra is a very slight hyperchromic displacement (intensity increase) of the longer wavelength maxima.

As shown in Table 1 and Figure 2 for the β -band there is both a bathochromic and hypochromic displacement (shift to longer wavelength and intensity decrease) as the number of alkyl groups increase in the naphthalene ring. The values of wavelength and absorptivities for the various isomers in each carbon number class are in ranges narrow enough to justify the use of averages. Table 1 presents the arithmetic averages determined for each class of methylnaphthalenes. A plot of carbon number vs. arithmetic average of molar absorptivity yields a linear relationship. However, for application to the present analysis the relationship shown in Figure 2 is shown to have more usefulness. This plot combines both the bathochromic and hypochromic shifts by plotting average absorptivity vs. average wavelength of the β -band for each class of methylnaphthalenes. Values for other alkylnaphthalene classes were added to the plot after the curve for methyl data was drawn. Points shown in squares for monoalkyl-, ethylmethyl-, trialkyl-, and tetraalkylnaphthalenes (where $R = C_{13}$ - C_{16}) were obtained from averages of 26 literature spectra.

While the absorptivities and wavelengths for each class fell into definite ranges, it must be pointed out that the β -band is not insensitive to isomerism. A close examination of the data reveals that in addition to the relationship of absorptivity with degree of substitution, it is also subject to position substitution effects.

TABLE 1. - Ultraviolet data for the β -band of C_{10} - C_{18} naphthalene classes

Class	Source	Average wavelength, $m\mu$	Average absorptivity
Naphthalene	Pure compound	220.7	933
Monomethylnaphthalenes	Pure compounds	223.7	754
Monoethylnaphthalenes	Pure compounds	224.8	709
Dimethylnaphthalenes	Pure compounds	227.3	612
Trimethylnaphthalenes	34 literature values	230.1	550
Tetramethylnaphthalenes	12 literature values	232.1	446
Pentamethylnaphthalenes	2 literature values	236.0	346
Hexamethylnaphthalenes	9 literature values	238.3	321
Heptamethylnaphthalenes	1 literature value	242.0	237
Octamethylnaphthalenes	2 literature values	254	205

TABLE 2. - Ultraviolet data for the β -band of individual C_{11} - C_{12} naphthalenes

Compound	Wavelength, $m\mu$	Absorptivity
1-Methylnaphthalene	223.7	657
2-Methylnaphthalene	223.7	850
1-Ethylnaphthalene	224.8	609
2-Ethylnaphthalene	224.8	808
1, 2-Dimethylnaphthalene	227.5	544
1, 3-Dimethylnaphthalene	227.8	564
1, 4-Dimethylnaphthalene	227.7	352
1, 5-Dimethylnaphthalene	227.3	571
1, 6-Dimethylnaphthalene	226.9	523
1, 7-Dimethylnaphthalene	227.2	692
1, 8-Dimethylnaphthalene	228.2	572
2, 3-Dimethylnaphthalene	226.2	653
2, 6-Dimethylnaphthalene	226.6	868
2, 7-Dimethylnaphthalene	227.3	785

The β -band of naphthalene has been assigned to longitudinal polarization by Klevens (26). The longitudinal direction is defined as being parallel to the long axis of the molecule while transverse is perpendicular to the long axis of the molecule. Jaffé (20) has discussed the importance of the position of substitution upon the longitudinal and transverse polarizations possible within the naphthalene molecule and the effects on wavelength and intensity. However, he does not discuss these effects with regard to the β -band. An examination of all the classes of naphthalenes shows no correlation of structure with wavelength within each class since the ranges are so narrow. It is to be expected that ring substitution will distort the charge distribution within the naphthalene ring and that this effect will influence the intensity of absorption. The following position substitution effects on the absorptivity of the β -band for four classes of naphthalenes were noted:

(1) For monomethylnaphthalenes, Table 2 shows that substitution in the 1-position causes a greater hypochromic shift relative to the value for naphthalene than 2-substitution.

(2) In the class of dimethylnaphthalenes, Table 2 shows that substitution in the 1,4-position produces the greatest hypochromic shift relative to the value for naphthalene while substitution in the 2,6-position produces the least.

(3) A study of the literature data on trimethylnaphthalenes shows that the 1,4,6-isomer has the lowest absorptivity, thus indicating again a greater hypochromic effect with substitution in the 1 and 4 positions.

(4) Within the class of tetramethylnaphthalenes, the 1,4,6,7-isomer has the lowest absorptivity value (320) while the 2,3,6,7-isomer has the largest (686).

Since, as previously stated, ethyl groups are present in coal tar neutral oils and, specifically, monoethylnaphthalenes, it was thought they should be included in the average absorptivities used for the determination of monoalkylnaphthalenes. An arithmetic average of 731 was obtained for the two classes. Since position substitution has a pronounced effect on absorptivity of monoalkylnaphthalenes, a further check on the validity of this average was made by calculating a weighted absorptivity. Data used in obtaining this weighted absorptivity was based on gas chromatographic analysis of each of these four compounds in the isolated naphthalene fractions from 18 individual neutral oils. A value of 757 was obtained which represents a difference of only 3.4 percent from the arithmetic average. In the same manner as for monoalkylnaphthalenes, a weighted average absorptivity was determined for dimethylnaphthalenes. A value differing from the arithmetic average was expected here since there is not an even distribution of the amounts of the 10 dimethyl- isomers in these neutral oils. For example, 1,8-dimethylnaphthalene has not been identified in any coal tar neutral oil. However, a value of 639 was obtained which differs only 4.2 percent from the arithmetic average of 612 for all 10 isomers. In summary, for analysis of coal tar neutral oils, tailored absorptivities of 757 and 639 were used for the mono- and dialkylnaphthalene classes respectively, and absorptivities obtained from the literature were used for the tri-, tetra-, and pentamethylnaphthalenes.

Ultraviolet Analysis. - Throughout successively eluted portions of a neutral oil a regular stepwise bathochromic shift of the β -band occurs and the wavelength of each shift is in good agreement with the wavelength average determined for each class of methylnaphthalenes shown in Table 1. Corresponding to each wavelength shift a peak occurs in the monitor chromatogram. Data from the ultraviolet spectra of individual tubes were used to construct absorbance distribution curves for the β -band of each class of naphthalene, as shown in Figures 1 and 3. The envelope of the ultraviolet absorbance curve is discontinuous, i. e., it is constructed of data from several wavelengths. The plot for a single wavelength was followed as long as that wavelength predominated, i. e., until a combination tube was reached. The absorbance plot was then continued at the new wavelength. In the neutral oil samples analyzed there were consistently six wavelength changes corresponding to C_{10} - C_{15} alkyl naphthalenes. A graphical method was utilized to resolve the individual absorbance distribution curves for each class. Using qualitative changes exhibited throughout the entire ultraviolet spectrum (naphthalene α - and para- bands also vary qualitatively with increasing degree of alkylation), it is possible to follow the key tubes representing the first appearance, the peak and the disappearance for each class of naphthalene, even in the presence of overlapping. These tubes and all combination tubes are then marked on the absorbance plot. The absorbance curve is then drawn according to this information. The dashed lines shown in Figures 1 and 3 indicate this deduced data. Knowledge of curve shapes and characteristic tailing was obtained from pure compound runs. After the absorbance curve for an individual class was constructed in this manner, the absorbance values for each tube were read from this resolved plot and the proper absorptivity used to calculate the weight of that class in a single tube according to the following equation:

$$w = \frac{A \times l4}{a}$$

where w = weight, milligrams;

$l4$ = volume of one tube, ml;

a = absorptivity of the naphthalene class at the β -band;

A = absorbance of the tube at the β -band.

Extensive interference from non-naphthalenic compounds was not encountered. Both ultraviolet and infrared spectra showed that the lower classes of naphthalene were sufficiently separated from the preceding classes of hydroaromatics, biphenyls, and monoaromatics. A small amount of overlapping introduced negligible error since these classes have minimum absorption in the region of the naphthalene β -band and, in addition, have significantly lower absorptivities at their maxima. When there was qualitative evidence of significant amounts of dibenzofurans, fluorenes, phenanthrenes, and anthracenes overlapping the higher naphthalene classes, there was a change in the shape of the distribution curve, as shown in Figure 3 for the tetramethylnaphthalene class. The amount of absorbance due to this interfering compound was graphically subtracted from the absorbance distribution plot, as shown by the shaded area, considering the shape of the naphthalene curve. In the instance of Figure 3, the compound was identified as a methyl dibenzofuran mixture from its ultraviolet bands. Since the method is graphical, it is not necessary to identify the compound to subtract its absorbance. If this graphical approach is prevented by too close an agreement of peak tubes of interfering compound and

naphthalene class, the standard quantitative method of solution of simultaneous equations can be applied. The absorptivities of these more strongly adsorbed compounds at the naphthalene β -band wavelength are minimum since their wavelength maxima are all in the range 250 to 260 μ .

Because of the unavailability of pure samples in the C_{14} - C_{15} naphthalene range, no realistic synthetic mixture could be tested. However, analysis of the relatively simple mixture shown in Figure 1, using absorptivities specific for the compounds present, gave individual errors of not more than 2 percent absolute. Another accuracy test was made on a mixture synthesized to duplicate the percentages of individual C_{10} - C_{13} naphthalenes in a neutral oil sample. This test mixture, containing 14 naphthalenes, gave an ultraviolet absorbance distribution curve that showed the same class elutions as obtained with neutral oils. Average class absorptivities were used to determine the amounts of each class. Results showed that no naphthalene class was in error more than 5 percent absolute.

The 18 neutral oils analyzed by this method varied in composition from 5 to 25 percent total alkyl naphthalenes. In spite of this composition variation, wavelengths of each class remained remarkably constant. These analytical procedures for coal tar neutral oils should be applicable to similar hydrocarbon oils from other sources, such as petroleum and shale oil.

REFERENCES

1. Abadir, B. J., J. W. Cook, and D. T. Gibson. Synthesis of Polymethylnaphthalenes. *J. Chem. Soc.*, 1953, pp. 8-17.
2. Adams, Norman G., and Dorothy M. Richardson. Aromatic Hydrocarbons in Some Diesel Fuel Fractions. *Anal. Chem.*, v. 23, No. 1, January 1951, pp. 129-133.
3. American Petroleum Institute Research Project 44. Catalog of Ultraviolet Spectra. Texas Agricultural and Mechanical University, College Station, Texas.
4. American Society for Testing and Materials. Standard Method of Test for Naphthalene Hydrocarbons in Aviation Turbine Fuels by Ultraviolet Spectrophotometry. ASTM Designation D1840-64, adopted 1964.
5. Barton, D. H. R., J. F. McGhie, M. K. Pradhan, and S. A. Knight. Constitution and Stereochemistry of Euphol. *J. Chem. Soc.*, 1955, pp. 876-886.
6. Bory, S., and P. Dietrich. Synthesis of 1, 2, 4, 6-Tetramethylnaphthalene. *Bull. Soc. Chim. France*, 1957, pp. 228-229.
7. Caglioti, L., H. Naef, D. Arigoni, and O. Jeger. Sesquiterpenes and Azulenes. CXXVI. Constituents of Asafetida. 1. Farnesiferol A. *Helv. Chim. Acta*, v. 41, 1958, pp. 2278-2292.
8. Cagniant, Denise, and Paul Cagniant. Arylaliphatic Hydrocarbons. I. Ultraviolet and Infrared Spectrographic Studies of Some 9- and 9,10-Alkylated Phenanthrene and Hydrophenanthrene Derivatives. *Bull. Soc. Chim. France*, 1957, pp. 1403-1416.

9. Carruthers, W., and A. G. Douglas. Constituents of High-Boiling Petroleum Distillates. II. Trimethylnaphthalenes in a Trinidad Oil. *J. Chem. Soc.*, 1955, pp. 1847-1850.
10. Carruthers, W., and J. D. Gray. 1,2,3,4,5,6- and 1,2,3,4,5,7-Hexamethylnaphthalene. *J. Chem. Soc.*, 1958, pp. 1280-1286.
11. Chang, Ta-Chuang Lo, and Clarence Karr, Jr. Gas-Liquid Chromatographic Analysis of Aromatic Hydrocarbons Boiling Between 202° and 280° in a Low-Temperature Coal Tar. *Anal. Chim. Acta*, v. 24, No. 4, April 1961, pp. 343-356.
12. Chrétien-Bessière, Yvonne. Alloocimene. *Ann. Chim. (Paris)*, Series 13, v. 2, 1957, pp. 301-370.
13. Clar, E. Polycyclic Hydrocarbons. Academic Press, Inc., New York, N. Y., v. 1, 1964, 487 pp.
14. Cocker, J. D., T. G. Halsall, and A. Bowers. The Chemistry of Gum Labdanum. II. The Structure of Labdanolic Acid. *J. Chem. Soc.*, 1956, pp. 4262-4271.
15. Coggeshall, Norman D., and Alvin S. Glassner, Jr. Ultraviolet Absorption Analysis for Naphthalenes. *Anal. Chem.*, v. 21, No. 8, May 1949, pp. 550-553.
16. Dannenberg, Heinz, and Dorothee Dannenberg-von Dresler. The Systematics of the Ultraviolet Absorption. III. Polycyclic Compounds With a Naphthalene System. *Chem. Ber.*, v. 89, 1956, pp. 1326-1333.
17. Evans, R. F., J. C. Smith, and F. B. Strauss. Alkylnaphthalenes. X. 1,4-Dimethylnaphthalene and Some Trialkylnaphthalenes. *J. Inst. Petrol.*, v. 40, 1954, pp. 7-13.
18. Friedel, R. A., and Milton Orchin. Ultraviolet Spectra of Aromatic Compounds. John Wiley & Sons, Inc., New York, N. Y., 1951.
19. Heilbronner, E., U. Fröhlicher, and Pl. A. Plattner. Ultraviolet Absorption Spectra of Trimethylnaphthalenes. *Helv. Chim. Acta*, v. 32, 1949, pp. 2479-2488.
20. Jaffé, H. H., and Milton Orchin. Theory and Applications of Ultraviolet Spectroscopy. John Wiley and Sons, Inc., New York, N. Y., 1962, p. 303.
21. Karr, Clarence, Jr., Edward E. Childers, and William C. Warner. Analysis of Aromatic Hydrocarbon Samples by Liquid Chromatography With Operating Conditions Analogous to Those of Gas Chromatography. *Anal. Chem.*, v. 35, No. 9, August 1963, pp. 1290-1291.
22. Karr, Clarence, Jr., Edward E. Childers, William C. Warner, and Patricia A. Estep. Analysis of Aromatic Hydrocarbons From Pitch Oils by Liquid Chromatography on Gas Chromatography Analog. *Anal. Chem.*, v. 36, No. 11, October 1964, pp. 2105-2108.

23. Karr, Clarence, Jr., Joseph R. Comberiat, Kenneth B. McCaskill, and Patricia A. Estep. Evaluation of Low-Temperature Coal Tars by a Rapid, Detailed Assay Based on Chromatography. *J. Appl. Chem.*, v. 16, No. 1, January 1966, pp. 22-27.
24. Klemm, L. H., and A. J. Kohlik. Polarographic Reduction of Some Alkyl-, Alkylene-, and Polymethylnaphthalenes. *J. Org. Chem.*, v. 28, No. 8, August 1963, pp. 2044-2049.
25. Klemm, L. H., David Reed, L. A. Miller, and B. T. Ho. Chemical Structure and Chromatographic Adsorbability of Aromatic Hydrocarbons on Alumina. *J. Org. Chem.*, v. 24, No. 10, October 1959, pp. 1468-1477.
26. Klevens, H. B., and J. R. Platt. Spectral Resemblances of Cata-Condensed Hydrocarbons. *J. Chem. Phys.*, v. 17, 1949, pp. 470-481.
27. Kruber, Otto, and Armin Raeithel. Coal-Tar Anthracene Oil. *Chem. Ber.*, v. 85, 1952, pp. 327-333.
28. Morton, R. A., and A. J. A. deGouveia. Chromophoric Groups. Part II. Absorption Spectra of Naphthalene, Hydronaphthalenes, and Related Compounds. *J. Chem. Soc.*, 1934, pp. 916-930.
29. Mosby, William L. The Ultraviolet Absorption Spectra of Some Highly Chlorinated Aromatic Systems. *J. Am. Chem. Soc.*, v. 77, No. 3, February 1955, pp. 758-760.
30. _____. The Ultraviolet Absorption Spectra of Some Polymethylnaphthalenes. *J. Am. Chem. Soc.*, v. 75, July 1953, pp. 3348-3349.
31. Neimark, M. E., I. E. Kogan, and M. M. Bragilevskaya. Spectrophotometric Determination of Naphthalene and Monomethylnaphthalenes. *Sb. Nauchn. Tr. Ukr. Nauchn.-Issled. Uglekhim. Inst.*, v. 14, 1963, pp. 105-110.
32. Ruzicka, L., H. Schinz, and P. H. Müller. Sesquiterpenes. LXII. A New Type of Sesquiterpene From *Cedrus atlantica* Leaf Oil. *Helv. Chim. Acta*, v. 27, 1944, pp. 195-206.
33. Schöpf, Clemens, Dieter Klein, and Ernst Hofmann. Samandarine and Related Alkaloids. V. The Preparation of Hydrocarbons by Dehydrogenation of Samandiol. *Chem. Ber.*, v. 87, 1954, pp. 1638-1660.
34. Snyder, Lloyd R. Applications of Linear Elution Adsorption Chromatography to the Separation and Analysis of Petroleum. II. Compound Class Separations by a Routine Micro Procedure. Determination of Gasoline Polyaromatics. *Anal. Chem.*, v. 33, No. 11, October 1961, pp. 1535-1538.
35. _____. Linear Elution Adsorption Chromatography. II. Compound Separability With Alumina as Adsorbent. *J. Chromatog.*, v. 6, No. 1, July 1961, pp. 22-52.

36. Snyder, Lloyd R., and H. Dale Warren. Linear Elution Adsorption Chromatography. VIII. Gradient Elution Practice. The Effect of Alkyl Substituents on Retention Volume. *J. Chromatog.*, v. 15, No. 3, August 1964, pp. 344-360.
37. Stoll, M., C. F. Seidel, B. Wilhalm, and M. Hinder. Odor and Constitution. XVI. The Constitution of Ambrinol. (Δ^4 -, Δ^9 -, and $\Delta^{5,10}$ -1,1,6-Trimethyl-6-hydroxyoctahydronaphthalene). *Helv. Chim. Acta*, v. 39, 1956, pp. 183-199.

ANALYSIS OF SULFUR IN COALS BY X-RAY FLUORESCENCE

Martin Berman and Sabri Ergun

Solid State Physics Group, Pittsburgh Coal Research Center
U.S. Bureau of Mines, Pittsburgh, Pennsylvania

ABSTRACT

Determination of the sulfur content of coals by X-ray fluorescence has been investigated. For preliminary studies on sulfur in both organic and pyritic forms, known amounts were added to sulfur-free carbon black.

Pyrite particle size was found to have a significant effect on fluorescence intensities. At constant pyrite content, fluorescence intensity gives a good measure of pyrite particle size in the range from 2 to 150 microns. For determination of sulfur content, samples must be ground to less than 2 microns.

The ratio of sulfur $K\alpha$ and $K\beta$ fluorescence emission is quite dependent on sulfur concentration but almost independent of bonding or sulfur form. The alpha to beta ratio thus is a very good measure of the sulfur concentration, requiring no standard or correction for changes in intensity of the X-ray beam. The alpha to beta ratio, in combination with the $K\alpha$ reading, permits a determination of total sulfur as well as the percentage in pyritic form.

A program is now in progress to determine the sulfur content of over 100 American coals by X-ray fluorescence.

A MICROMETHOD FOR TOTAL SULFUR DETERMINATION IN
NONLEADED LIGHT HYDROCARBON FEEDSTOCKS

A. Attari

Institute of Gas Technology, Chicago, Illinois

ABSTRACT

Sulfur poisoning adversely affects the life and performance of nickel catalysts used in hydrocarbon reforming and similar operations. The need for a dependable procedure for total sulfur determination led to development of the method described in this paper. The sulfur compounds in a weighed sample are converted to SO_2 by combustion in an oxyhydrogen burner, and oxidized to SO_3 by passage of the combustion products through a hydrogen peroxide solution. An aliquot of the washings is then reduced to H_2S in a solution of hydriodic acid. The resulting H_2S is converted to methylene blue for colorimetric measurement; at the acid concentration used in this method, methylene blue has two absorption peaks: 670 and 745 $\text{m}\mu$. The method is so sensitive that 2 μg of sulfur in a 100 cc volume yields a perceptible color development. By adjusting the amount of sample taken, or the aliquot of sulfate solution, one can determine sulfur levels in the range of 0 to 500 ppm by weight. The only limitation is contamination of low-sulfur samples if the apparatus is not thoroughly rinsed and cleaned after use with high-sulfur samples. Interferences are from metals such as Ca, Ba, and Pb, which cause insoluble sulfates.

Partial Combustion of Fuel Oil with Oxygen
and Application to Smelting Iron Ore

by Jerome Feinman and
David A. Muskat*

Applied Research Laboratory
United States Steel Corporation
Monroeville, Pennsylvania

Much interest in alternative smelting processes based on cheaper fuels than metallurgical coke has developed during the past decade. Many processes have been developed, however, none of these processes have proven competitive with the blast furnace in the United States. In this context, it was decided to study a proposed smelting process in which all the reducing gases and heat for smelting come from the partial combustion of fuel oil and/or pulverized coal with oxygen at the bottom of a shaft reactor. Some anticipated advantages of such a process over the blast furnace are elimination of the stoves and associated equipment for heating the blast, reduction or elimination of coke requirements, and production of hot metal at much higher rates than are presently obtained with blast furnaces.

Preliminary heat and material balances indicated that the proposed process is feasible. Several important factors associated with the operation of a partial-combustion burner and with the operation of the reactor, however, could not be investigated theoretically. With respect to burner operation, the extent of conversion of fuel oil with oxygen to CO and H₂, the nature of any solid carbon formed during partial combustion, and the stability of combustion were the most important factors to be determined experimentally. As for the operation of the reactor, it was not known whether smooth flow of materials and effective contact between gases and solids could be achieved without the leavening action provided by coke in the blast furnace. In addition, it was not known whether sufficient residence time can be obtained to complete reduction at the high throughput rates assumed in the theoretical analysis.

Theoretical and Practical Considerations

Figure 1 shows that the theoretical flame temperature for stoichiometric partial combustion of No. 6 fuel oil with oxygen to produce CO and H₂ is 3375 F. With 10 percent excess oxygen, the flame temperature would be approximately 4000 F. If 10 percent un-gasified carbon were formed with stoichiometric oxygen, the flame temperature would be approximately 3700 F. Thus, the required temperatures for smelting iron oxide are theoretically attainable. Whether they could be obtained in practice, however, remained to be determined.

* Present address - Lubrizol Company, Painesville, Ohio

In most commercial applications, combustion refers to the rapid oxidation of a material with the evolution of large quantities of heat. Usually, the specific rates of the chemical reactions occurring in the combustion process are so rapid that physical transport phenomena control the rate of combustion. These physical characteristics are directly related to the degree of mixing of the reactants. A device known as a burner is used to prepare and introduce the reactants into the reaction zone in such a manner as to produce an efficient rate of combustion.

The most effective burner for high-intensity combustion would mix the fuel with the oxygen before introduction into the combustion chamber. Many gas burners premix all or most of the air or oxygen needed for combustion with the gas and produce a high-temperature flame. A bunsen burner premixes only as much air as can be aspirated; its flame is therefore not as hot nor as well defined as the flame of burners utilizing completely premixed air and fuel because some of the air needed for combustion must come from the surroundings of the flame. When all aspirated air to the burner is shut off, the flame becomes long and poorly defined because all the air must mix with the gas by diffusional means, a much slower method of mixing.

Because liquid fuels cannot be appreciably premixed before burning, the rate of combustion is controlled by the mixing in the combustion zone. To facilitate combustion, liquid fuels are usually injected into the combustion zone through an atomizing nozzle. There are three types of atomizers: (1) pneumatic nozzles that use air, steam, or some other gas to atomize the liquid; (2) high-pressure nozzles that force the liquid through a small orifice; and (3) mechanical devices that use rotating discs to break up the liquid. The energy used to atomize the liquid is greatest for the first type, which usually produces a spray of finer droplets than the other types.

There are two common methods for providing good mixing of the reactants in the combustion zone. The first is direct impingement of the fuel and air jets, each introduced into the combustion zone at different angles. In the second method, opposite radial velocity components are imparted to the two streams by the use of vanes in each injector tube. For efficient operation, most burners are designed to use one of these methods.

Liquid fuels such as fuel oil burn according to the following simplified mechanisms:

1. The volatile components in the oil are vaporized
2. The vapors react with oxygen, evolving sufficient heat to propagate the combustion. If sufficient oxygen is not immediately available to react with all the carbon in the vaporized portion of the fuel, the unreacted hydrocarbons will crack to form solid carbon particles and hydrogen.

3. The nonvolatile matter (primarily solid carbon) is burned. This carbon, as well as any carbon formed by the cracking of hydrocarbons, is consumed by a relatively slow solid-gas reaction mechanism.

Previous workers have found that the reaction time of the solid residue is as much as 10 times that of the volatile matter.^{1,2)}* These experiments were performed in an atmosphere containing an excess of oxygen. The increase in burning time for cases in which there is a deficiency of oxygen, such as in a partial-combustion process, would probably be even greater. It is therefore desirable to minimize the amount of solid carbon formed during primary combustion. The minimum solid carbon would be comprised of oil residue, with none being formed by cracking of volatiles.

When atomization is good, the rates of evaporation of volatiles and reaction of volatiles with oxygen are very rapid. Therefore, to prevent any of the volatiles from cracking, oxygen must be made available before the hydrocarbon vapors reach the cracking temperature. Because the oxygen and oil are not premixed, very rapid mixing must occur as soon as these reactants enter the combustion chamber. Because this mixing can only occur by eddy and molecular diffusion, it is evident that mixing is normally the limiting factor in establishing the rate of combustion. This conclusion is based on work done under conditions of complete combustion, and is probably even more restrictive under conditions of partial combustion.

Description of Burner System and Operating Procedure

In view of the theoretical and practical considerations, it was apparent that the combustion chamber would have to be constructed of a refractory capable of withstanding very high temperatures in both oxidizing and reducing atmospheres. It was also apparent that because of the small volume of oxygen needed per unit of fuel compared with a complete combustion burner operating on air — only 1/16 the volume of reacting gas and 1/3 the oxygen is required for partial combustion using oxygen — satisfactory mixing of the reactants would be considerably more difficult. If sufficient mixing were not provided, flame stability would decrease, localized excessive temperatures would result, and large quantities of solid carbon would be formed that would greatly increase the time needed to complete the gasification process; additional combustion-chamber volume would be needed to produce a given amount of reducing gas.

These factors were considered in selecting a commercial fuel-oil burner that was adaptable for use as a partial-combustion burner. An air-atomizing vortex burner was procured that fulfilled these requirements. In addition to the fine atomization obtainable with this burner, the main oxygen stream had a counterclockwise motion imparted to it by

*See References

means of vanes in the windbox. This arrangement provided one of the most efficient means available in a commercial burner for mixing the fuel oil and oxygen.

Figure 2 shows details of the oil-injection nozzle, the center cone, the windbox vane detail and the oxygen nozzle comprising the essential parts of the burner, Figure 3 is a section view of the assembled burner, and Figure 4 is a section view of the atmospheric test chamber.

Figure 5 shows a schematic piping diagram for the burners. The oil rate is obtained by measuring the change in weight of the oil-supply barrel with time. A positive-displacement pump transports the oil against a constant delivery pressure maintained by the pressure-regulating valve. The oil rate is controlled manually with an air-operated control valve. The pressure switches are connected to an annunciator that warns when the oil pressure deviates from a preset range; a solenoid valve in the line enables the oil flow to be stopped rapidly.

The primary oxygen flow is measured by a calibrated rotameter and is controlled manually by a needle valve. The pressure switch in the oxygen line is connected to the annunciator panel to indicate a low-pressure oxygen supply; a solenoid valve enables the oxygen flow to be stopped rapidly.

The system was piped to provide for either air or oxygen atomization. The atomizing flow rate was measured by a calibrated rotameter. Electric resistance heaters were installed in both the primary oxygen and the atomizing lines so that these streams could be heated during cold-weather operation.

Figure 6 shows a schematic diagram of the electrical wiring for one burner system. The pressure switches are connected to an annunciator that rings an alarm and flashes a light when any of the supply pressures deviate from a preset range. The solenoid valve switches are arranged so that the atomizing gas flow has to be started before the oil and oxygen to provide a safe start-up.

To become familiar with the operating characteristics of the burner, tests were made using only air and No. 6 fuel oil. A typical chemical analysis of the No. 6 fuel oil is shown in Table I. Although the burner performed as expected under complete-combustion conditions, burner operation became unstable as the air rate was decreased. Apparently, the heat released per unit volume of fuel became so low that the flame could not propagate itself effectively. The next step was to use oxygen for primary combustion gas and air for atomization.

During these initial tests using oxygen, the burner was being fired at 40 to 50 pounds of oil per hour using zero to 10 percent excess oxygen, and with an atomizing pressure of 40 to 60 psig. The pressure drop across the windbox of the burner (a measure of the energy)

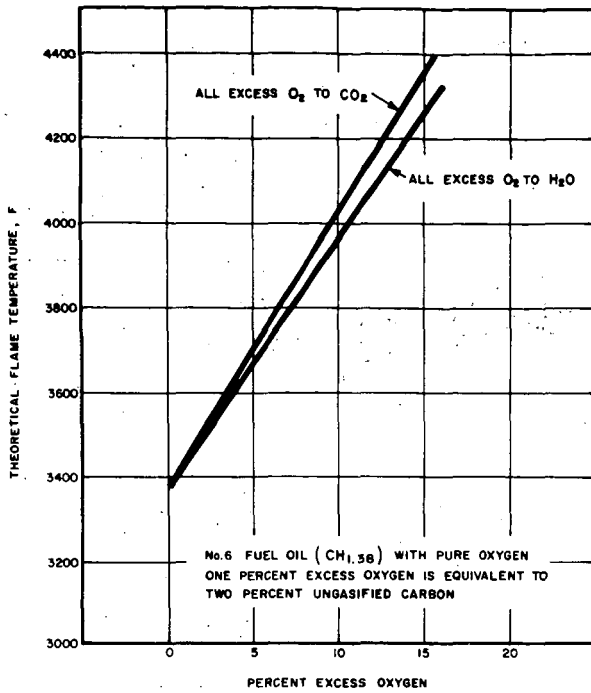


FIGURE 1 THEORETICAL FLAME TEMPERATURES FOR PARTIAL COMBUSTION OF BUNKER C FUEL OIL VERSUS EXCESS OXYGEN

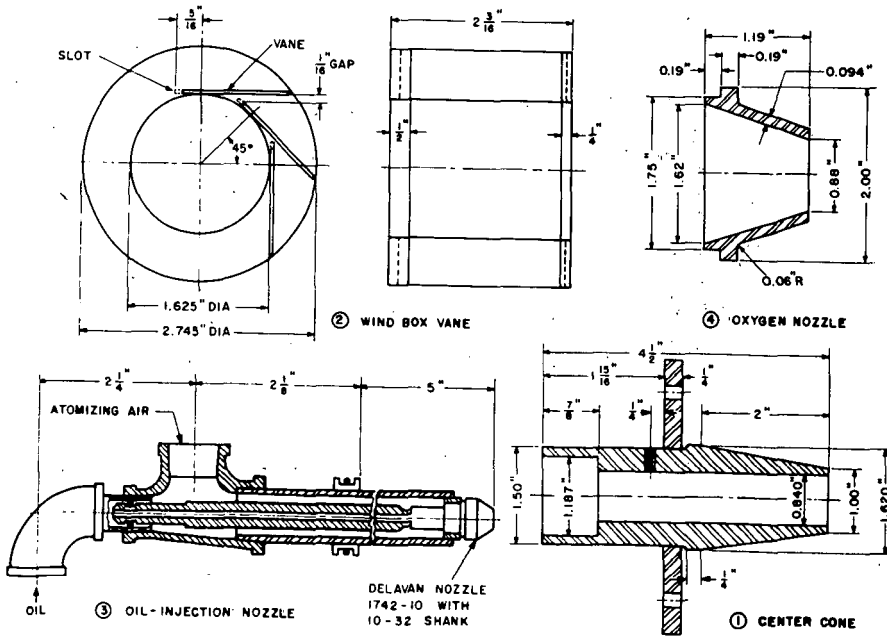


FIGURE 2 DETAILS OF BURNER PARTS

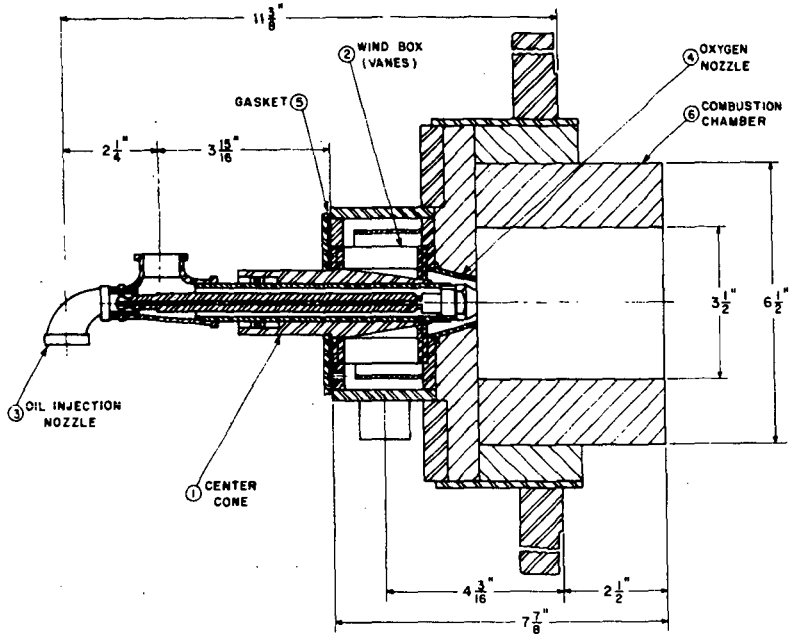


FIGURE 3 SECTION VIEW OF ASSEMBLED BURNER

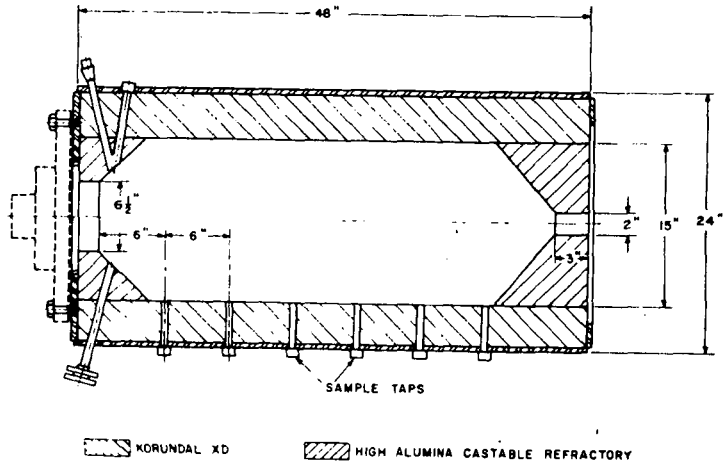


FIGURE 4 ATMOSPHERIC TEST CHAMBER

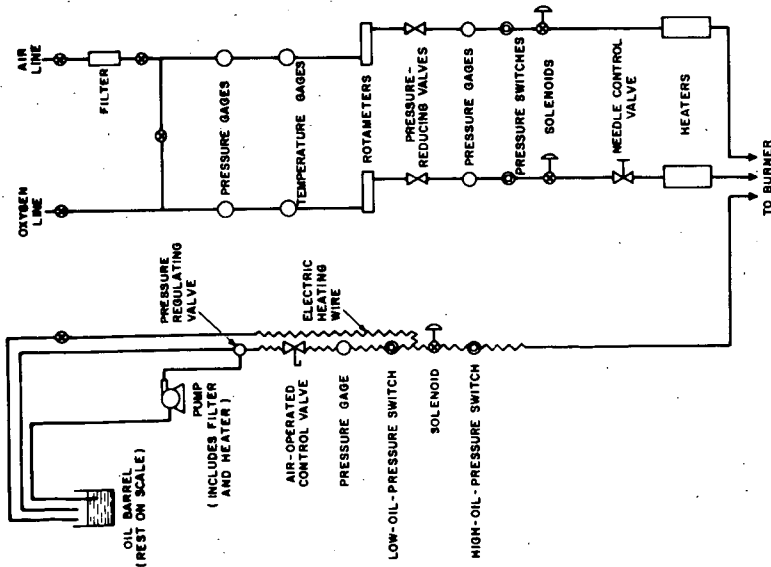


FIGURE 5 PIPING DIAGRAM FOR PARTIAL - COMBUSTION BURNER

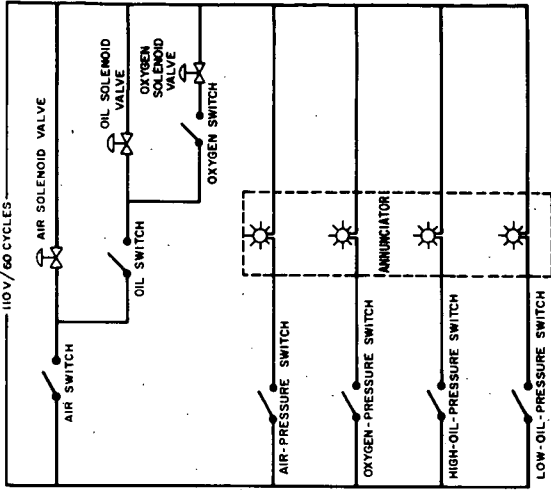


FIGURE 6 SCHEMATIC ELECTRICAL DIAGRAM FOR PARTIAL - COMBUSTION BURNER SYSTEM

released to the gas stream for mixing the reactants) was approximately two inches of water. In addition to poor conversions (the fraction of carbon in the oil that is gasified) during these studies, hard carbon would rapidly build up in the combustion chamber. This would direct the flame back onto the burner tip and force a shutdown. The hard carbon build-up was attributed to a combination of coarse atomization and lack of turbulence in the chamber, and probably occurred when oil droplets impinged on the hot refractory surface. It was obvious that finer atomization and increased turbulence in the chamber were necessary to prevent formation of hard carbon. Finer atomization was obtained by increasing the atomizing pressure. Increased turbulence in the combustion chamber was obtained by increasing the pressure drop across the windbox. This was done by decreasing the gap between the vanes in the windbox (part 2, Figure 2) from 1/16 inch to 1/64 inch, and decreasing the diameter of the oxygen nozzle (part 4, Figure 2) from 1 inch to 0.88 inch. These changes eliminated the hard-carbon build-up, but did not appreciably improve conversion. It was later determined that erosion of the nozzle tip had been the major cause of coarse atomization at 40 psig atomizing pressure, and that satisfactory operation at this atomizing pressure was possible with a new nozzle. When these changes were made it was possible to operate the burner continuously for extended periods (at least 8 hours) and a test program was begun to determine the operating conditions for most efficient fuel conversion. The independent variables chosen were oil rate, percent excess oxygen, and atomizing pressure. The range of conditions studied are listed in Table II.

Testing began when the walls of the atmospheric test chamber became incandescent. The independent variables chosen for the test were established and 30 minutes was allowed for attainment of steady-state conditions. Two gas samples, one 3 feet and one 1.5 feet from the burner nozzle, were then taken from the inside wall of the test chamber using an uncooled 1/4-inch-diameter stainless-steel tube. These samples were analyzed by gas chromatography for CO, CO₂, H₂, and N₂. Several samples were analyzed with a mass spectrometer to determine the quantities of other hydrocarbons (such as CH₄, C₂H₂, and C₂H₆) being formed. The mass-spectrometer results indicated that less than 1.5 percent of the total product gas was made up of constituents other than CO, CO₂, H₂, and N₂; the chromatograph results were therefore used to calculate material balances. Elemental balances for hydrogen, carbon, and oxygen were used to calculate the quantities of soot and water vapor, and the total moles of dry gas formed. A check on the consistency of the data was possible by a nitrogen balance.

Analysis of the data from this program showed that the burner was not very efficient (cf. results below). Because it was believed that the original nozzle was the major source of trouble, studies were also made using a special spray nozzle designed for operation over a wider range of fuel rates. Figure 7 is a detailed drawing of this nozzle.

Results of Burner Tests

Most commercial burner systems are operated under complete combustion conditions and efficiencies are usually expressed as thermal output per unit of fuel consumed. In the case of partial-combustion systems, it is more meaningful to consider the degree of gasification of the fuel. In the present application this type of burner has a dual purpose — to produce reducing gas and to produce sufficient heat to melt the solid products in a smelting operation. Thus, the formation of a small amount of CO_2 and H_2O is not necessarily detrimental to the performance of the process. However, it is possible that any ungasified carbon leaving the combustion zone will remain as such in its passage through the reactor and thus represent an unrecoverable loss of energy. In the analysis of the present data, therefore, the percent excess oxygen was considered as the independent variable, the percent ungasified carbon as the dependent variable, and the fuel rate, atomizing pressure, and sampling location as the parameters.

Figure 8 shows the data obtained inside the test chamber 3.0 feet and 1.5 feet from the original nozzle tip while operating at an oil rate of 45 to 50 pounds per hour; atomizing pressure is the parameter. It is clear that atomizing pressure has little effect on fuel conversion, probably because atomizing pressure has little effect on the mixing of the oil and oxygen. This would not be true at very low atomizing pressures (up to about 20 psig) where atomization is coarse and the rate of evaporation becomes a limiting step in the burning process. It is concluded that for all the atomizing pressures studied, the fineness of atomization was sufficient to maintain an evaporation rate greater than the reactant mixing rate, thereby making burner performance independent of atomizing pressure. This result held at the higher oil rates and also for the special spray nozzle.

Figure 9 represents the data when considering the fuel rate as a parameter. It is clear that fuel rate has no significant effect on conversion. This result is probably due to the fact that the decreased residence time for the higher fuel rates is compensated for by increased turbulence and concomitant improvement in mixing.

Figure 10 is a plot of percent ungasified carbon versus percent excess oxygen for comparable data using the original nozzle and the special spray nozzle. Better conversions were obtained with the special spray nozzle.

In all cases, better conversions were obtained 3 feet from the nozzle tip than 1.5 feet from the tip. This distance would be expected to directly affect the conversion since the extent of mixing is a function of that distance (in terms of increased residence time). In addition, the burning times of the solid residue and soot are probably comparable to the residence time of the gas in the test chamber. Thus, even with perfect mixing, a difference in conversion would exist between the two sampling locations.

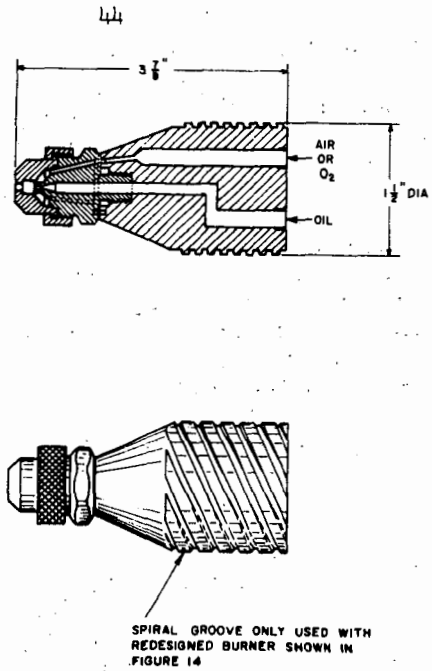


FIGURE 7 SPECIAL SPRAY OIL INJECTION NOZZLE

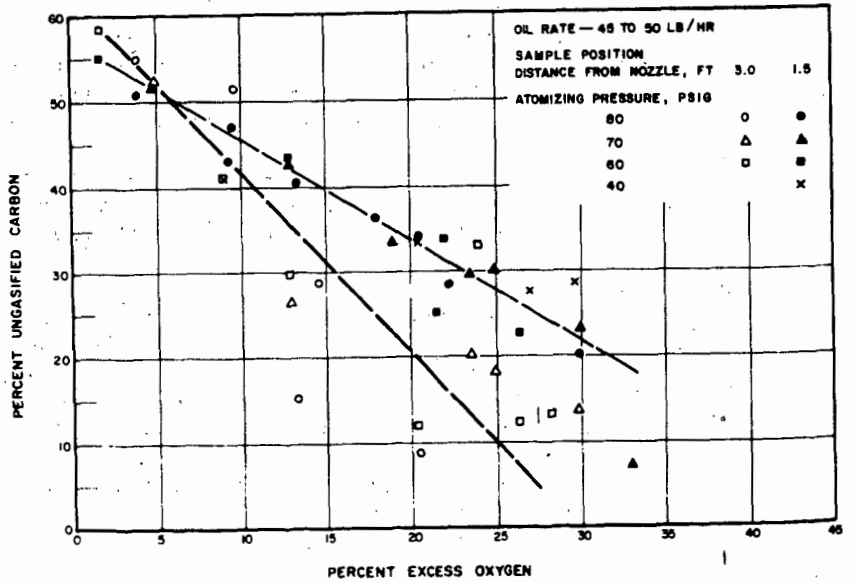


FIGURE 8 EFFECT OF ATOMIZING PRESSURE AND SAMPLING POSITION—ORIGINAL NOZZLE

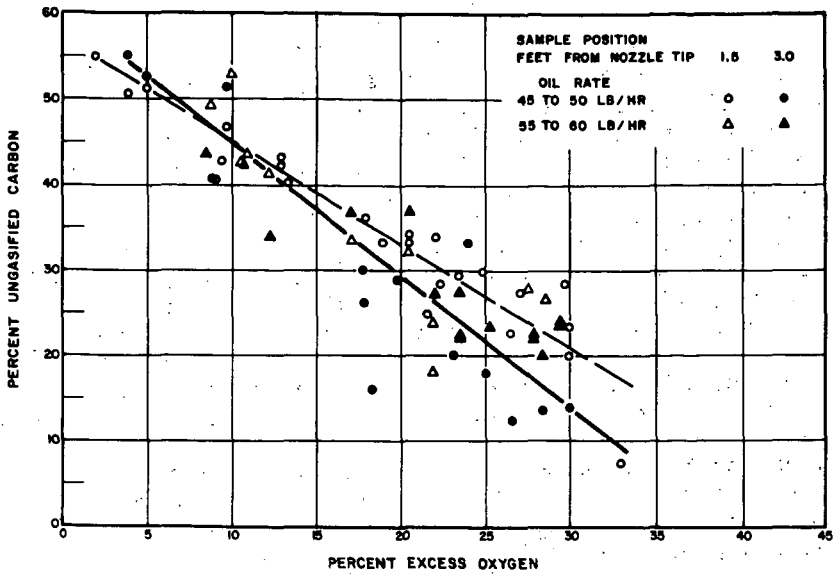


FIGURE 9 EFFECT OF FUEL RATE AND SAMPLING POSITION—ORIGINAL NOZZLE.

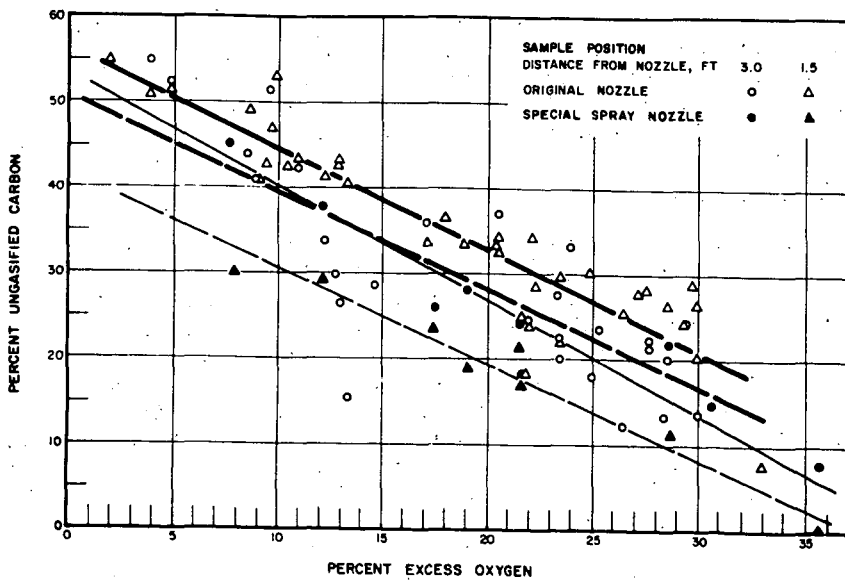


FIGURE 10 EFFECT OF SAMPLING POSITION AND NOZZLE DESIGN

Under all conditions, with less than 15 percent excess oxygen, the ungasified carbon was greater than 20 percent. With ideal mixing of the reactants, any ungasified carbon would represent solid carbon from nonvolatile matter in the oil and not from cracking of the volatiles. However, the oil contained greater than 90 percent volatile matter. Thus, at least half of the ungasified carbon formed came from cracking of volatiles. This is so because, with perfect mixing, the volatiles would probably burn as rapidly as they evaporate,⁵⁾ and the quantity of ungasified carbon would be 10 percent or less, depending on the sampling position and burning time of the residue.

The results of other work done on evaporation rates and combustion rates of fuel droplets³⁾ indicate that 0.3 to 0.6 seconds (the average residence time available for a drop to react in our apparatus) is far in excess of the time needed to evaporate and burn the volatile matter. It is therefore believed that the present system could, with perfect mixing of the reactants, gasify all carbon contained in the volatile matter and produce a product gas containing less than 10 percent ungasified carbon. Because gasification of solid residue is about 10 times slower than gasification of volatiles, conversions better than 90 percent would require longer residence time than can be obtained in the test chamber. In any event, the technical feasibility of the proposed smelting process should not be restricted by the low conversions obtained in the test chamber. This conclusion is based on the knowledge that, even when operating with 20 percent excess oxygen, the gas produced will be reducing to FeO. Table III shows the results of a representative run and a comparison of the actual CO_2/CO and $\text{H}_2\text{O}/\text{H}_2$ ratios with the equilibrium ratios for 2000 F. Although the $\text{H}_2\text{O}/\text{H}_2$ ratio is only moderately reducing, the CO_2/CO ratio is substantially reducing to FeO. In addition, it must be remembered that the operation of the proposed process will provide enough solid carbon in the burden to reduce these complete combustion products and for solution in the hot metal produced.

Pilot-Plant Design

Figure 11 is a picture of the pilot plant comprising of a shaft reactor, a double-hopper arrangement for feeding solids, an off-gas system, and a control room that houses most of the equipment for operating the burners. Figure 12 shows a cross-sectional diagram of the reactor, which is constructed in four sections: the hearth, the lower stack (containing two diametrically opposed burner mounting assemblies), the upper stack, and the top head. The reactor shaft is a 10-foot straight section, 1 foot in diameter, that flares to 2 feet where it is attached to the hearth. The hearth is 2 feet in diameter and 2 feet high. The reactor is lined with 18 inches of refractory material; the inner face of high-alumina brick is backed by a layer of fire-clay brick and a layer of low-conductivity castable refractory. The refractory is separated from the steel shell by a one-inch layer of asbestos block insulation.

Eight flanged ports for measuring stack temperatures and pressures, and for obtaining gas samples are located at four levels of the stack.

Table I

Chemical Analysis of No. 6 Fuel Oil

	<u>Weight Percent</u>
Carbon	87.24
Hydrogen	11.19
Oxygen	0.69
Nitrogen	0.27
Sulfur	0.59
Ash	0.02
Volatile Matter	94.56
Fixed Carbon	5.42

Table II

Range of Variables Studied in the Test Chamber

<u>Oil Rate, lb/hr</u>	<u>Atomizing Pressure, psig</u>	<u>Excess Oxygen, %</u>
48	80, 70, 60, 40	0 to 30
58	80, 70, 60	0 to 30

Table III

Results of Representative Burner Operation with No. 6 Fuel OilTest Number 181

Oil Rate	56.4 lb/hr
Atomizing Air Rate	3.39 scfm*
Primary Oxygen Rate	15.05 scfm
Excess Oxygen	21.6%
Ungasified Carbon	17.0%

Product Gas Analysis, Mole Percent

CO ₂	5.5		
CO	43.1		
H ₂	27.7		
H ₂ O	17.2		
N ₂	6.5		
$\frac{CO_2}{CO} = 0.128$		$\frac{H_2O}{H_2} = 0.621$	
$\frac{CO_2}{CO} = 0.390$		$\frac{H_2O}{H_2} = 0.675$	
eq		eq	

Equilibrium ratios are for 2000 F

* 70 F and 1 atm

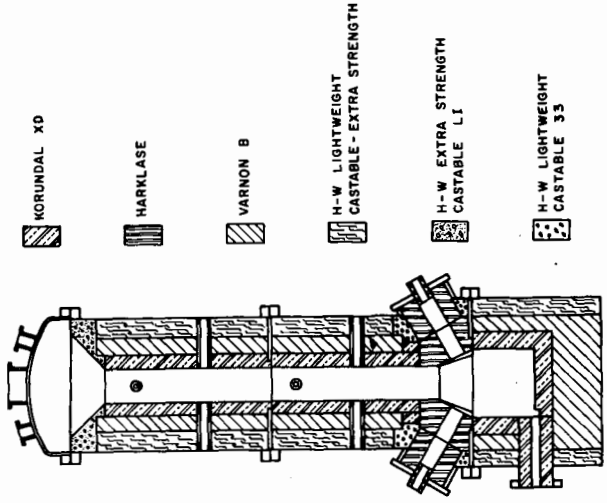


FIGURE 12 CROSS-SECTION OF FUEL-OIL OXYGEN SMELTING REACTOR

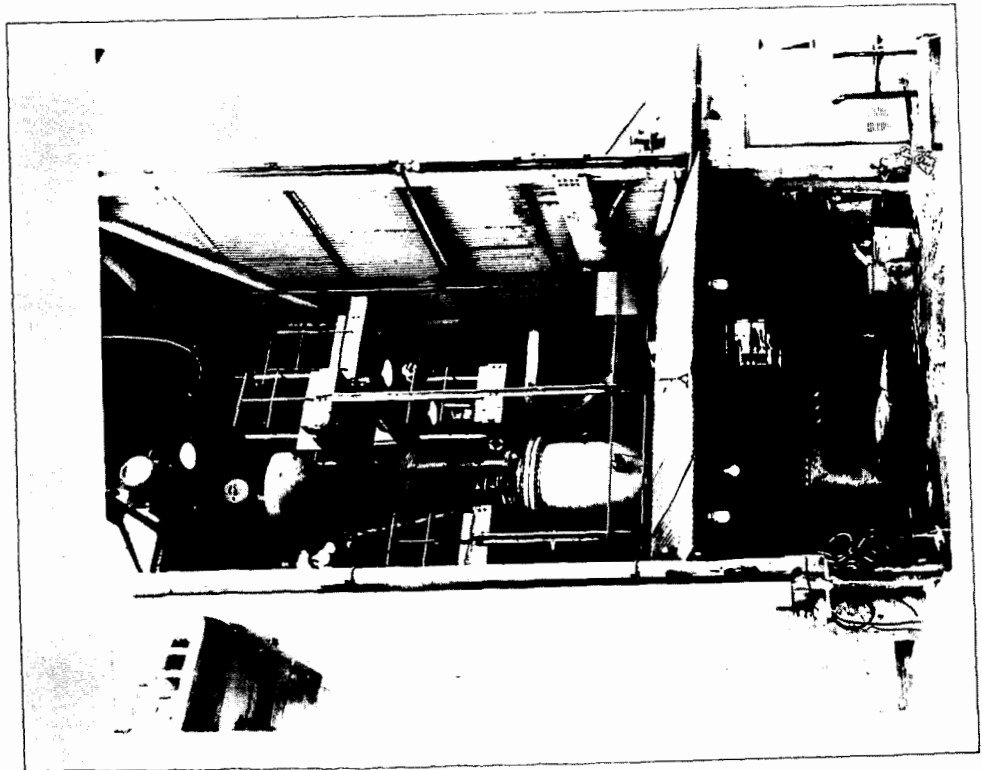


Figure 11. Picture of Pilot Plant

Partial-Combustion Studies in Pilot Plant

In the atmospheric test chamber the combustion efficiency (expressed as the percent of carbon gasified) was low; at least 15 percent excess oxygen (over the theoretical oxygen for combustion to CO and H₂) was needed for 80 percent gasification. These low conversions were caused by the low residence times and high heat losses in the test chamber. In addition, it was learned that the oil rate and the atomizing pressure had very little effect on the combustion efficiency. The percent excess oxygen and the residence time were the only variables that significantly affected combustion efficiency; gasification increased with increased excess oxygen and further distance from the burner.

A test program was run in the pilot plant to verify and extend the results obtained in the atmospheric test chamber. The ranges of the independent operating variables are listed in Table IV. Each burner test consisted of two hours of operation at the test conditions. A set of gas samples (bottom, top, and off-gas) was taken after one hour and after two hours of operation. Material balances were then calculated from the operating data and chemical analysis of the samples.

The results are plotted in Figure 13 as percent ungasified carbon versus percent excess oxygen for the special spray nozzle and for the original nozzle. The results obtained in the atmospheric test chamber are also shown for comparison. Conversions in the reactor were much better than in the test chamber because of the longer residence time and higher temperatures. Conversions for the special spray nozzle were significantly better than for the original nozzle. As in the atmospheric-test-chamber operation, there was no significant effect of the atomizing pressure or the oil rate on the burner performance.

There is considerable scatter in the data in Figure 13. This scatter is attributed primarily to poor gas mixing and distribution and to the fact that the material balances are very sensitive to small differences in nitrogen concentration. It is therefore instructive to study the results of a 24-hour test with constant-burner operating conditions. Gas samples were taken at the bottom and top of the reactor, and from the off-gas line every hour during this run. The other operating variables were recorded periodically so that an average material balance could be calculated for the day of operation. The material flows were held constant during the whole operation; there was less than 5 percent variation in any of the flows. The average operating data and results are presented in Table V. There was more ungasified carbon at the bottom of the reactor than at the top or in the off-gas. This result was expected because the studies made in the atmospheric test chamber showed that gasification increased with longer residence times. The increase in ungasified carbon between the top and the off-gas sections was unexpected and may be due to carbon deposition in this part of the system. Most of the short-duration tests in the reactor showed this same trend; there was a slightly higher amount of ungasified

Table IV

Operating Ranges for Burner Test Program

Excess Oxygen, %	- 5 to 25
Oil Rate, lb/hr	40 to 90
Atomizing Pressure, psig	40 to 70
Sampling Position	Bottom of Reactor Top of Reactor Off-Gas System

Table V

Summary of Average Operating Conditions and Results of 24-Hour Burner Test (2 Burners)

Oil Rate	73.4 lb/hr/burner
Atomizing Air Rate	6.57 scfm/burner
Primary Oxygen Rate	18.23 scfm/burner
Atomizing Pressure	70 psig
Percent Excess Oxygen	17.7

<u>Dry-Gas Analyses,</u> <u>Vol. %</u>	<u>Bottom</u>	<u>Top</u>	<u>Off-Gas</u>
CO	52.6	51.9	52.3
CO ₂	4.1	3.2	3.2
H ₂	34.6	36.4	35.8
N ₂	8.7	8.5	8.7

<u>Wet-Gas Analyses,</u> <u>Vol. %</u>	<u>Bottom</u>	<u>Top</u>	<u>Off-Gas</u>
CO	46.4	49.6	48.9
CO ₂	3.5	3.1	3.0
H ₂	30.5	34.8	33.5
H ₂ O	11.9	4.4	6.3
N ₂	7.7	8.1	8.2

Percent Ungasified C	10.0	-3.1	0.1
----------------------	------	------	-----

Nitrogen-Balance Error ~ 0.7%
(Independent Data Check)

carbon in the off-gas line than at the top of the reactor and conversions at both of these locations were much higher than at the bottom of the reactor.

These results of the burner tests run with an unfilled reactor are summarized as follows:

1. Burner rates were varied from 40 to 90 pounds of oil per hour with no significant difference in burner performance.
2. Atomizing pressures were varied from 40 to 70 psig with no significant difference in burner performance.
3. Stable burner operation was obtained from minus 10 to plus 25 percent excess oxygen.
4. The burners could be operated continuously for at least 5 days with no noticeable nozzle erosion.
5. Combustion chambers cast from high-purity magnesium oxide and burned at about 2800 F performed very well.

Burner Redesign

Several problems associated with burner design were brought into focus during the reactor-test program. First, in the original design the combustion chamber was located very close to the outside mounting flange. Heat losses were therefore unnecessarily high and the mounting flange was susceptible to high-temperature damage. In addition, removal of the burner for inspection invariably broke the combustion chamber, and this meant a complete rebuilding of the burner. And finally, the inspection and replacement of burner nozzles that plugged during operation was time consuming.

Figure 14 shows a drawing of the revised burner design. This design eliminates all the problems discussed above without sacrificing any features of the original design that are necessary for efficient combustion. The combustion chamber was relocated closer to the stack, thereby minimizing heat losses and protecting the mounting. The unitized system could be quickly removed and replaced if any trouble occurred; also, the system retained the vortex action of the primary oxygen input.

Operation of Pilot Plant as a Steel Melter

After the operation of redesigned partial-combustion burners was demonstrated to be satisfactory with a coke-filled stack, it was planned to study the operation of the system as a steel melter. Steel punchings 1 inch in diameter and 3/8-inch high and small coke were used as the burden. The pilot plant was operated successfully as a melter for four consecutive days (including one day for start-up). Table VI presents a summary of the operating conditions and results. The oil rate during

Table VI

Summary of Operating Conditions and
Results for Melting Operation

	<u>Period 1</u>	<u>Period 2</u>
Duration, hours	42	24
Oil Rate, lb/hr	100	100
Atomizing Air Flow, scfh	720	720
Atomizing Pressure, psig	~70	~70
Primary Oxygen Flow, scfh	1530	1530 (100% O ₂)
Excess Oxygen, %	~20	~20
Theoretical Flame Temperature, F	4275	4275
Burden Ratio, lb coke/lb steel	0.25	0.11
Approximate Casting Rate, lb/hr	85	160

Oil Analysis, wt %

C	87.03
H	11.09
N	0.29
O	0.95
S	0.59

Metal Analysis, wt %

	<u>Charge</u>	<u>Product</u>
Fe	98.9	~98
Si	0.13	<0.01 to 0.29
S	0.031	0.11 to 0.18
C	0.37	0.2 to 2.6

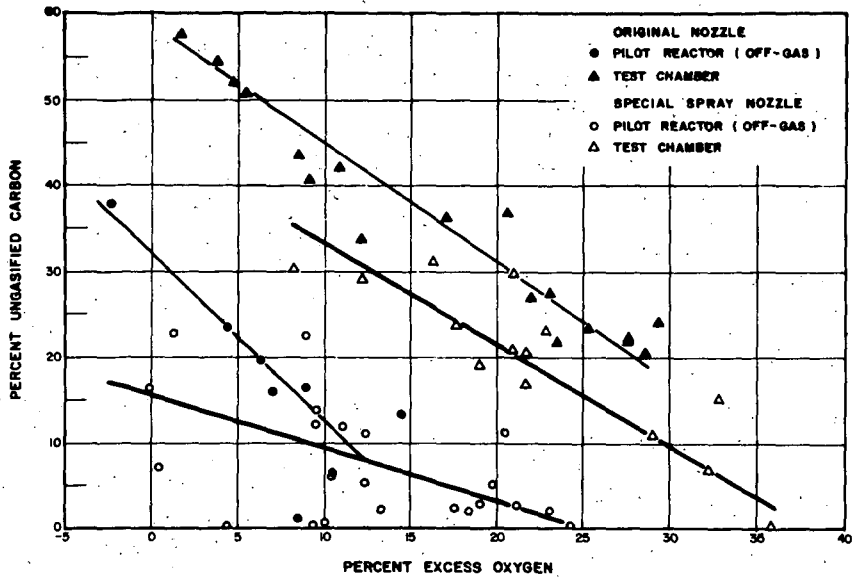


FIGURE 13 CONVERSION VERSUS EXCESS OXYGEN

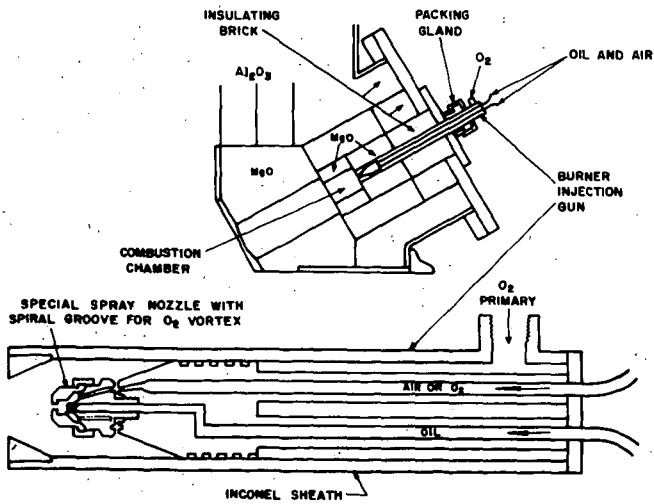


FIGURE 14 SCHEMATIC DIAGRAM OF NEW BURNER DESIGN

this operation was 100 lb/hr (for two burners); the burners were operated with about 20 percent excess oxygen, and the atomizing air pressure was 70 psig. The burden movement was smooth, and hot metal was successfully removed from the hearth during this operation. During the first day and a half of melting operation, the coke-to-steel weight ratio was 0.25 and the melting rate was 85 lb/hr. During the rest of this period, the coke-to-steel ratio was decreased to 0.11 and the melting rate was 160 lb/hr. Inspection of the system after the shutdown showed that the reactor and the burner guns were in excellent condition.

Operation of Pilot Plant as a Smelter

The pilot plant was operated as a smelter with a burden of 90 percent self-fluxing sinter and 10 percent coke. Table VII presents a summary of the steady-state operating conditions and results. About 12 hours after the first charge, small amounts of molten metal were tapped. The rate of burden movement gradually increased for the next 7 hours until it reached a steady state. For the next 13 hours operation was very good. The charging rate averaged 340 lb/hr and was very steady. Casts were made every two hours and little difficulty was encountered in getting the material to flow. Operation of the burner was very smooth. The operation ended when the burden hung at the base of the feed hopper and then slipped 1-1/2 hours later, thereby charging 500 pounds of cold material into the stack. This plugged the stack and caused a complete shutdown. Considerable damage was done to the refractory in the hearth and lower stack.

As shown in Table VII, the total carbon rate was 1300 lb/THM, of which the coke supplied about 300 lb/THM, and the fuel oil 1010 lb/THM. This low total fuel and coke ratio is very encouraging because of the small size of the pilot reactor, which inherently has relatively large heat losses. Also encouraging was the fact that burden movement was excellent in spite of the low coke ratio, and there were no indications that an even lower coke ratio would not work well.

Many serious problems were encountered during the operation of the pilot plant, primarily with the construction and performance of the refractories around the burners. There were many failures; however, it is believed that these failures can be attributed to the small size of the plant. Because the plant has a relatively high ratio of surface area to volume, heat losses were high and the burners must be operated at higher temperature (higher excess oxygen) to compensate. In a larger plant the operating conditions would not be as severe. In any event, the results indicate, at least from the standpoint of burden movement and permeability, that very high "fuel-injection" levels — approaching "cokeless" operation — can be achieved in shaft processes for smelting iron ore.

Table VII

Summary of Operating Conditions and Results
For Smelting of Self-Fluxing Sinter

A. Raw Material Analyses, Weight Percent

<u>Coke</u>		<u>Sinter</u>		<u>No. 6 Fuel Oil</u>	
C	88.26	Fe _T	60.52	C	87.36
H	1.82	O	24.50	H	10.92
N	0.96	SiO ₂	5.72	O	0.87
S	0.75	Al ₂ O ₃	1.02	Ash	0.012
O	2.55	CaO	6.93	S	0.55
Ash	5.66	MgO	0.89		
Moisture	8.53	TiO ₂	0.15		
		C	0.15		
		S	0.009		
		M _m	0.093		
		P	0.054		
		FeO	11.91		
		Fe ₂ O ₃	73.29		
		Combustion Oxygen	99.5 percent O ₂		

B. Input Data

No. 6 Fuel Oil, lb/hr	119.1
Coke, lb/hr	37.8
Sinter, lb/hr	340.0
Atomizing Air, moles/hr	1.73 (11.16 scfm)
Primary Oxygen, moles/hr	4.78 (30.82 scfm)

C. Output Data

Average Off-Gas Analysis (approximate volume %, based on 3 samples), Dry Basis

CO	49.0
CO ₂	12.7
H ₂	28.25
N ₂	9.9

Material Balance - Based on N₂

Dry Volume	14.0 moles/hr
H ₂ O	2.96 moles/hr
Total soot plus dissolved carbon	2.6 moles/hr

Table VII

(continued)

Summary of Operating Conditions and Results
For Smelting of Self-Fluxing Sinter

Independent Oxygen Balance

Input	=	Output
7.83 moles/hr	=	6.69 moles/hr

D. General Data*

Solid Carbon Consumption, lb/hr	30.5
Solid Carbon Ratio, lb/THM	~298
Total Carbon Consumption, lb/hr	134.5
Total Carbon Ratio, lb/THM	~1312
Metal Rate, lb/hr	~205

*Metal rate based on input

References

1. Masdin, E. G., and Thring, M. W., "Combustion of Single Droplets of Liquid Fuel," Journal of the Institute of Fuel, Vol. 35, No. 257, p 251, June 1902.
2. Thring, M. W., The Science of Flames and Furnaces, pp. 198, 199, 256, John Wiley and Sons, Inc., Second Edition, 1906.
3. Masdin, E. G., and Thring, M.W., *ibid*, pp. 254, 255.

"THE REACTION OF COKE WITH CARBON DIOXIDE"

H. C. Hottel, G. C. Williams and P.C. Wu

Chemical Engineering Department
Massachusetts Institute of Technology
Cambridge, Massachusetts 02139

Earlier studies of the kinetics of the CO_2 -C reaction have generally been deficient for one or both of two reasons: either the data were based on imprecise methods of determining the extent of reaction (e.g., product gas analysis, reactant weight decrease, pressure variation) or the data did not yield information concerning local- or point-reaction rates, which are the kind of data required for formulating kinetic mechanisms. Most commonly the data were on reaction in a tube of finite length, packed with carbon.

The present studies were of mono-layers of carbon particles resting on a screen up through which the reactant gas mixtures were passed, the system being maintained isothermal. Details of the apparatus and experimental techniques are given by Wu (1). The reactant gases were CO_2 , CO_2 - N_2 mixtures, and CO_2 - CO mixtures. Before each run the system was evacuated, following which reactant gas was passed through for 10 to 15 minutes. Because of the high reactivities of H_2O and O_2 relative to CO_2 the gas mixture was dried by passage through a bed of Drierite and then stripped of trace oxygen by contact with reduced copper turnings at 415°C . After the furnace had reached the desired temperature level the screen with the carbon particles was introduced by a magnetically operated slide mechanism the smooth operation of which prevented disturbance of the carbon bed. After a specified time the carbon bed was quickly removed, cooled and weighed. The decrease in weight of the carbon and the time of reaction were used to determine the specific reaction rate for each run.

The solid reactant used was from the same lot used by Gilliland et al (2) and by Graham (3) in fluidized beds. The effect of particle size from 80-100 mesh to 10 mm diameter was determined in the present studies. The coke contained 9.5 weight per cent ash and a small percentage of V.C.M. Reaction rates, R , mg c/g.c. min., are expressed on an ash-free basis and corrected for loss of V.C.M. as a function of reaction time, temperature and particle size on the basis of experiments made in pure N_2 . The maximum weight loss correction for V.C.M. amounted to 1.5% of the initial weight of the particles.

The various reaction rate terms used are defined as follows:

(1) The instantaneous specific reaction rate R_i is defined as the rate of decrease in weight of carbon based on unit weight W of carbon at the fractional residual carbon $W/W_0 = F$:

$$R_i = \frac{-dW}{W d\theta} = \frac{-d \ln W}{d\theta} = \frac{-d \ln (1-F)}{d\theta} \quad (1)$$

(2) The initial specific reaction rate R_0 is defined as the rate of decrease in weight of carbon based on unit weight of carbon at $F=0$:

$$R_0 \equiv - \left(\frac{dW}{W d\theta} \right)_{F=0} \equiv - \left(\frac{d \ln (1-F)}{d\theta} \right)_{F=0} \equiv \left(\frac{dF}{d\theta} \right)_{F=0} \quad (2)$$

(3) The average specific reaction rate R_{av} is defined as the time mean of the instantaneous specific reaction rate R_i from $F=0$ to $F=F$:

$$R_{av} \equiv \frac{\int_0^{\theta} R_i d\theta}{\theta} \equiv \frac{\int_0^{\theta} \frac{-dW}{W} d\theta}{\theta} \equiv \frac{W_0 - \frac{dW}{W} - \ln(1-F)}{\theta} \equiv \frac{-\ln(1-F)}{\theta} \quad (3)$$

The experimental results, all obtained at a total pressure of 780 mmHg, can be classified into the following two groups:

1. Experiments using New England coke particles of 50-60 mesh.

The gas flow rate, except in the velocity runs, was maintained constant.

(a) N_2 blank runs: Typical results are listed in Table 1, as fractional decrease in weight of the sample, F_{N_2} , calculated from the data on an ash-free basis at different temperatures.

(b) CO_2-N_2 runs: Five temperatures (1500, 1600, 1700, 1800 and 1900°F) were investigated. The time of reaction was adjusted for each run to give approximately 10% reaction. In Figure 1 the values of the average specific reaction rate R_{av} are plotted vs the partial pressure of CO_2 on semi-logarithmic coordinates. For each pair of curves the upper one shows R_{av} calculated on an ash-free basis, and the lower one shows that calculated on an ash-free basis, after being corrected for V.C.M. based on the N_2 blank runs.

(c) CO_2-CO runs: These data are shown in Figure 2.

(d) Velocity runs: The temperatures investigated were the same as in the CO_2-N_2 runs. Since the gas flows were in the laminar region a linear plot of R versus the reciprocal of the gas flow rate gave straight lines which could be extrapolated on a straight line through the data points to the origin, corresponding to the reaction rate in pure CO_2 , uncontaminated by the CO produced.

TABLE 1

Evolution of VCM as a function of time and temp. in N_2 50-60 mesh particles.

TEMP. °F	1500		1600		1700		1800		1900		
$F_{N_2} \times 10^3$	8.8	7.9	10.3	8.1	15	11.6	19	14.5	11	9	6.7
θ , min	610	463	240	100	120	60	90	60	30	15	10

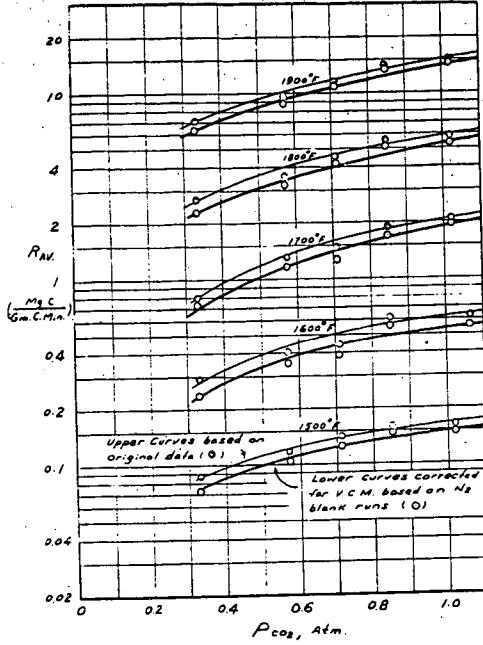


Figure 1. Effect of Partial Pressure of CO_2 and Temperature on Reaction Rate of 50-60 Mesh Coke Particles. Total Pressure 1.026 atm; H_2 as Diluent.

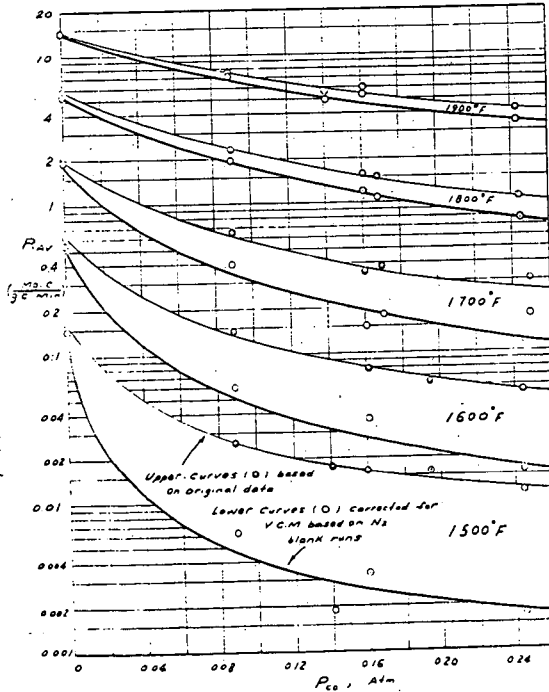


Figure 2. P_{AV} vs. P_{CO} For CO_2-CO Runs (New England Coke, 50-60 Mesh)

2. Experiments using New England coke particles of different sizes, reacting with pure carbon dioxide at 1800°F.

(a) N₂ blank runs: The fractional gasification in N₂ for the 8-12 mesh particles at any given time was about 60 per cent of that for the 50-60 mesh data shown in Table 1 and that for the 80-100 mesh particles was about 50 per cent greater. The effect of further increase in particle size up to nearly 10 mm diameter was a very small, less than 10 per cent decrease in gasification below that for the 8-10 mesh particles.

(b) Time runs: Reaction runs were made with samples of particle sizes between 8-100 mesh. Six different particle sizes were used, namely, 8-12, 16-20, 30-40, 50-60, 70-80, and 80-100 mesh. Each sample weighed about 0.1 gram. The values of R_{av} calculated from the corrected data are plotted vs θ in Figure 3 together with lines of constant F.

Effect of Particle Size

DISCUSSION OF RESULTS

From slopes of the curves of R_{av} vs θ in Figure 3 values of R_i were calculated and extrapolation of these to $F=0$ gave R_0 . Values of R_0 and the maxima of R_i are shown as a function of initial particle diameter in Figure 4.

From Figure 3 it is clear that the reaction rate is influenced not only by the fractional decrease in weight of carbon, F, but also by the diameter of the coke particle, D.

For all sizes investigated, R_i initially increased, reached a maximum, and then declined with further reaction. There was a pronounced trend for the maximum to occur at larger F values when smaller particles were used.

The shift of $R_{i(max)}$ to larger values of F with decrease in particle size can be explained as being due to the presence in the coke of ash, which amounts to 9.5%. In the case of the large particles, only a relatively small fraction of the weight of the particle has to be reacted to form a substantial layer of ash on the surface. The ash coating then makes the carbon less accessible to the reacting gas, and the reaction rate falls off. However, in the case of the small particles, a large fraction of the weight of the particle must be burned away to produce the substantial ash layer that retards further reaction.

The effect of initial particle size on the specific reaction rate as shown in Figure 3 may be explained as follows: (1) In the larger size range, 2-10 mm, the reaction occurs in a thin porous coke layer dependent in thickness on the ratio of the rate of diffusion of CO₂ into the particle to the rate of reaction on the surfaces of the pores but independent of particle diameters, thus the rate is proportional to the superficial surface area of the particles - a slope of minus unity in Figure 3. (2) As the particle size is further reduced, 1.5 to 0.5 mm, the thickness of the

diffusion-reaction zone becomes comparable with the particle radius and all of the particle volume becomes active, specific reaction rate becomes nearly independent of particle size. (3) With further decrease in particle size it is possible that the average depth of the pores in which reaction occurs is also reduced thus accounting for the increase in specific reaction rate as the particle size is reduced from 0.5 to 0.17 mm. It should also be noted that the initial apparent density of the coke particles (1.0 g/cc for massive particles) increased from 2.0 g/cc to 2.8 g/cc as the particle size was reduced in this size range, probably due to a loss of ash in the grinding and sieving process. This could also be advanced as an explanation for the increase in specific reaction rate as size decreases in this size range.

Effect of Fractional Reaction

In other experiments (1) with ash-free electrode carbon gasified in CO₂ it was found that, presumably because of an increase in surface area with progress of reaction, the instantaneous specific reaction rate was a linear function of the weight fraction gasified:

$$R_i = R_o \left(1 + \frac{m}{R_o} F\right), \text{ where } m/R_o \text{ was } 14 \text{ for } 50\text{-}60 \text{ mesh particles.}$$

In the present experiments the effect of the ash as shown in Figure 3 is apparently to accumulate to such an extent that the increase in surface area due to reaction is finally offset by the accumulation of ash.

The present data on coke can be correlated by the empirical expression

$$R_i = R_o \left(1 + \frac{m}{R_o} F\right) e^{-5.5DF^{1.85}}$$

in which the exponential represents the retarding effect of the ash and m is a function of initial particle diameter

$$m = \frac{10(2 + \log_{10} D)}{R_o}, \quad D \text{ in mm}$$

It is interesting to note that m for 50-60 mesh from this equation for coke is 13 vs the 14 reported for electrode carbon. The studies of Goring (4), Oshima and Fukuda (5) and of Duffy and Leinroth(17) show similar results on high-ash cokes.

Kinetics

1. Langmuir-Hinshelwood derivation

Hinshelwood et al (16) presented the following derivation as representative of the simplest application of the early ideas of Langmuir (6) on the effect of surface adsorption on heterogeneous reactions. Note that Langmuir himself did not present the following derivation, and in fact stated in 1915 (7) that he did not believe

carbon dioxide was adsorbed in the reaction of carbon with carbon dioxide. He gave instead the first step of the mechanism of Semechkova and Frank-Kamenetzky.

Hinshelwood et al made the assumption that both the reactant, CO_2 , and the retarding product, CO , are adsorbed as such on the carbon surface, and that the rate of reaction is proportional to the fraction, s , of the surface covered by the reactant. The mechanism can then be expressed by the following equations:



in which equations, (...) represents gas in the adsorbed state.

The surface consists of equivalent and independent reaction sites, each of which can be occupied by one CO_2 or one CO molecule. When a steady state on the surface is attained, the rate of reaction per unit surface is then given by:

$$\text{Rate} = k_5 s_1 = \frac{k_5 k_1}{k_2 + k_5} P_{\text{CO}_2} \quad (7)$$

$$1 + \frac{k_3}{k_4} P_{\text{CO}} + \frac{k_1}{k_2 + k_5} P_{\text{CO}_2}$$

2. Derivation of Semechkova and Frank-Kamenetzky (8)

The assumptions made are that carbon dioxide is not adsorbed as such, but reacts with the carbon to give an atom of oxygen which remains on the surface, and a molecule of carbon monoxide which passes into the gas phase. The adsorbed oxygen atom, taking up an atom of carbon from the surface forms gaseous carbon monoxide at a steady rate. Carbon monoxide present in the gas phase is always in equilibrium with carbon monoxide in the adsorbed state on the surface (this is the sole part of the reaction scheme which is identical with the previous derivation). There is a distinction between the adsorbed oxygen and the adsorbed carbon monoxide. The following equations express the mechanism:



in which CO^* represents an O atom adsorbed on carbon, and (CO) represents CO in the adsorbed state.

When a steady state on the surface is attained, the rate is found to be:

$$\text{Rate} = k_7 s_3 = \frac{k_6 P_{\text{CO}_2}}{1 + \frac{k_3}{k_4} P_{\text{CO}} + \frac{k_6}{k_7} P_{\text{CO}_2}} \quad (11)$$

It is seen that also this expression is of the same form as equation (7).

3. Modified Semechkova and Frank-Kamenetzky Derivation (1)

In this derivation the assumption is also made that carbon dioxide is not adsorbed as such, but reacts with the carbon to form a gaseous carbon monoxide molecule, and an adsorbed oxygen atom, which is next transformed at a steady rate, not to gaseous CO, but to (CO) , the adsorbed CO, the concentration of which on the surface is in equilibrium with the CO in the gas phase.

The following equations represent this mechanism:



At steady surface state the following relations hold:

$$\text{Rate} = k_8 s_3 = \frac{k_6 P_{\text{CO}_2}}{1 + \frac{k_3}{k_4} P_{\text{CO}} + k_6 \left(\frac{1}{k_8} + \frac{1}{k_4} \right) P_{\text{CO}_2}} \quad (15)$$

which equation is seen to be of the same form as (7) and (11) and of the general type

$$R = \frac{K_1 P_{\text{CO}_2}}{1 + K_2 P_{\text{CO}} + K_3 P_{\text{CO}_2}} \quad (16)$$

The applicability of the Langmuir type equation can be tested, and the constants involved evaluated by application to the data obtained in both $\text{CO}_2\text{-N}_2$ and $\text{CO}_2\text{-CO}$ runs shown in Figs. 1 and 2. It is evident that where the surface is completely characterized by F, as shown before, the instantaneous specific reaction rate at any F could be used for this evaluation. However, R_0 was chosen as a reference value for testing the validity of the proposed Langmuir equation. The procedure used was as follows:

In the case of the CO₂-N₂ runs, the term K₂ P_{CO} is 0, if the effect of the CO generated during the reaction can be neglected. The equation can hence be reduced and rearranged to:

$$\frac{P_{CO_2}}{R_O} = \frac{K_3}{K_1} P_{CO_2} + \frac{1}{K_1} \quad (17)$$

If the proposed equation fits the data, then for a specific reaction temperature when P_{CO₂}/R_O is plotted vs P_{CO₂} on linear coordinates a straight line with slope K₃/K₁ and intercept 1/K₁ should result, from which values of K₁ and K₃ can be evaluated. The data for 1900°F are shown in Figure 5; the intercept gives K₁ = 28.6 and the slope gives K₂ = 0.56.

When the equation is applied to the CO₂ - CO runs, rearrangement of the equation to a more convenient form is possible by substituting P_{CO₂} + P_{CO} = π, where π is the total pressure on the reaction system. The rearranged equation then becomes

$$\frac{P_{CO_2}}{R_O} = \frac{K_2 - K_3}{K_1} P_{CO} + \frac{1 + K_3 \pi}{K_1} \quad (18)$$

For a specific reaction temperature when P_{CO₂}/R_O is plotted vs P_{CO} on linear coordinates, a straight line with slope K₂-K₃/K₁ and intercept 1+K₃π/K₁ should be obtained. With the aid of the values for K₁ and K₃ calculated from the results of the CO₂-N₂ runs at the same temperature, K₂ can then be evaluated from the slope of this line. Figure 6 shows the 1900°F data, the slope is 0.6 from which K₂ = 18.

The data for the other temperatures were similarly treated and over the range of variables investigated, R_O for 50-60 mesh particles could be represented by a Langmuir type equation of the following form:

$$R_O = \frac{K_1 P_{CO_2}}{1 + K_2 P_{CO} + K_3 P_{CO_2}}$$

The values of K₁, K₂ and K₃ are listed in Table 2 and shown on logarithmic-reciprocal temperature coordinates in Fig. 6.

TABLE 2
Langmuir Equation Constants

(50-60 mesh)

Constants	Reaction Temperature, °F				
	1500	1600	1700	1800	1900
K ₁ (mg.C./gm.C.min.atm)	0.23	0.9	3.18	10.2	28.5
K ₂ (atm ⁻¹)	423	178	78	36	18.
K ₃ (atm ⁻¹)	0.5	0.45	0.39	0.35	0.56

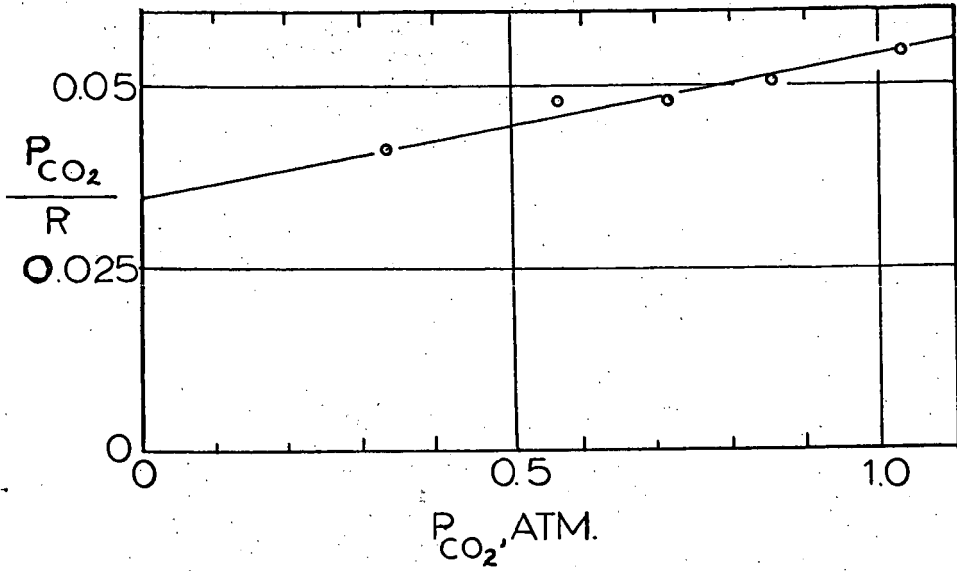


Figure 5. Test of Langmuir Isotherm
1900 F., 50-60 Mesh

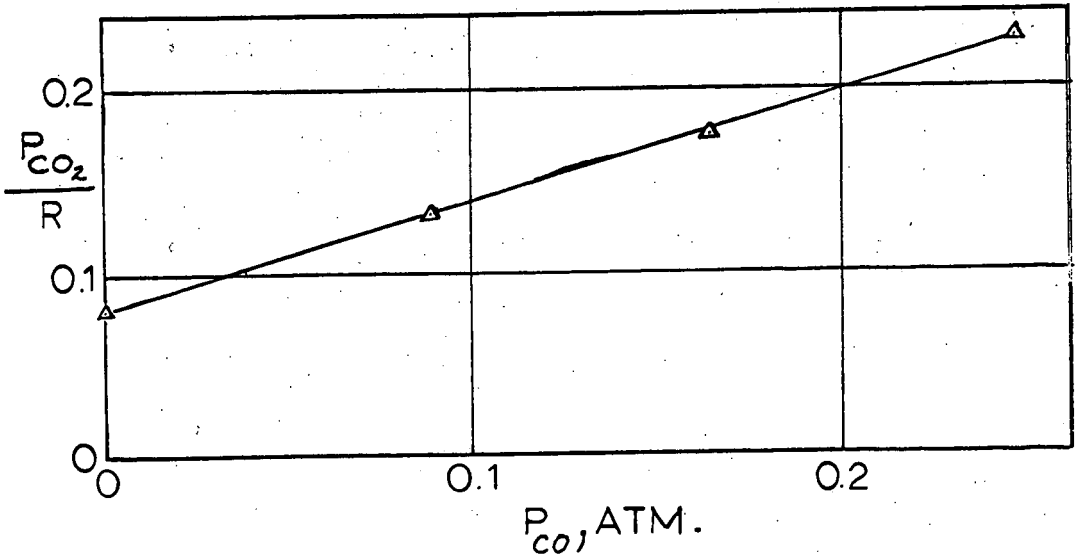


Figure 6. Test of Langmuir Isotherm
1900 F., 50-60 Mesh

From the straight line shown on Fig. 6 the values of K_0 and E were calculated for each constant and are listed in Table 3 :

TABLE 3

Values of E and K_0 in $K = K_0 e^{-E/RT}$

(50-60 mesh)

E_1 111,000 (Btu/lb mole)	K_{10} 5.2×10^{11} (mg C/gm C min atm)
E_2 - 72,500 "	K_{20} 3.6×10^{-6} (atm ⁻¹)
E_3 - 11,000 "	K_{30} 3×10^{-2} (atm ⁻¹)

It is to be noted that, if the equation describes a rate affected by surface adsorption of CO and CO₂, i.e., if the Langmuir-Hinshelwood derivation is substantially correct, then the signs of the three E's are as expected. E_2 and E_3 are associated with adsorption phenomena which should become less important as the temperature rises, whereas E_1 ($= E_2 + E_3$) is the primary measure of effect of temperature on reaction rate.

4. The Temkin adsorption isotherm

A major theoretical deficiency of the Langmuir adsorption isotherm is the implicit assumption of uniform heat of chemisorption and hence of surface activity. For most real surfaces the heat of adsorption changes with the degree of occupation of the surface (9), (10), (11) and (12). A linear decrease in heat of adsorption with fractional surface coverage leads to an isotherm for which the fractional surface coverage is proportional to the logarithm of the pressure of the adsorbing gas. This isotherm has been named after Temkin (13) although the concept appears in the works of earlier Russians (14), (15)

If the heat of adsorption, q , falls linearly with the fraction of surface occupation, S ,

$$q = q_0 (1 - \beta S)$$

the isotherm is given by

$$S = \frac{RT}{q_0 \beta} \ln A_0 P \quad (19)$$

where, β = a constant

q_0 = a constant

$A_0 = a_0 e^{q_0/RT}$

a_0 = constant

If it is assumed that chemisorption of CO₂ is fast compared with subsequent surface reactions and that the rate of surface reaction is directly proportional to the fraction of the surface covered then

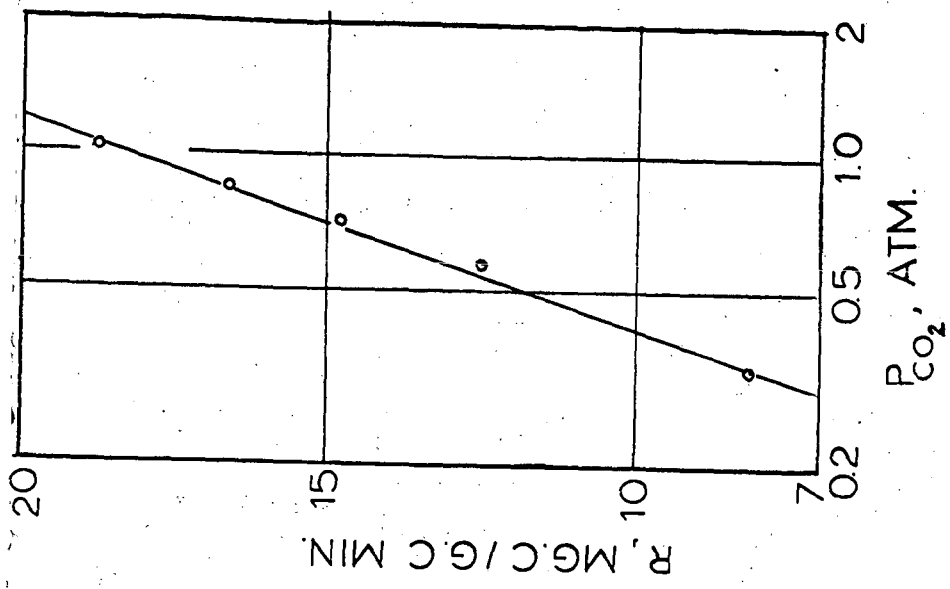


Figure 8. Test of Temkin Isotherm, 1900 F.

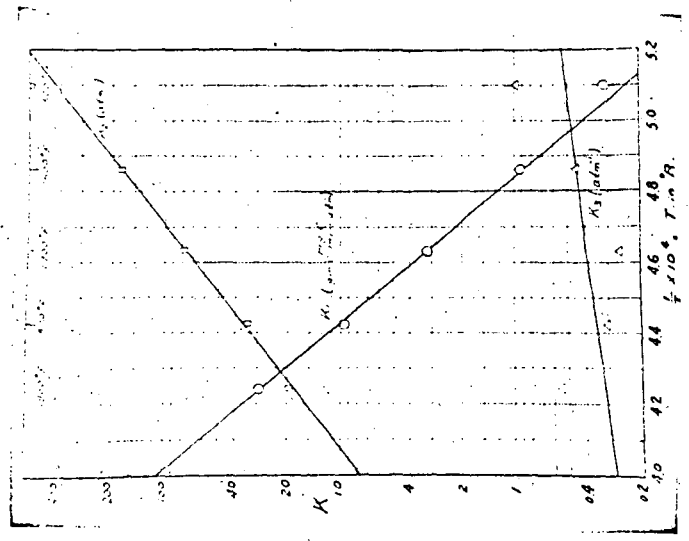


Figure 7. Arrhenius Plot of Reaction Rate Constants, 50-60 Mesh Coke.

$$R_o = \frac{k e^{-E/RT}}{\beta q_o} RT \ln A_o + \frac{k e^{-E/RT}}{\beta q_o} RT \ln P_{CO_2} \quad (20)$$

$$R_o = a(T) + b(T) \ln P_{CO_2} \quad (21)$$

Thus a plot of reaction rate versus logarithm of the pressure should be linear. Fig. 7 shows the data for 50-60 mesh particles in pure CO₂ at 1900°F. The data for other temperatures are correlated equally well.

From Eqs. 19, 20 and 21

$$\frac{a}{b} = \ln a_o + \frac{q_o}{RT} \quad (22)$$

Thus a plot of a/b versus $1/T$ should give a straight line with slope q_o/R . The present data give a value of heat of adsorption of CO₂ of 2400 Btu/lb mole and an intercept $\ln a_o = 1.4$ at $1/T = 0$.

Since q_o probably does not vary greatly with temperature b/T should be exponential in $1/T$. This was found to be so, giving a value $b/T = 81 \times e^{-45,600/RT}$.

No attempt has been made to treat the CO₂-CO mixture data using the logarithmic adsorption isotherm.

ACKNOWLEDGEMENT

This work was supported by funds from Bituminous Coal Research, Inc.

LITERATURE CITATIONS

1. Wu, P. C. "The Kinetics of the Reaction of Carbon with Carbon Dioxide" Sc. D. Thesis, Chem. Eng., MIT (1949).
2. Gilliland, E. R., Lewis, W. K., McBride, G. T., Ind. Eng. Chem., 41, 1213 (1949).
3. Graham, H. S., "Gasification of Carbon by Steam and Carbon Dioxide in a Fluidized Powder Bed", Sc.D. Thesis, Chem. Eng., MIT (1947).
4. Goring, G. E., "Effect of Pressure on the Rate of CO₂ Reduction by High Temperature Coke in a Fluidized Bed", Sc.D. Thesis, Chem. Eng., MIT (1949).
5. Oshima, Y., and Fukuda, Y., Fuel in Sc. and Pract. Vol. XI, 4, 135 (1932).
6. Langmuir, I., J. Am. Chem. Soc., 38, 2221 (1916).
7. Langmuir, I., J. Am. Chem. Soc., 37, 1154-1156 (1915).

8. Semchikova, A. F. and Frank-Kamenetzky, D. A., *Acta Physicochim.*, U.S.S.R., 12, 879 (1940).
9. deBoer, H. J., "Advances in Catalysis", Academic Press, Vol. VIII, 139 (1956).
10. *ibid* Vol. IX, 472 (1957).
11. Redmond, J. P. and Walker Jr., P. L., *J. Phys. Chem.*, 64, 1093 (1960).
12. Trapnol, B.M.W., "Chemisorption", Academic Press, 104, 124 (1955).
13. Temkin, M. and Pyzhev, J., *Acta Physicochim. U.S.S.R.*, 12, 327 (1940).
14. Frumkin, A. and Slygin, A., *Acta Physicochim.*, U.S.S.R., 3, 791, (1935).
15. Zeldowitsch, J., *Acta Physicochim.*, U.S.S.R., 1, 961 (1934).
16. Hinshelwood, C. N., Gadsby, J., and Sykes, K. W., *Proc. Roy. Soc.*, No. 1009, Vol. 187, 129-151 (1946).
17. Leinroth, Jr., J. P. and Duffy, Jr., B. J., "The Rate of Gasification of Anthracite Coke by Carbon Dioxide in a Fluidized Bed", S. M. Thesis, Chem. Eng., MIT (1947).

Reduction of Incendivity of Hot Gases to Methane and Coal Dust

J. M. Singer,^{1/} N. E. Hanna,^{2/} R. W. Van Dolah,^{3/} and J. Grumer^{4/}

Bureau of Mines, Pittsburgh, Pennsylvania

ABSTRACT

Hot gases produced by explosives are known to constitute a possible ignition hazard in coal mines. Experiments in the large test gallery of the Bureau of Mines have established that sodium chloride reduces the incendivity of explosives. In the present investigation the effect of sodium nitrate was explored. This study was conducted in two phases. Gallery experiments showed that sodium nitrate reduced the incendivity of certain explosives to 8 percent natural gas in air, but increased their incendivity to coal dust predispersed in air. Laboratory experiments using hot jets from explosions of stoichiometric mixtures of methane-oxygen-nitrogen showed that both sodium chloride and sodium nitrate reduced the incendivity to methane, to mixtures of coal dust and methane, and to coal dust. The difference between the gallery and laboratory results with respect to coal dust is attributed to temperature-time effects. In the gallery experiments, the sodium nitrate probably forms sodium oxide which affects the incendivity of the hot gases. In the hot jet case, it is possible that the nitrate is not as completely decomposed and has a different effect on incendivity.

INTRODUCTION

The hot gases produced by explosives constitute a possible ignition hazard in coal mines. Components of explosives known to affect incendivity of explosives are sodium nitrate and sodium chloride. Large scale gallery experiments with sodium chloride had confirmed that it reduces the incendivity of explosives,^{5/} but the effect of sodium nitrate had not been systematically explored. As sodium nitrate is an oxidant, it was conceivable that it might increase the incendivity of explosives to methane or coal dust dispersed in air. On the other hand it might have an inhibiting action similar to that of sodium chloride. The present study sought to determine whether sodium nitrate inhibits or promotes the ignition of mixtures of methane, coal dust, or both with air.

In one phase of this study, an investigation was conducted in a gallery 6-1/3 feet in diameter, with a 20 foot long section filled with 8 percent natural gas or coal dust predispersed in air. Concentrations of coal dust in air were about 300 mg/liter. This and the 8 percent natural gas concentration in air are both much higher than the lean flammability limit of the respective fuel. Explosives containing natural and synthetic sodium nitrate were fired in the gallery and their incendivity

-
- ^{1/} Research chemist, Explosives Research Center, Bureau of Mines, Pittsburgh, Pa.
 - ^{2/} Research chemist, Health and Safety Research and Testing Center, Bureau of Mines, Bruceton, Pa.
 - ^{3/} Research director, Explosives Research Center, Bureau of Mines, Pittsburgh, Pa.
 - ^{4/} Project coordinator, Flame Dynamics, Explosives Research Center, Bureau of Mines, Pittsburgh, Pa.
 - ^{5/} Hanna, N. E., G. H. Damon, and R. W. Van Dolah. Probability Studies on the Incendivity of Permissible Explosives Effect of Small Percentages of Sodium Chloride, BuMines Rept. of Inv. 5463, 1959, 22 pp.

was determined by the Bureau's standard up-and-down method.^{6/} Sodium nitrate reduced the incendivity to methane but increased the incendivity to coal dust. Another phase of the study sought to model gallery conditions through small scale laboratory experiments in which the ignition sources were small pulsed hot gas jets produced by explosions of stoichiometric mixtures of methane-oxygen or such mixtures diluted with nitrogen. These small jets were "salted" or not, so that the relative promoting or inhibiting effect could be determined. The fuel-air mixtures exposed to these jets when not salted were fuel-lean mixtures of methane plus coal dust (hybrid mixtures) or coal dust. Concentrations of coal dust and methane in the hybrid air mixtures were generally below concentrations at their lean flammability limits. The oxygen index [oxygen/(oxygen + nitrogen)] of the ignition source was the index of incendivity. It was used to vary the temperature of the hot jet which increased as the oxygen index was increased. Temperatures of these jets are noted in table 1 along with other characteristics. The ability of the technique to detect changes in incendivity was confirmed by experiments with sodium chloride. Sodium nitrate was found to reduce the incendivity of the hot gases with respect to all three of the fuel systems. This experimental technique should make it possible to survey a large number of ignition inhibitors to select the materials which are most effective in reducing the ignition hazard of hot gases from detonating charges in coal mines.

ACKNOWLEDGEMENT

The authors wish to thank Bituminous Coal Research, Inc., Monroeville, Pa. for furnishing the ultrafine grind of coal dust.

EXPERIMENTAL EQUIPMENT AND PROCEDURE

Gallery Experiments

Equipment used in these experiments were the same as those used to evaluate the permissibility of explosives according to schedule 1-H.^{7/} The first experiment had a 2 x 3 factorial design and was conducted by firing from a stemmed cannon into 8 percent natural gas-air mixtures (gallery test 7).^{7/} Its purpose was to compare the six explosive formulations in table 2, which are based on the composition of two different permissible explosives (A and B). The samples based on composition A contained about 4 percent sodium nitrate; those based on composition B contained 10 percent sodium nitrate. Both synthetic (99.5% pure) and natural (98.5% pure) sodium nitrate was used, with the natural in two ranges of particle size. The average particle diameter of the coarse natural, ground natural, and synthetic sodium nitrate was 1,170, 317, and 437 microns, respectively. Each of the six explosives was carried through the up-and-down sequence, varying the weight of explosive to obtain W₅₀ values.^{8/} Ten pairs of ignition-nonignition results were obtained in each up-and-down sequence.

The second experiment was also given a 2 x 3 factorial design to compare the incendivity of the same explosives to coal dust (300 mg/liter) predispersed in air. The coal dust was of Pittsburgh Seam coal; its average particle diameter was 80 microns and the proximate analysis was 2.0 percent moisture, 34.9 percent volatile, 55.4 percent fixed carbon, and 7.6 percent ash. In this experiment, 5.5 kilos of

^{6/} Hanna, N. E., P. A. Richardson, and R. W. Van Dolah. An Improved Method for Evaluating the Incendivity of Explosives to Coal Dust: A Preliminary Report. Restricted International Conference of Directors of Safety in Mines Research, Sheffield, England, 1965, Paper No. 12.

^{7/} Federal Register, March 1, 1961, v. 26, No. 39. Title 30 - Mineral Resources, Schedule 1-H, p. 1761.

^{8/} W₅₀ is weight of explosive producing 50 percent probability of igniting a natural gas-air atmosphere; W₅₀ values increase as incendivity decreases.

Table 1. - Characteristics of hot turbulent gas jets. (ignition sources)

Oxygen index <u>1</u> /	Adiabatic flame temperature, ° K	Observed <u>2</u> / maximum temperature, ° K	Jet velocity, <u>3</u> / m/sec	Length <u>3</u> / of jet, cm
1.0	3050	2740	137	12.8
.75	2975	2650	98	9.0
.50	2813	2480	59	6.4
.35	2620	2270	36	5.4
.30	2510	2510	28	5.0
.26	2400	2020	22	4.7
.21	2200	1820	16	4.3

1/ O₂/(O₂ + N₂) of stoichiometric mixture containing methane.

2/ Experimental values determined by the sodium D line reversal technique.

3/ Velocity of advance of head of jet from orifice. Velocity was constant between time zero and growth of jet to maximum length (point of sharp decrease in luminosity and start of break-up of jet).

Table 2. - Incendivity of products from explosives containing sodium nitrate and sodium chloride

	A formulations				B formulations			
Chemical analysis:								
Moisture	0.3	0.2	0.2	0.4	0.3	0.4	0.3	0.4
Nitroglycerine	8.8	8.7	8.8	10.6	10.7	10.5	10.7	10.5
Nitrocellulose	.3	.3	.3	.3	.3	.2	.3	.2
Ammonium nitrate	68.3	67.6	68.1	57.6	57.1	56.9	57.1	56.9
Sodium nitrate	1/ 3.8	2/3.9	3/3.8	1/10.3	2/9.3	3/9.9	2/9.3	3/9.9
Sodium chloride	9.2	9.5	9.1	10.4	10.1	9.8	10.1	9.8
Antacid	.4	.3	.5	.3	.5	.5	.5	.5
C.C.M. ^{4/}	8.9	9.8	9.2	10.1	11.6	11.8	11.6	11.8
Physical properties:								
Apparent specific gravity	1.06	1.05	1.05	0.84	0.82	0.81	0.82	0.81
Grams wrapper per 100 g explosive	7.3	7.7	7.3	8.2	8.5	8.5	8.5	8.5
Ballistic mortar, percent strength of TNT	96	97	96	89	89	90	89	90
Rates of detonation, meters per second	2470	2360	2480	2630	2570	2580	2570	2580
Oxygen Balance, grams oxygen per 100g explosive	-11.6	-13.3	-12.5	-15.5	-18.1	-19.1	-18.1	-19.1
Incendivity, Gallery Results:								
W50, grams ^{5/}	615	600	590	670	650	670	650	670
WCD, grams ^{6/}	300	290	490	80	90	90	90	90

1/ Coarse natural nitrate, average particle size 1171 microns.

2/ Fine synthetic nitrate, average particle size 437 microns.

3/ Ground natural nitrate, average particle size 317 microns.

4/ Carbonaceous combustible material.

5/ Weight for 50 percent probability of ignition in 8 percent natural gas-air; stemmed cannon shots.

6/ Weight for 50 percent probability of ignition in predispersed coal dust (300 mg/liter) - air; suspended shots.

coal dust was dispersed in the first section of the gallery 1/2 second before firing an explosive charge suspended in the center of this section which was isolated from the rest of the gallery by a paper diaphragm. The coal dust was spread evenly over a length of 30-grain per foot detonating cord laid in a 20-foot long steel Vee trough made from 6-inch by 6-inch angle and mounted 7 inches above the gallery floor; the detonation of the cord disperses the dust. With this test arrangement, $W_{CD}^{9/}$ were determined, again using up-and-down technique.

LABORATORY EXPERIMENTS

The effect of sodium nitrate on incendivity of hot gas jets was investigated using mixtures in air of methane, coal dust, or hybrid mixtures of the two as the acceptor charge. The coal dust was an ultrafine grind (83.5 percent less than 17 microns) of Pittsburgh Seam, Mathies mine coal. The elemental composition in percent by weight was: $H_2 = 5.3$, $C = 78.9$, $O_2 = 8.0$, $N_2 = 1.6$, $S = 1.3$, and ash = 4.9. The proximate analysis in percent by weight was: Moisture, 0.7; volatile matter, 37.0; fixed carbon, 57.5; and ash, 4.8. All gases were obtained in cylinders and were chemically pure grade except for air. Sodium chloride and sodium nitrate of chemically pure grade were ground to minus 20 micron particle size.

The hot gas ignition apparatus (figure 1) and coal dust disperser (figure 2) have been described earlier.^{10/} The explosion vessel consists of two chambers, one

Figure 1. - Hot Gas Ignition Apparatus.

Figure 2. - Coal Dust Disperser.

partially within the other (figure 1). The small chamber A (76 cc) was capped and communicated with the large chamber B (2.1 liters) through a straight channel, 0.5 cm in diameter and 1.0 cm long. After purging and filling chamber A with a stoichiometric methane-oxygen-nitrogen mixture, the cap was removed and the contents were spark-ignited near the channel opening. The explosion products vented through the channel into the flammable mixture in chamber B. These jets differed in temperatures as shown in table 1, both by their calculated theoretical temperatures assuming adiabatic combustion, and by measured temperatures using the sodium D line reversal technique. Natural gas used in these experiments contained about 91 percent methane and 6 percent ethane. Chamber B was equipped with top plates having an array of small venting holes, a blowout pressure release diaphragm at the sidewall, and viewing windows. The outer face of the diaphragm was inerted with nitrogen to eliminate spurious luminosity due to secondary combustion in surrounding air of the hot, partially burned explosion products. The premixed coal dust-methane-air mixture to be ignited flowed through chamber B at approximately 140 cc/sec, giving a constant average linear upward speed of 2.2 cm/sec.

In determining an ignition limit, the coal dust concentration was held constant and the methane concentration was increased until ignition occurred. The salt being investigated for its inhibiting or promoting action was added to chamber A prior to spark ignition by mechanically vibrating the duster (figure 1, view C) that had previously been filled with the requisite amount of additive. Amounts placed in

9/ W_{CD} is the weight of explosive producing 50 percent probability of igniting a coal dust atmosphere. W_{CD} values increase as incendivity decreases.

10/ Singer, J. M. Ignition of Mixtures of Coal Dust, Methane and Air by Hot Laminar Nitrogen Jets. Ninth International Symposium on Combustion, 1963, Academic Press, Inc., New York, N. Y., pp. 407-414.

Singer, J. M. Ignition of Coal Dust-Methane-Air Mixtures by Hot Turbulent Gas. BuMines Rept. of Inv. 6369, 1964, 24 pp.

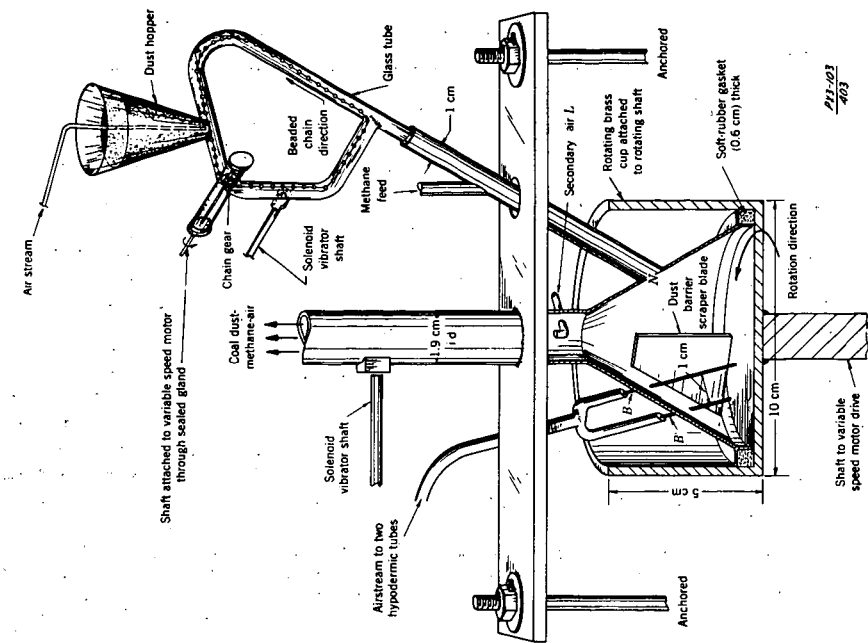


Figure 2. - Coal Dust Disperser.

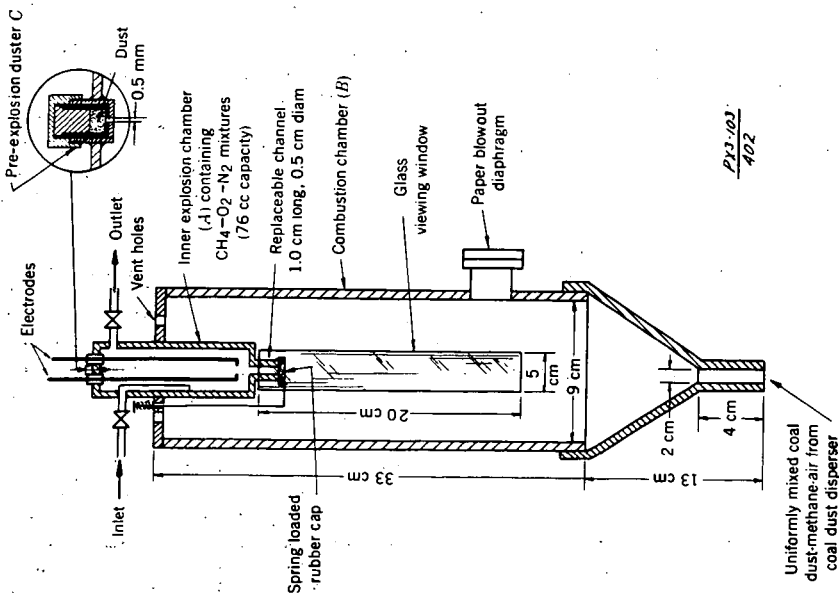


Figure 1. - Hot Gas Ignition Apparatus.

chamber A are stated in figure 3. The actual amount of additive entrained by the

Figure 3. - Effects of sodium salts on incendivity of hot jets to methane-coal dust-air mixtures.

hot jet is not known. The criteria of ignition after the hot jet entered chamber B was the luminosity observed throughout B, and the simultaneous luminous flame shooting out of the ruptured pressure release diaphragm. Duplicate runs made at each ignition point showed that methane-in-air concentrations were reproducible to 0.15 percentage units, oxygen indices to within 0.02 units and coal dust concentrations to within 20 percent. Coal dust concentrations were determined on separate runs by filtering the entire mixture at different levels of chamber B through a 4 cm diameter glass-wool cartridge and weighing after a selected time interval. Local concentrations of dust were determined by filtering through a paper extraction thimble on a 1.0 cm diameter iso-kinetic sampling probe. Local concentrations of dust at various heights and radii of chamber B were constant to within 20 percent. Concentrations of fuel in chamber B at the ignition limit are termed "lower ignition limits", and correspond to lower flammability limits, except that ignition limits are dependent on apparatus factors.

The coal dust disperser in figure 2 was continuously fed by an endless beaded-chain carrier that removed dust from the hopper at a rate determined by its rotation speed. Methane was added through an inlet to the dust disperser. Not all of the air could be added through the air jets; the balance was added through duct L. Hypodermic needles, dust carrier tubes, and chamber B were continuously vibrated to facilitate dust movement and to prevent dust deposition.

RESULTS AND DISCUSSION

Gallery Experiments

The W_{50} values obtained for the six samples are given in table 2. The values for the three explosives containing the low percentage of sodium nitrate varied from 590 to 615 grams; and the values of the three high sodium nitrate explosives varied from 650 to 670 grams. A statistical analysis of these data showed that the type and fineness of the sodium nitrate had no significant effect on the incendivity of the explosives to natural gas air mixtures. However, the samples with the high sodium nitrate content were consistently less incendive than those with low sodium nitrate concentrations.

The W_{CD} values for the low sodium nitrate explosives (a) formulation varied from 290 to 490 grams; the W_{CD} values for the high sodium nitrate explosives (b) formulations varied from 80 to 90 grams. As in the previous experiment the type and fineness of the sodium nitrate does not appear to have any significant effect on the incendivity to coal dust. The 10 percent sodium nitrate explosives were more incendive in coal dust-air atmospheres than the 4 percent sodium nitrate explosives. The reverse was the case for natural gas-air, but differences were much smaller.

The concentration of other constituents of the explosives were changed; nitro-glycerin increased about 17 percent between A and B formulations, ammonium nitrate decreased by 18 percent, sodium chloride increased by 10 percent and the combustible carbonaceous matter increased by 19 percent. The sodium nitrate increase was much greater, being about 155 percent. The net result of these changes in chemical composition is that the oxygen balance is more negative for the B formulations than for the A group of explosives. (The oxygen balance is the deficiency or excess of oxygen required for stoichiometric explosion, in units of grams of oxygen per 100 grams of explosive.) Problems of interpretation due to changes in composition, other than changes in sodium nitrate concentration will be discussed later.

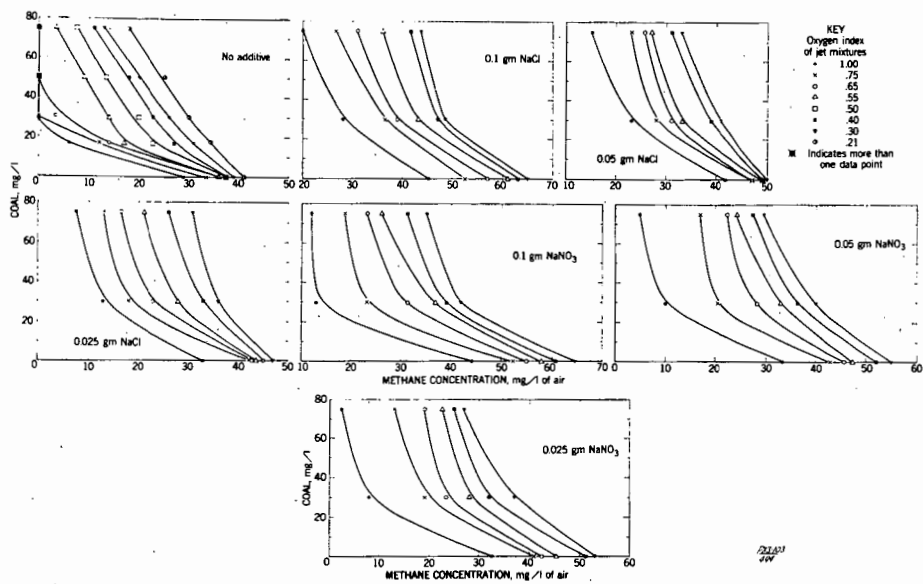


Figure 3. - Effects of Sodium Salts on Incendivity of Hot Jets to Methane-Coal Dust-Air Mixtures.

Laboratory Experiments

Lower ignition limits with and without sodium nitrate in the hot gas jet which served as an ignition source are shown in figure 3; no ignition is obtainable to the left of any curve with the jet used. Each jet is characterized by its oxygen index. The fuel-air mixtures subjected to these jets range from methane-air (lean limit of flammability for methane, 35 mg/liter) to hybrid mixtures of methane-coal dust-air to coal dust-air mixtures (stoichiometric concentration of coal dust used, 109 mg/liter). As the incendiivity of the hot jet is decreased by decreasing the oxygen index or adding sodium salts, the lower ignition limits are displaced upward for constant methane concentration and to the right for constant coal dust concentration. Table 3 gives the reduction in incendiivity as measured by an increase in oxygen index of the jet required to ignite a given fuel mixture; the composition of the fuel mixture is given in terms of concentrations of methane and coal dust. Table 4 summarizes in another way, the change in incendiivity due to the sodium salts. As the incendiivity of the jet decreases due to the salts (comparisons for constant oxygen index and coal concentrations) more methane must be added to the fuel mixture to keep it ignitable. The increase in methane is indicated in table 4 by the increase in total fuel concentration.

The data for sodium chloride shows that the hot jet technique is capable of demonstrating the known effectiveness of sodium chloride in reducing incendiivity.^{5/} The data for sodium nitrate parallel the trend of the sodium chloride data, but at a lesser level of effectiveness. Both salts reduce incendiivity of the hot jet toward methane, a hybrid mixture of methane and coal dust or coal dust only. This result was not the case in the gallery experiments in which sodium chloride reduced incendiivity to gas and to coal dust, but sodium nitrate only reduced incendiivity to gas while increasing incendiivity to coal dust.

It is difficult, without further investigation, to pinpoint the reason for the difference in the two sets of results. The gallery determinations were done with coal dust concentrations of 300 mg/liter in air, and the average particle diameter of the coal dust was 80 microns. The coal dust used in the hot jet determinations was of a much finer grind; concentrations used were below 80 mg/liter. It is not known whether these differences would lead to any specific chemical effect between coal dust and sodium nitrate. There are also differences between the two sets of formulations of the explosives (table 2). The overall changes in stoichiometry between formulations A and B resulted in more combustible materials being present in the products of explosion of the B formulation than in those of the other. Perhaps secondary burning in air may have contributed to the greater incendiivity of the B formulations, rather than the greater concentration of sodium nitrate. However, afterburning of the richer fuel concentration in the explosion products should increase incendiivity to natural gas as well as to coal dust unless the ignitibility of coal dust is far more dependent than gas on the temperature of the ignition source.^{11/}

The striking difference in the two experiments may be due to the condition of the sodium nitrate when the hot gases are injected into the fuel-air mixture. In the case of the gallery experiments, the nitrate may be completely reacted with fuel materials in the detonation front or shortly thereafter. A usually assumed product of its reaction is sodium oxide. In the hot jet experiment it is possible that less sodium oxide is formed in the time available. Thus the possibility exists that sodium compounds derived either from sodium chloride or sodium nitrate in the detonation gases may be a specific inhibitor for the ignition of methane, and that sodium oxide may have a specific ignition promoting mechanism for coal dust. In the hot jet case, sodium chloride and sodium nitrate may play essentially equal roles.

^{11/} Singer, J. M. and J. Grumer. Equivalences of Coal Dust and Methane at the Lower Ignition Limits of Their Mixtures. Restricted International Conference of Directors of Safety in Mines Research, Sheffield, England, 1965, Paper 13, 22 pp.

Table 3. - Incendivity of hot gas jets: minimum oxygen indices of jets required to ignite coal dust-methane-air mixtures.

Fuel Compositions		Additives in ignition jet ^{1/}						
Coal dust Concentration, mg/liter	Methane Concentration, mg/liter	No additive	0.1 gm NaCl	0.1 gm NaNO ₃	0.05 gm NaCl	0.05 gm NaNO ₃	0.025 gm NaCl	0.025 gm NaNO ₃
0	35	0.54	n ^{2/}	n	n	0.95	0.94	0.94
	40	.23	n	n	n	.80	.80	.77
	45	.21	n	1.0	0.88	.65	.44	.55
	50	.21	0.86	.81	.30	.50	.21	.40
30	0	.75	n	n	n	n	n	n
	10	.60	n	n	n	1.0	n	0.9
	20	.50	n	0.80	1.0	.75	0.70	.70
	30	.21	0.90	.60	.70	.65	.50	.50
50	40	.21	.65	.38	.35	.30	.26	.30
	0	.65	n	n	n	n	n	n
	10	.55	n	n	n	0.9	1.0	0.85
	20	.30	n	0.80	1.0	.73	.65	.65
75	30	.21	0.80	.60	.55	.53	.40	.35
	40	.21	.55	.26	.26	.30	.21	.21
	0	.60	n	n	n	n	n	n
	10	.45	n	n	n	0.85	0.85	0.80
75	20	.21	1.0	0.73	0.88	.70	.70	.65
	30	.21	.70	.45	.45	.30	.35	.30
	40	.21	.45	.21	.21	.21	.21	.21

1/ Weight of additive in primary chamber before ignition.

2/ n = Not ignitable with oxygen index of unity.

Table 4. - Total concentrations^{1/} of coal dust and methane at the lower ignition limits of their mixtures with and without the additives sodium chloride and sodium nitrate.

Additives in ignition jet ^{2/}	None		0.1g NaCl		0.1g NaNO ₃		0.05g NaCl		0.05g NaNO ₃		0.025g NaCl		0.025g NaNO ₃								
	1.0	0.55	0.3	1.0	0.55	0.3	1.0	0.55	0.3	1.0	0.55	0.3	1.0	0.55	0.3						
Oxygen index of jet	1.0	0.55	0.3	1.0	0.55	0.3	1.0	0.55	0.3	1.0	0.55	0.3	1.0	0.55	0.3						
Coal dust concentration, mg/l:																					
0	0.45	0.55	0.59	0.68	0.92	0.95	0.68	0.88	0.95	0.62	0.71	0.72	0.52	0.71	0.80	0.50	0.65	0.70	0.50	0.69	0.79
30	.30	.46	.65	.68	.90	.96	.48	.82	.89	.60	.75	.86	.42	.75	.82	.48	.68	.81	.40	.68	.83
50	.45	.58	.75	.80	1.03	1.12	.62	.93	1.02	.73	.92	1.0	.53	.91	.99	.53	.83	.95	.50	.83	.93
75	.65	.70	.85	.94	1.13	1.27	.80	.98	1.15	.90	.98	1.1	.72	.95	1.01	.70	.94	1.02	.65	.95	.98

1/ Fraction of stoichiometry of coal dust-methane-air for complete combustion.

2/ Weight of additive in primary chamber before ignition.

The effect of additives on ignition has been examined recently by several investigators. The experiments of Singer using hot laminar nitrogen jets^{12/} and hot pulsed jets^{13/} as ignition sources indicated that (1) gaseous inhibitors were more effective when added to hot laminar nitrogen jets than to the fuel mixtures to be ignited, and (2) inhibitors suppressed ignition by hot pulsed turbulent jets less efficiently than ignition by hot continuous laminar jets. In ignition by hot pulsed turbulent jets, higher temperatures and high rates of heat and mass transfer to the dust mixtures nullified the effect of the volatile inhibitors. In hot continuous laminar jets, the same compounds were powerful ignition suppressors, apparently because they inhibited slow chemical reactions coupled to the slow diffusion of oxygen and fuel into the slower moving hot gases.

Most of the work reported by other investigators^{14/} concerns suppression of flames of gas mixtures by well-known inhibitors such as halogenated hydrocarbons and alkali metal compounds. Flame inhibition mechanisms suggested for gas mixtures usually relate the condition that chain branching of the active species will equal chain breaking in flames of mixtures with a minimum (or zero) flame velocity or in flames at the upper and lower flammability limits. Dust inhibitors are presumed to act either as coolants or as chemical inhibitors attacking free radicals responsible for chain reaction. One explanation is that the efficiency of a chemical inhibitor is related to the ease of removal of a free valence electron by a colliding radical. Sodium nitrate and sodium chloride are classed as both thermal and chemical inhibitors.

^{12/} First work cited in footnote 10.

^{13/} Second work cited in footnote 10.

^{14/} Abrams, M. C. Chemical Flame Quenching Theory. Pyrodynamics, v. 1, 1964, pp. 131-141.

Dewitte, M., J. Vrebosch, and A. Van Tiggelen. Inhibition and Extinction of Premixed Flames by Dust Particles. Combustion and Flame, v. 8, No. 4, Dec. 1964, pp. 257-266.

Dolan, J. E. The Suppression of Methane/Air Ignitions by Fine Powders. Sixth Symposium (International) on Combustion, Reinhold Publishing Co., New York, pp. 787-794.

Dolan, J. E. and J. B. Dempster. The Suppression of Methane-Air Ignitions by Fine Powers, J. Appl. Chem. v. 5, 1958, pp. 510-517.

Rosser, W. A., S. H. Inami, and H. Wise. The Effect of Metal Salts on Premixed Hydrocarbon-Air Flames, Combustion and Flame, v. 7, June 1963, pp. 107-119.

Van Tiggelen, A. University of Louvian, Final Technical Report on Contract DA-91-591-EUC-1072, March 1960.

CONCLUSIONS

1. The incendiivity to methane or natural gas-air mixtures was reduced by the presence of sodium nitrate in explosives or in hot jets from methane-oxygen-nitrogen explosions.
2. The incendiivity to methane-coal dust-air mixtures was reduced by sodium nitrate in the hot jets.
3. The incendiivity to coal dust was increased by sodium nitrate in explosives and decreased by sodium nitrate in the hot jets.

AN ANALYSIS OF POROUS-PLATE COMBUSTION SYSTEMS

by

S. A. Weil
 W. R. Staats
 R. B. Rosenberg

Institute of Gas Technology
 Chicago, Illinois

INTRODUCTION

In the porous-plate combustion system, an unburned gaseous fuel-oxidant mixture is fed into the upstream side of a porous solid. The combustion or reaction zone is near the downstream surface. The variety of possible pore structures and solid materials offers a variety of reaction areas. They include combustion in the gas phase above the solid (a flame), in pores large enough to permit essentially ordinary flames, in pores too small to permit ordinary flames, on the pore surfaces within a catalytic porous medium, and combinations of these.

This paper presents a theoretical analysis of combustion in and above a non-catalytic solid with fine pores. Its purpose is to indicate the limits of steady-state operation of such a system, and the operating characteristics as they depend on flow rate.

The location of the combustion zone is deduced from the model, rather than included in the assumptions. Potentially, the porous plate can operate either as a preheater or as a reactor. In the first case, the incoming gases are heated in the plate and most of the combustion occurs above it. In the other case, most of the combustion occurs in the plate. The characteristics of both mechanisms are of interest here. The quantitative results are necessarily inseparable from the assumed chemical kinetics and physical properties. These have been chosen to correspond to reasonably real systems, but in any case, they demonstrate the types of operating boundaries to be encountered in such systems.

THE HYPOTHETICAL MODEL

The system is defined to be unidimensional, with a semi-infinite porous solid. Within the porous phase, the gas and solid temperatures are equivalent, and the pores are sufficiently fine that the equations applicable to a homogeneous phase can be used. The chemical kinetics are the same within the pores as in the gas phase outside the solid.

The equations to describe the energy and mass transfer in this system are based on those presented by Spalding.¹ To solve the equations, even numerically, a relationship between the local temperature and composition is extremely convenient. In the porous phase, the assumption of no mass diffusion generates this relationship. In the gas region, the assumption of a Lewis number of 1, as originally suggested by Semenov,² serves this purpose.

Furthermore, the formulation of the overall kinetics of the reaction is most conveniently set in terms of mass fraction of the fuel (for a lean system) and the temperature, in the manner used by Spalding.³ The resulting steady-state equations, in terms of reduced variables, are:

For the region outside the solid

$$d^2\tau/dy^2 - d\tau/dy + a \tau^m / g^2 \lambda^2 = 0 \quad (1)$$

$$a = \tau_f - \tau \quad (2)$$

For the porous region

$$r_k d^2\tau/dy^2 - d\tau/dy + a^n \tau^m P/g^2 \lambda^2 = 0 \quad (3)$$

$$a = 1 - \tau + r_k d\tau/dy \quad (4)$$

where

τ = temperature above the feed gas temperature relative to the adiabatic temperature rise

y = distance \times gas specific heat \times gas mass velocity / gas thermal conductivity

a = fuel mass fraction relative to inlet fuel mass fraction

r_k = mean solid thermal conductivity relative to that of the gas

g = mass velocity relative to the adiabatic burning velocity

n = overall order of reaction in terms of fuel fraction

τ^m = temperature dependence of reaction rate

P = porosity of the solid

λ^2 = constant

The interaction of the system with the surroundings occurs only by radiation to and from the porous-plate surface. With this, the conditions at the boundaries are:

$$y = -\infty: \tau = 0, d\tau/dy = 0 \quad (5)$$

$$y = \infty: \tau = \tau_f, d\tau/dy = 0 \quad (6)$$

$$y = 0: \epsilon \tau^s = g(1 - \tau_f) + \epsilon \tau_b^s \quad (7)$$

$$\tau_f = 1 + r_k (d\tau/dy)_{y < 0} - (d\tau/dy)_{y > 0} \quad (8)$$

if y is zero at the surface, τ_f is the final gas temperature, τ_b is the temperature of the surroundings, and $\epsilon \tau_b^s$ is the radiation law for the solid.

The solution of Equations 1 through 8 for a specified g and τ_b consists of finding a temperature distribution in the porous phase from 3 and 5, and one in the gas phase from 1 and 6, that can be linked up at the surface in accordance with 7 and 8. Two, one, or no solutions may exist, for a given flow rate and surrounding temperature, depending on the operating parameters.

Although reaction occurs in both phases, the solutions correspond to the porous phase acting primarily as a heater, with the major combustion in the gas phase, or to the major combustion occurring in the porous phase. In this paper, these regimes are referred to as preheater and reactor, respectively, to emphasize the role of the porous solid.

The lack of a steady-state solution must imply the impossibility of stable operation for the particular input and surrounding temperature. Also, more than one steady-state solution may exist for any given set of conditions. On the other hand, the existence of a steady-state solution does not necessitate stable operation, since other factors may be involved.

RESULTS

In the primary example used for analysis, values of the parameters are $n=2$, $m=10$, $\epsilon=1.17$, $S=3$ and $P=0.3$. As shown in previous work,³ $m=10$ is appropriate for methane-air systems. For a 105 percent aerated flame with an adiabatic flame temperature of 2190°K, the values for ϵ and S correspond to a black-body radiation law. Two values of r_k were studied, 5 and 20, corresponding to insulating and high-conductivity porous solids, respectively.

In Figure 1, a typical set of temperature distribution curves is presented. Note that Equations 3, 4, and 5 define the temperature distribution in the porous phase with the flow rate as the only operating parameter. The maximum τ increases monotonically with flow rate. Any finite flow rate will yield a porous phase steady-state solution. However, the whole system has a valid steady-state solution only if a surface consistent with Equations 6, 7, and 8 exists. The location of the surface with respect to the temperature distribution of the porous phase depends on the surrounding temperature and on the solution for the gas phase.

In Figure 2, the steady states for a surroundings temperature (τ_b) of 0.4 are shown for $r_k=5$ in terms of the surface and final gas temperatures. This is the behavior of these systems when τ_b is low. The lower input limit is the same for the solid behaving as a reactor or as a preheater. It is not zero if τ_b is greater than zero. The upper input limit of the preheater region corresponds to the situation when all the incoming radiation goes into preheating the gas. Another notable characteristic is the maximum in the surface temperature vs. feed rate curve for preheater operation. Thus, a maximum yield of radiation energy exists for this type of operation.

The choice when there are two possible steady states at a given flow rate presumably is determined by the path to the steady state. If the burner is started cold at a flow rate within the preheat region, it will behave as a preheater. If it is started at a higher rate where the solid is a reactor, a reduction in flow rate would keep the system in that regime. The type of instability which results from a reduction of the flow rate beyond the lower input limit is not known from this analysis. However, the extent of reaction is 46 percent within the solid at the lower limit, which would indicate that the system would go into flashback.

In Figure 3, the characteristics of the same system ($r_k=5$) at high surrounding temperatures are illustrated with $\tau_b=0.6$. At low flows, no steady states are possible. The regimes, in order of increasing flow rate, then consist of one in which only preheater behavior is possible, one in which both preheater and reactor behavior is possible, and one in which only reactor behavior is possible. These results imply the existence of two lower limits, depending on operation as a preheater or as a reactor. Again, this type of analysis cannot anticipate the behavior at these bounds, in particular whether the lower limit for the reactor corresponds to a discontinuous transition to preheater behavior or directly to flashback.

The equivalent system, but with a higher relative thermal conductivity for the porous phase, $r_k=20$, is similar to the $r_k=5$ system in most aspects. The separation of the lower bounds for preheater and reactor occurs at lower surrounding temperatures, as shown in Figure 4. At higher temperatures, another type of behavior appears. For $\tau_b=0.6$, (Figure 5) there is a flow region too high for preheater activity and too low for reactor behavior.

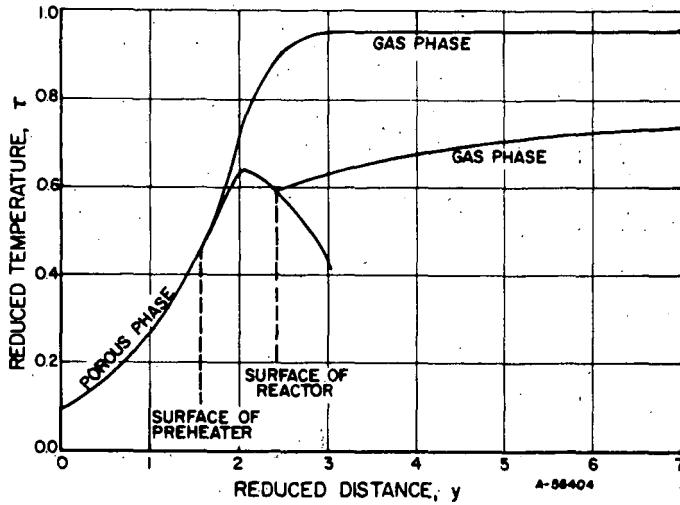


Fig. 1.—TEMPERATURE DISTRIBUTIONS IN POROUS SOLID AND GAS PHASES WITH POROUS PHASE ACTING AS PREHEATER AND AS REACTOR,
 $\tau_b = 0.4$, $r_k = 5$.

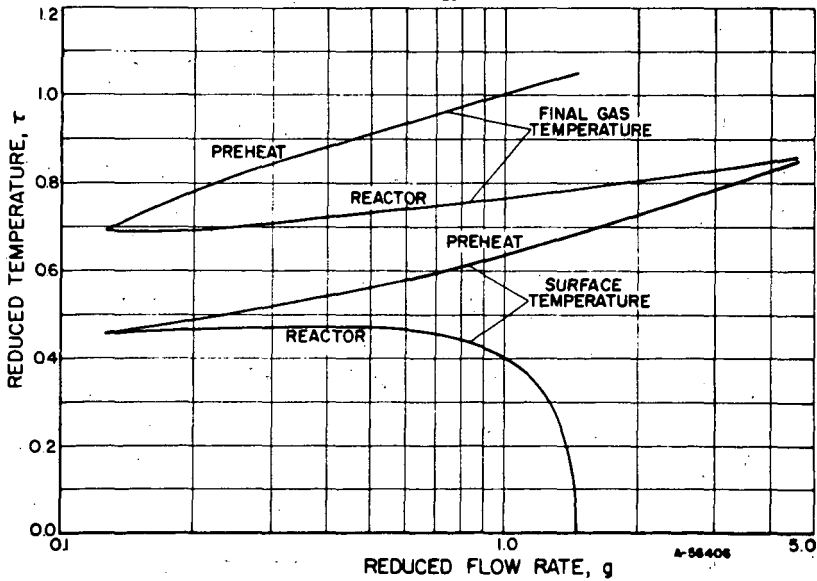


Fig. 2.—FINAL GAS TEMPERATURE AND TEMPERATURE OF THE SURFACE OF THE POROUS SOLID AS FUNCTIONS OF GAS FLOW RATE,
 $\tau_b = 0.4$, $r_k = 5$.

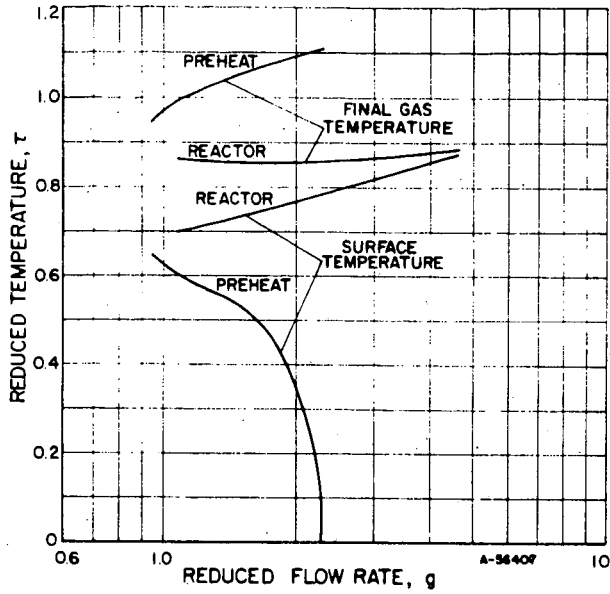


Fig. 3.—FINAL GAS TEMPERATURE AND TEMPERATURE OF THE SURFACE OF THE POROUS SOLID AS FUNCTIONS OF FLOW RATE, $\tau_b = 0.6$, $r_k = 5$.

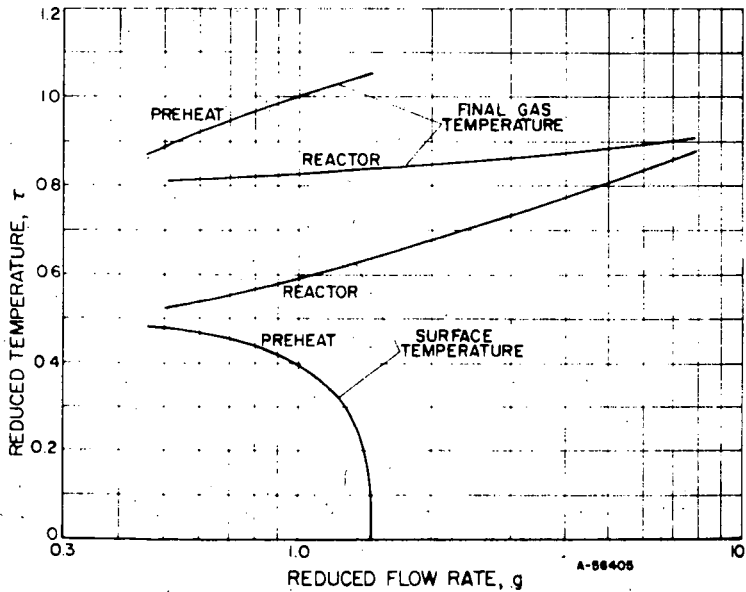


Fig. 4.—FINAL GAS TEMPERATURE AND TEMPERATURE OF THE SURFACE OF THE POROUS SOLID AS FUNCTIONS OF GAS FLOW RATE, $\tau_b = 0.4$, $r_k = 20$.

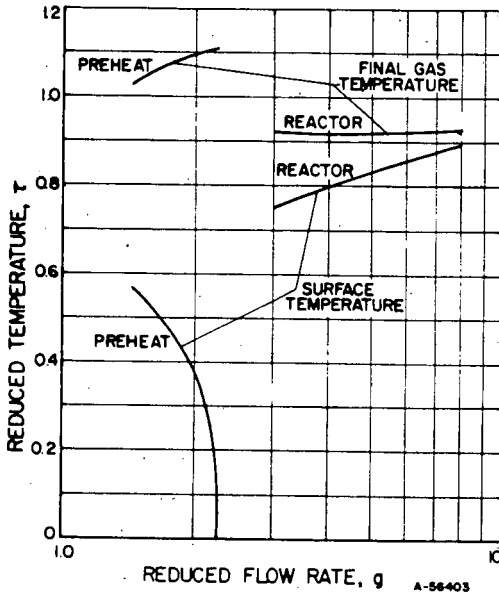


Fig. 5.—FINAL GAS TEMPERATURE AND TEMPERATURE OF THE SURFACE OF THE POROUS SOLID AS FUNCTIONS OF GAS FLOW RATE, $\tau_b = 0.6$, $r_k = 20$.

SUMMARY

The theoretical analysis demonstrates the existence of heat input limits (limits of steady-state operation) for a noncatalytic porous-plate burner. It indicates the relative location of these limits and the effect of the temperature of the surroundings. The analysis also shows the surface temperatures as a function of input and surrounding temperature.

The porous plate can operate in two ways:

- 1) As a preheater — The incoming gases are preheated as they pass through the plate, with most of the combustion occurring above the plate.
- 2) As a reactor — The fuel-air mixture reacts primarily in the plate rather than above it.

Three different input limits for steady-state operation are shown to exist:

- 1) An upper limit for operation as a preheater.
- 2) A lower limit for preheater operation.
- 3) A lower limit for reactor operation.

Limits 2 and 3 can be identical under some conditions.

The porous plate can sometimes act either as a preheater or as a reactor at a given input. In such a case, it may be difficult to visually differentiate between the two mechanisms since the plate surface temperatures are often similar. The appropriate mechanism can be determined most readily by determining the effect of variations in the input rate on the surface temperature.

REFERENCES CITED

1. Spalding, D. B., "II. One-Dimensional Laminar Flame Theory for Temperature — Explicit Reaction Rates," Combustion and Flame 1, 296-306 (1957) September.
2. Semenov, N. N. "Thermal Theory of Combustion and Explosion. III. — Theory of Normal Flame Propagation," NACA Technical Memorandum No. 1026 (1942) September.
3. Weil, S. A., "A Study of Porous Plate Flameholders," Institute of Gas Technology Research Bulletin No. 35 (1964) August.

FORMATION OF NITROGEN OXIDES IN AERATED METHANE FLAMES

R. B. Rosenberg and D. S. Hacker

Institute of Gas Technology, Chicago, Illinois

INTRODUCTION

An investigation to determine the kinetics of the formation of the oxides of nitrogen produced in aerated methane flames is currently in progress at IGT. Under controlled flow conditions, the location and concentration of the oxides of nitrogen — nitric oxide, NO, and nitrogen dioxide, NO₂ — were experimentally measured in a premixed bunsen-type flame and on a premixed flat flame. The compositions of the primary stream (fuel-oxidant) and the secondary stream were varied. This paper summarizes the highlights of the work to date. The study is sponsored by the American Gas Association under its PAR (Promotion-Advertising-Research) Plan.

EXPERIMENTAL TECHNIQUE

The data on NO₂ were obtained with a Mast nitrogen dioxide analyzer. The concentrations of NO were initially determined by use of a catalytic probe which converted the NO to NO₂ for later analysis with the Mast. The NO concentrations are currently being obtained by homogeneously oxidizing the NO to NO₂ with oxygen at high pressure prior to analysis. Spot checks by the phenyldisulfonic acid technique are made on the concentration of oxides of nitrogen in the water condensed from the flue gas sample stream. These have not shown significant quantities of nitrogen oxides in most cases.

The reproducibility of the data is very good for runs made on the same day. The worst variations observed for runs on different days were about ±2 ppm. Most of the data showed smaller variations than this.

EXPERIMENTAL RESULTS

Figure 1 shows a bunsen flame which had a primary feed stream consisting of methane with 67 percent of the stoichiometric air required for complete combustion, and a secondary feed stream of air. Figure 2 shows the concentrations of NO and NO₂ measured at various positions in this flame. It can be seen that NO forms in a narrow region near the outside edge of the flame. It then diffuses both toward the center of the burner and into the secondary air stream. It oxidizes rapidly to NO₂ in the secondary air stream. Very little NO₂ is found in the burning gas.

Table 1 shows the average concentration of NO + NO₂ (NO_x) at each height above the burner. This average value corresponds to the concentration of NO_x which would have to be uniformly distributed over the cylindrical cross-section to yield the same total concentration shown at each height in Figure 2. Table 1 shows that the formation of NO_x occurs only where the flame is present. Above the tip of the flame, i.e., at heights greater than 7.2 cm, the concentration is seen to remain constant within experimental uncertainty. This suggests that the flame is acting as more than a source of heat, and may be participating chemically in the formation of NO_x.

Table 1.—AVERAGE NO_x CONCENTRATION AT VARIOUS HEIGHTS ABOVE FLAMEHOLDER WITH A CONICAL FLAME OF 67+ PRIMARY AERATION (Primary Flow Rate 15.6 CF/hr)

Height Above Flameholder, cm	Average NO _x Concentration, ppm	
	Corrected for Temperature Profile	Uncorrected
0.5	--	1.3
1.8	--	1.7
3.7	3.6	2.9
7.2	4.8	4.5
9.7	--	3.9
15	4.5	4.2

Figure 3 shows the results obtained when argon was substituted for nitrogen in the primary stream, with air retained as the secondary stream. The concentration of argon was varied so that the difference between the heat capacities of argon and nitrogen would not be a factor. The data show a lower concentration of NO_x when argon is substituted for nitrogen. Thus, it is seen that the nitrogen which^x reacts to form NO_x is supplied by both the primary and secondary streams, with somewhat more being^x supplied by the secondary.

Tables 2 and 3 show the effect of primary mixture flow rate (heat input) and of primary aeration on NO_x concentration at a height of 15 cm above the burner. The

Table 2.—EFFECT OF PRIMARY MIXTURE FLOW RATE (67% PRIMARY AIR) ON THE CONCENTRATION OF NO_x 15 cm ABOVE FLAMEHOLDER

Primary Mixture Flow Rate, CF/hr	NO _x at Various Radial Positions, ppm		
	0.0 cm	1.2 cm	2.4 cm
12.1	2.7	4.1	3.7
15.6*	3.1 ± 1.0	4.5 ± 0.9	3.5 ± 0.5
20.0	3.5	4.2	3.6
25.0†	1.2 ± 0.5	5.7 ± 0.3	4.8 ± 0.1

* Average of 4 runs

† Average of 2 runs

Table 3.—EFFECT OF PRIMARY AERATION ON THE CONCENTRATION OF NO_x 15 cm Above Flameholder

Primary Aeration,	Primary Mixture Flow Rate, CF/hr	NO _x at Various Radial Positions, ppm		
		0.0 cm	1.2 cm	2.4 cm
67.3*	15.6	3.1 ± 1.0	4.5 ± 0.9	3.5 ± 0.5
67.3	20.0	3.5	4.2	3.6
50.0	18.2	1.9	4.4	3.4
67.3†	25.0	1.2 ± 0.5	5.7 ± 0.3	4.8 ± 0.1
90.0†	30.0	4.8 ± 1.1	5.1 ± 0.5	5.4 ± 0.4
110.0†	29.1	3.1 ± 0.1	2.8 ± 0.2	3.0 ± 0.2
120.0	26.3	1.2	1.7	1.9

* Average of 4 runs

† Average of 2 runs

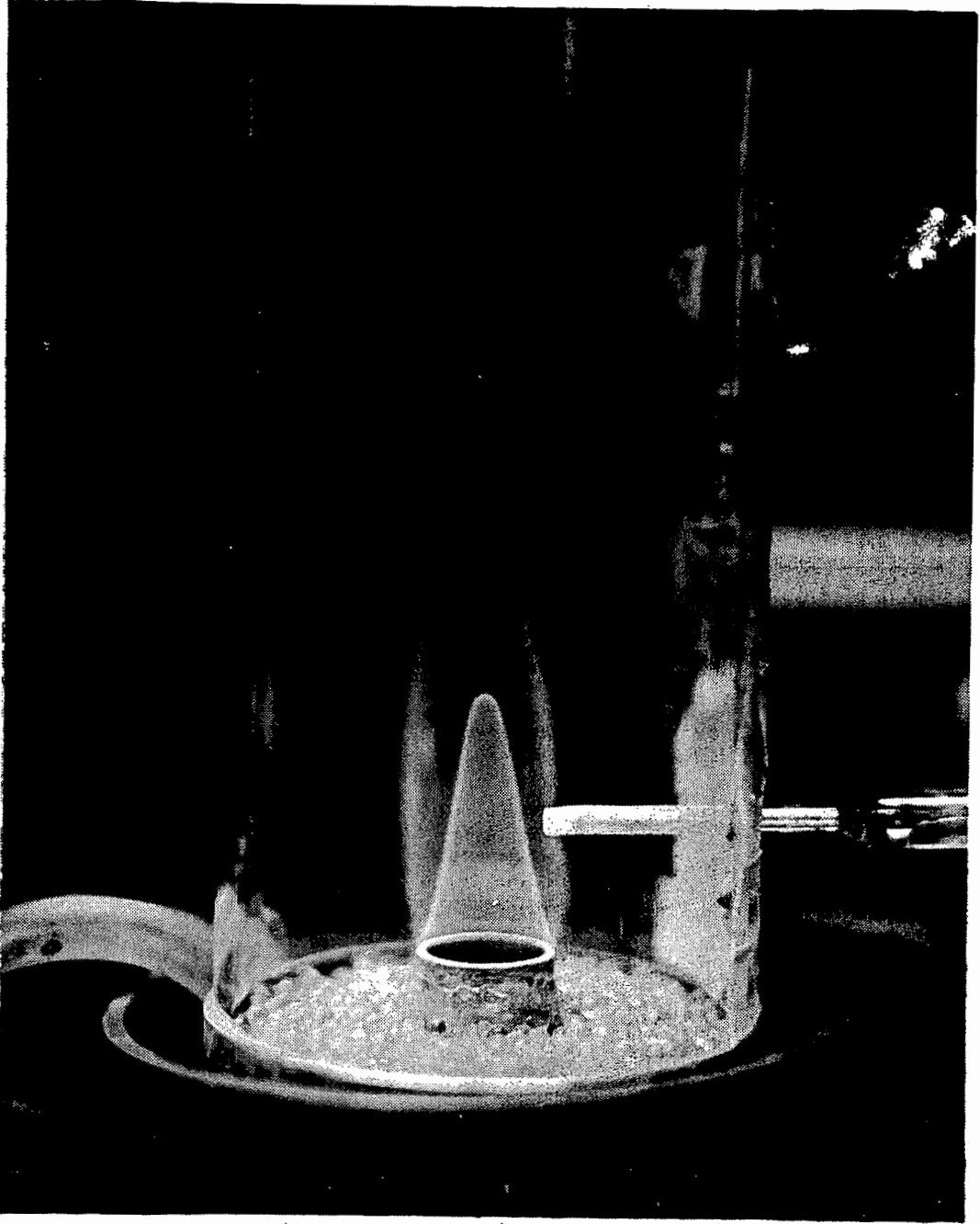


Figure 1.—QUARTZ PROBE AND 67% AERATED FLAME

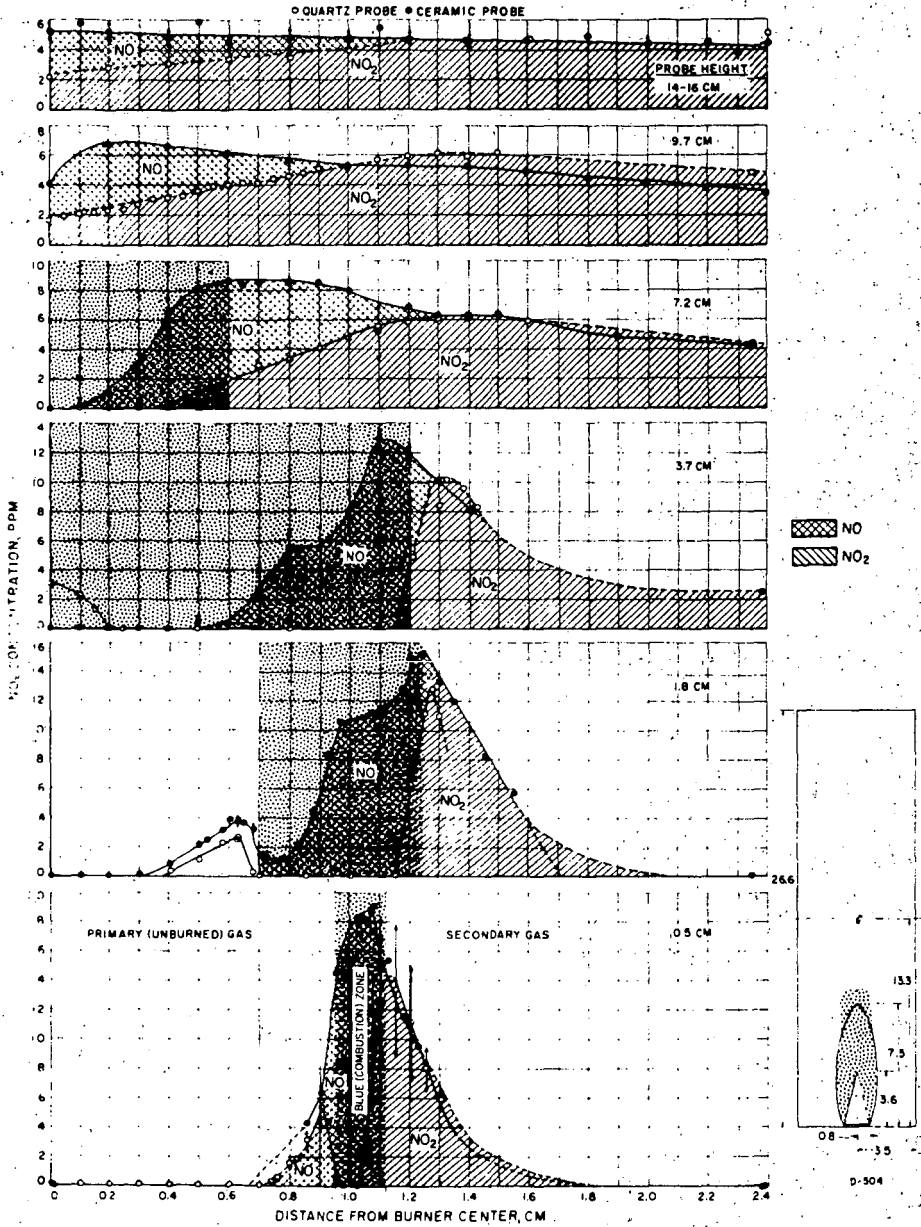


Figure 2.—NITROGEN OXIDE PROFILES AT VARIOUS HEIGHTS WITH 67% PRIMARY AERATED CONICAL FLAME

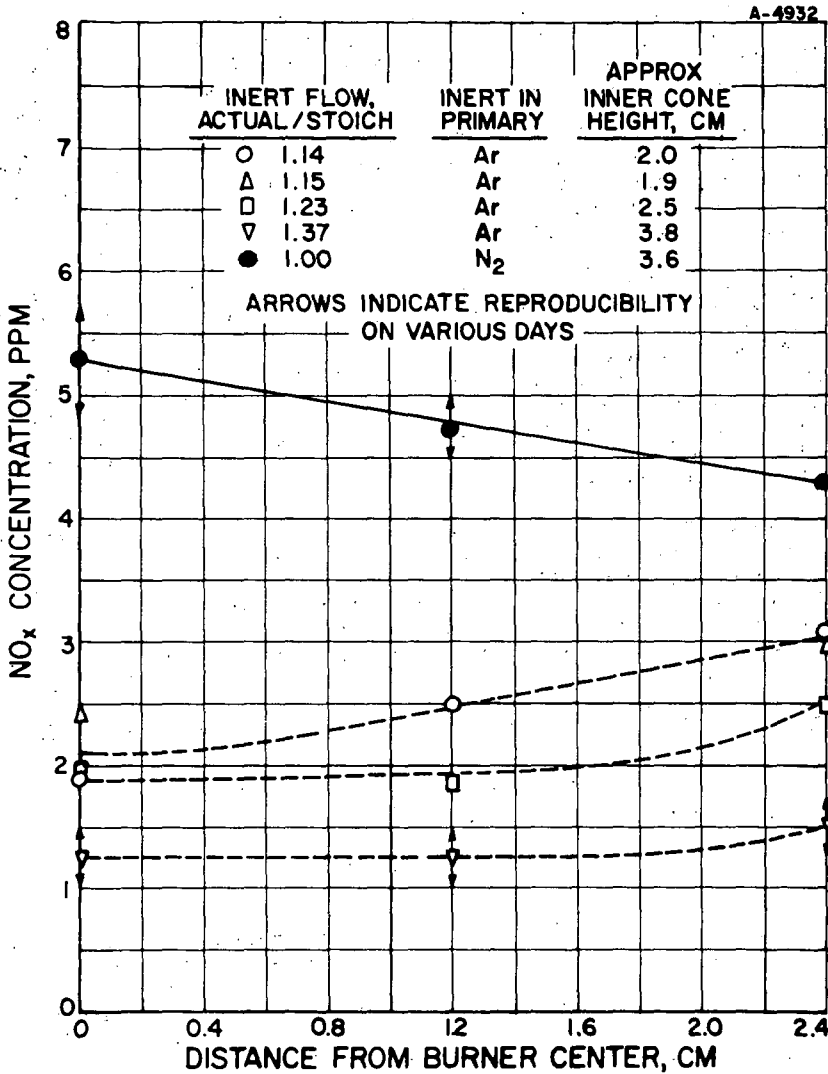


Figure 3.—CONCENTRATION OF NO_x 15 CENTIMETERS ABOVE THE FLAMEHOLDER OF A CONICAL CH₄-Ar-O₂ FLAME WITH 67% OF STOICHIOMETRIC O₂ IN THE PRIMARY STREAM

primary mixture flow rate has no apparent effect over the range of 12 to 20 CF/hr. There appears to be a small change in the concentration of NO_x as the input is increased to 25 CF/hr. The flow rate of the secondary stream has no effect over the same range.

The effect of primary aeration is not large over the range of 67 to 90 percent primary air. However, a strong decrease in the concentration of NO_x is observed when the primary mixture is made fuel-lean. Figure 4 shows the NO_x and NO_2 concentration profiles of a flame with 110 percent primary aeration. In contrast to the fuel-rich primary mixture (Figure 2), the primary oxide of nitrogen that is present is NO_2 , rather than NO . The flame with the fuel-lean primary has only a single, small combustion zone as opposed to the two larger combustion zones with the fuel-rich primary. This may account for the decreased NO_x with the fuel-lean primary.

The shape and position of the reaction zone for the formation of NO_x from a bunsen or conical flame made a kinetic analysis difficult. Consequently, the experimental work was changed from a bunsen to a flat flame stabilized by a flameholder consisting of a collection of stainless steel capillary tubes. A more detailed series of data are being obtained with this burner.

One of the most interesting observations illustrated is in Figure 5, where the concentration of NO_2 along the centerline is shown as a function of height above the burner. The NO_2 is seen to form very close to the flame (which is at a height of about 0.1 cm), and then rapidly decompose. The NO_2 concentration decreases to zero with the fuel-rich and stoichiometric primary mixtures. However, some NO_2 is found at all heights above the burner with the fuel-lean primary mixtures. These data were obtained with nitrogen as the secondary gas. A similar effect is observed when argon is the secondary. However, the decomposition of NO_2 is greatly decreased when air is the secondary.

Figure 6 shows the effect of this decomposition on the relative concentrations of NO and NO_2 when an argon or air secondary is used with a primary mixture of 100.5 percent aeration. It is seen that there is more NO_2 present at a height of 1.1 cm with air than with argon. However, in either case, the primary oxide of nitrogen is NO near the burner centerline, but it is NO_2 near the secondary. Figure 7 shows that almost no NO is present at 0.1 cm above the burner. NO_2 is the primary oxide of nitrogen at all radial positions.

There are three significant observations to be drawn from this stoichiometric flame:

- 1) NO_2 is the oxide of nitrogen which is formed in the flame.
- 2) Some of this NO_2 decomposes to NO .
- 3) NO also forms by another mechanism in the combustion products above the flame.

These observations do not necessarily contradict the data from the bunsen flame, since there are a considerable number of differences between the two systems.

There are two regions of formation of NO_x by a flat flame. Figure 8 shows that NO_2 is formed from a methane-air primary stream with an argon secondary. This NO_2 , which must have formed in the flame, is seen to decompose. Figure 9 shows that NO_2 is formed from a methane-argon-oxygen primary stream with an air secondary. This NO_2 , which forms where the primary and secondary stream are mixing, does not appear to decompose to any significant extent. Temperature differences between these two regions may explain the different decompositions observed, since the same relative effect is noted when NO_2 is added to the primary mixture of a methane-argon-oxygen flame with an argon secondary. The decomposition is much greater near the center of the burner than near the secondary. We

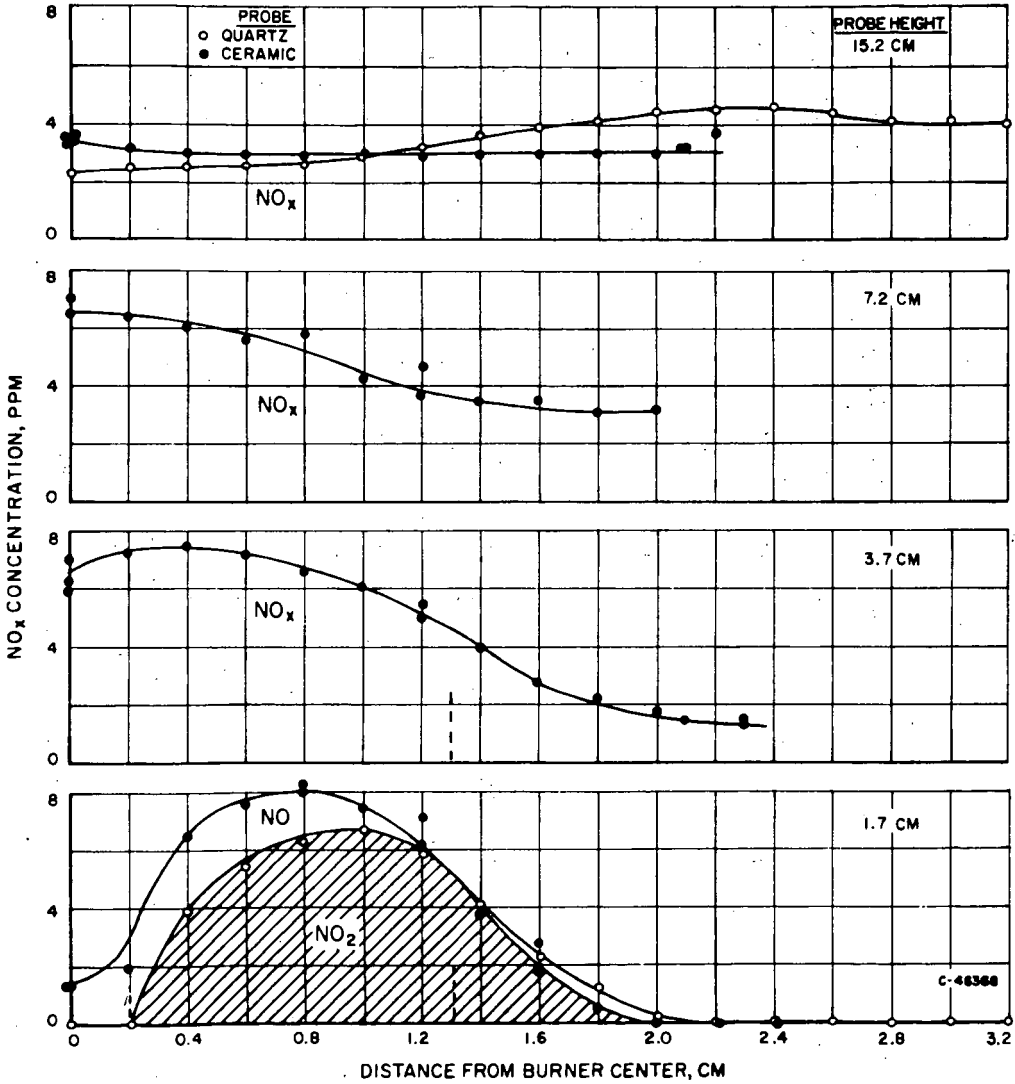


Figure 4.—NO_x CONCENTRATION PROFILES AT VARIOUS HEIGHTS WITH A 110% PRIMARY AERATED CONICAL FLAME

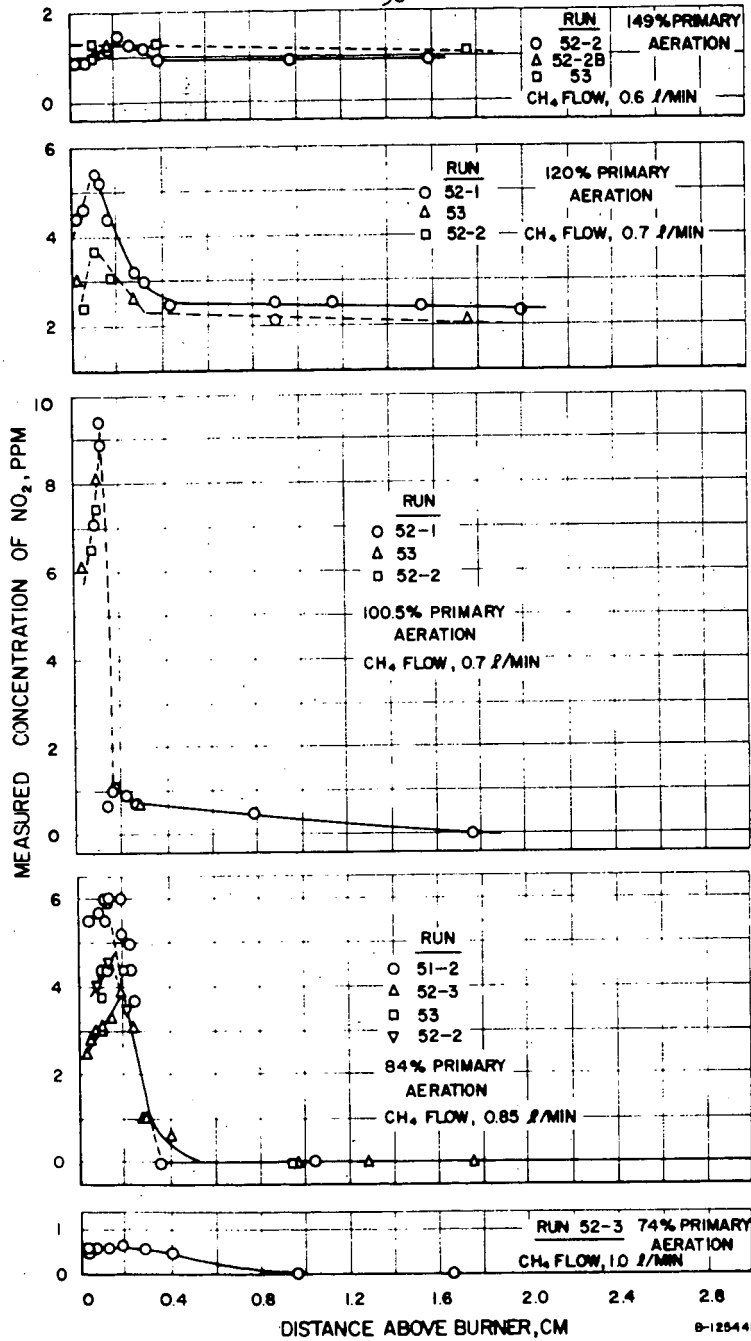


Figure 5.—AXIAL CENTERLINE CONCENTRATION PROFILES OF NO₂ FROM FLAT METHANE-AIR FLAMES WITH A SECONDARY NITROGEN ATMOSPHERE

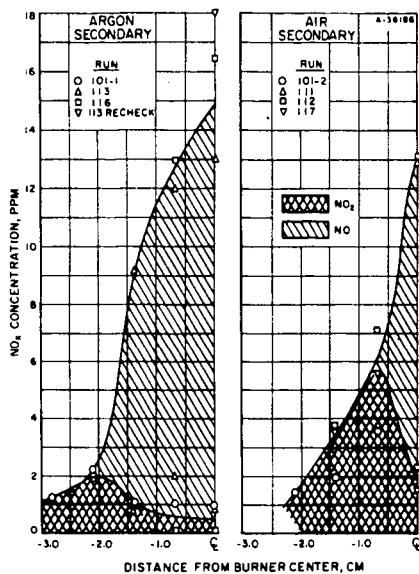


Figure 6.—NO_x CONCENTRATION FOR A CH₄-AIR STOICHIOMETRIC FLAME AT A HEIGHT OF 1.1 cm ABOVE THE BURNER

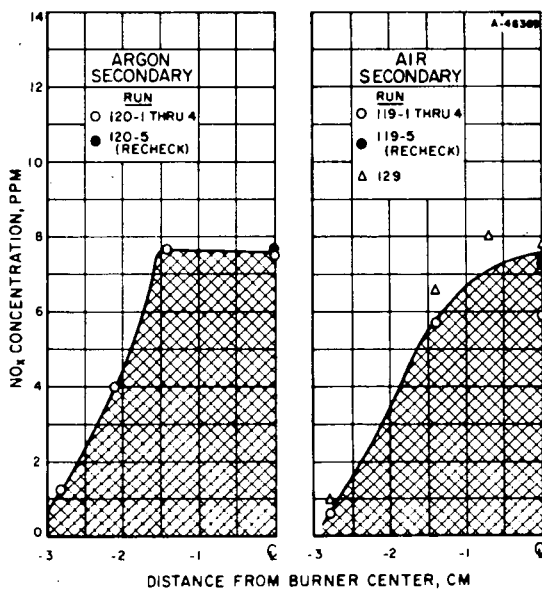


Figure 7.—NO_x CONCENTRATION FOR A CH₄-AIR STOICHIOMETRIC FLAME AT 0.1 cm ABOVE THE BURNER

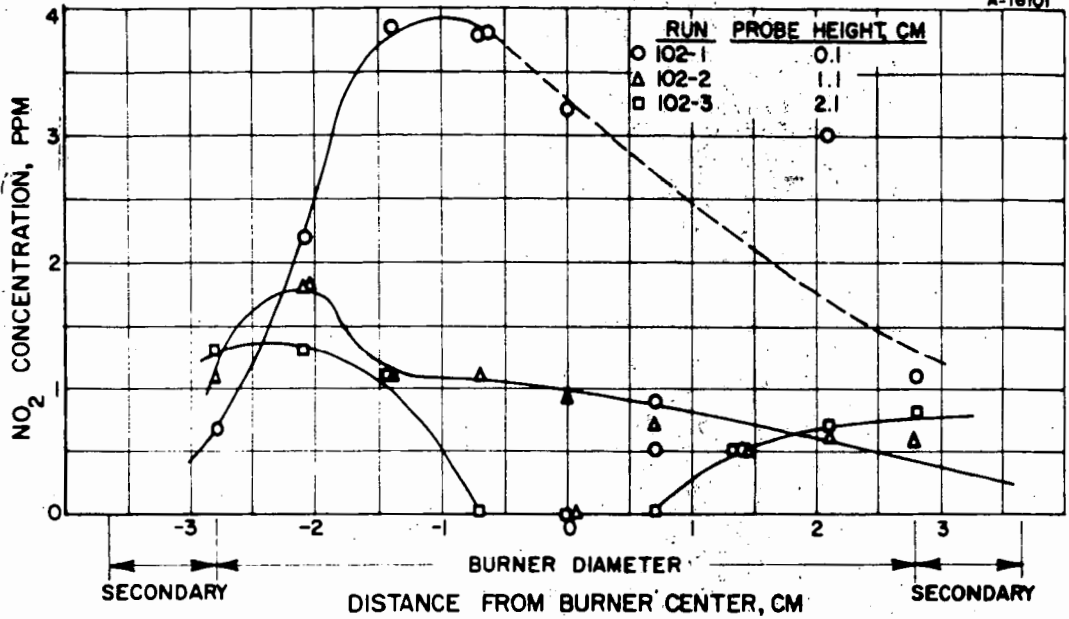


Figure 8.—FORMATION OF NO₂ FROM A STOICHIOMETRIC FLAT CH₄-AIR FLAME WITH A SECONDARY ARGON STREAM

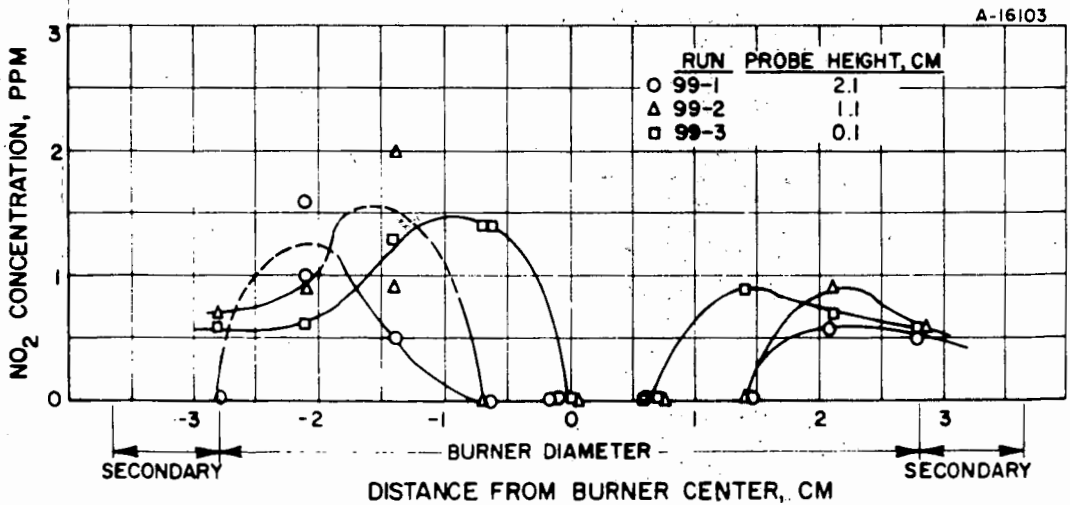


Figure 9.—FORMATION OF NO₂ FROM A STOICHIOMETRIC CH₄-Ar-O₂ FLAME WITH A SECONDARY AIR STREAM

are aware that there is some oxidation of NO to NO₂ in our sampling system. At present, the fraction oxidized appears to be small. We are interpreting the measured NO₂ as being primarily from the flame.

Theoretical equilibrium and kinetic studies are currently in process. Figure 10 shows the calculated concentration of NO_x in equilibrium¹ with the combustion products from flames of various compositions and various temperatures. At these temperatures, (above 1500°K), the ratio of the concentration of NO to that of NO₂ is more than 300:1. This ratio increases as the temperature increases or the oxygen concentration decreases.

The region where NO_x forms in the bunsen flame has relatively steep axial and radial temperature gradients. The estimated temperature range is from 2200° to 3100°R. The flat flame provides a radial region of more than 2.4 cm of very uniform temperature. The axial temperature gradient is only about 25°C/cm. The temperature above the flat flame has been estimated, with corrected thermocouple readings and published correlations,²⁻⁴ to be about 1500° ± 100°C (2700°R).

Thus, there are no indications that total concentrations in excess of equilibrium are being formed from stoichiometric or fuel-lean flames. However, the ratio of NO to NO₂ is not characteristic of the high-temperature equilibrium. This may be due to the oxidation in the sampling system.

The kinetics of this system are extremely complex because of the flame reactions. However, it is possible to compare the values measured in this system with the amount of NO that would be formed in air heated to the same temperature for the same length of time. The kinetic model (in which M represents any other species) used for this calculation is:

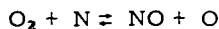
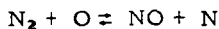
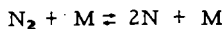


Table 4 gives the calculated rates at various temperatures. It is of interest to note that the rates of the bimolecular reaction and the atomic reactions to form NO are comparable at these temperatures. At higher temperatures, the atomic reactions will predominate.

Table 4.—RATES OF FORMATION OF NITRIC OXIDE IN AIR AT VARIOUS TEMPERATURES

Temperature, °K	Rate of Formation of Nitric Oxide, ppm/sec	
	NO = 100 ppm	NO = 10 ppm
1600	0.90	1.02
1800	69	73
2000	2150	2210

The time required for the combustion products to pass from 0.1 to 1.1 cm above the burner is about 0.026 second. During this time, the stoichiometric combustion products are observed to form a 10 ppm increase in NO_x.

If the same time factor is applied to the kinetics of heated air, the calculated concentrations are 1.8 ppm at 1800°K, and 57 ppm at 2000°K. It should be noted that:

1) The rate constants for this kinetic model are not well established, and the values

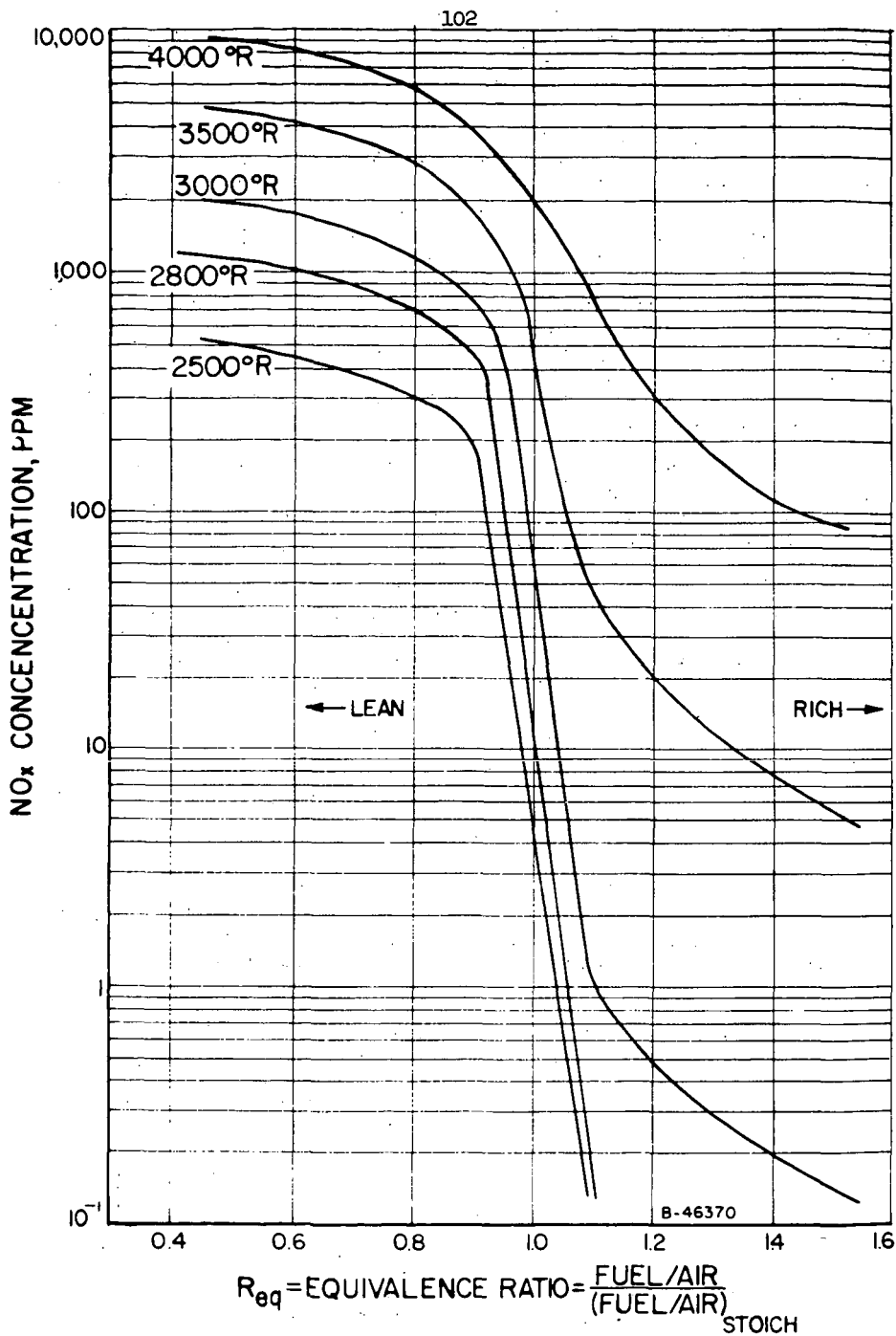


Figure 10.—EQUILIBRIUM OF NO_x WITH COMBUSTION PRODUCTS OF VARIOUS METHANE-AIR FLAMES

used in this calculation are among the highest that were found.⁵

2) The oxygen concentration of air is much larger than that of the stoichiometric combustion products by about 2 orders of magnitude.

3) The estimated temperature of the system is close to 1800 °K.

Thus, it appears likely that, upon completion of the theoretical analysis and with accurate temperature and composition measurements, it will be found that nitrogen oxides form in a flame faster than in heated air.

REFERENCES

1. Rossini, F. D., Pitzer, K. S., Arnett, R. L., Braun, R. M. and Pimental, G. C., "Selected Values of Physical and Thermodynamic Properties of Hydrocarbons and Related Compounds." Pittsburgh: Carnegie Press, 1953.
2. "Symposium on Gas Temperature Measurement," J. Inst. Fuel 12, S1-S108 (1939) March (Supplementary issue).
3. Weil, S. A., "Burning Velocities of Hydrocarbon Flames," Institute of Gas Technology Research Bulletin No. 30 (1961) March.
4. Weil, S. A., "A Study of Porous Plate Flameholders," Institute of Gas Technology Research Bulletin No. 35 (1964) August.
5. Wray, K. L., "Chemical Kinetics of High Temperature Air," Avco Research Rept. 104. Everett, Mass.: Avco-Everett Research Laboratory, 1961.

FLAME CHARACTERISTICS CAUSING AIR POLLUTION I. EMISSION
OF OXIDES OF NITROGEN AND CARBON MONOXIDE

Joseph M. Singer
Edwin B. Cook
Joseph Grumer

U.S. Bureau of Mines, 4800 Forbes Avenue,
Pittsburgh, Pennsylvania

ABSTRACT

This investigation is part of a program by the Bureau of Mines, sponsored by the Public Health Service, to determine the factors that govern emission of air pollutants by domestic and industrial gas combustors. Methods based on kinetic and thermodynamic theory are proposed for predicting concentrations of nitrogen oxides and carbon monoxide in the combustion gases of flames, specifically of lean, stoichiometric, and rich propane-air flames. These theoretical data are compared with concentrations observed experimentally downstream of flat grid-type burner flames (approximately 25,000 Btu/hr) that were used to simulate gas appliances such as water and space heaters. Air pollutant concentrations were computed for (1) flames chemically perturbed by recycling flue gases into the primary fuel-air mixtures; (2) flames thermally perturbed by cooling the burned gases at different rates; and (3) flames perturbed by combinations of these two effects. In general, experimental and computed concentrations agreed to within a factor of 2 to 4 with the experimental values always being higher than the theoretical. Cooling the burned gases and recycling cold flue gases (with and without excess air) reduced the relative amount of nitric oxides. Carbon monoxide concentrations were substantially reduced by recycling flue gases only when the cooling rates were less than about 5000-10000°R per second.

TRACE ORGANIC COMPOUNDS IN NATURAL GAS COMBUSTION

by

J. A. Chisholm, Jr. and D. L. Klass

Institute of Gas Technology
Chicago, Illinois 60616

INTRODUCTION

Complete combustion is decidedly easier to obtain with natural gas than with any other fossil fuel.⁵ Under normal operating conditions, the flue products of natural-gas-burning equipment are relatively free of unburned hydrocarbons and partial combustion products. However, under fuel-rich conditions, small quantities of organic derivatives are produced. The investigation reported in this paper to identify and determine the quantities of these trace compounds, particularly when combustion occurs under low-aeration conditions, was carried out at the Institute of Gas Technology, with financial support of the American Gas Association.

Classical wet chemical procedures lack the sensitivity and selectivity for analyses of these trace organic compounds. Consequently, highly sensitive instrumental methods were used, with modifications whenever necessary.

EQUIPMENT

The source of combustion products was the burner system shown in Fig. 1. It consists of a burner, transite base, and glass chimney. When the burner is operated at the low flow rates employed in this study, a bunsen-type flame is obtained. Disturbance of the flame by air currents, and dilution of the exhaust gases by surrounding air, were prevented by enclosing the burner in a pyrex glass chimney. Samples of flue products were withdrawn either from the top of the chimney or through the probe.

Early in the investigation, the base of the burner system was modified as shown in Fig. 2; a secondary air chamber, with 1/8-in. steel spheres in it to facilitate diffusion, was installed.

The burner was operated on 1000 Btu natural gas similar in composition to that shown in Table 1, and numerous experiments were carried out under a variety of conditions. Since space does not permit a detailed description of the experimental techniques, only a few comments can be made here.

Combustion conditions varied from fuel-rich to stoichiometric operation. The extreme fuel-rich variable corresponded to flow rates of 2 CF/hr of natural gas, no primary air, and 10 CF/hr of secondary air. Stoichiometric conditions corresponded to flow rates of 2 CF/hr of natural gas and 17.5 CF/hr of primary air. Secondary air was employed in selected stoichiometric experiments. Sufficient experiments were carried out to insure the reproducibility of the analytical determinations under the specific operating conditions. All determinations of specific

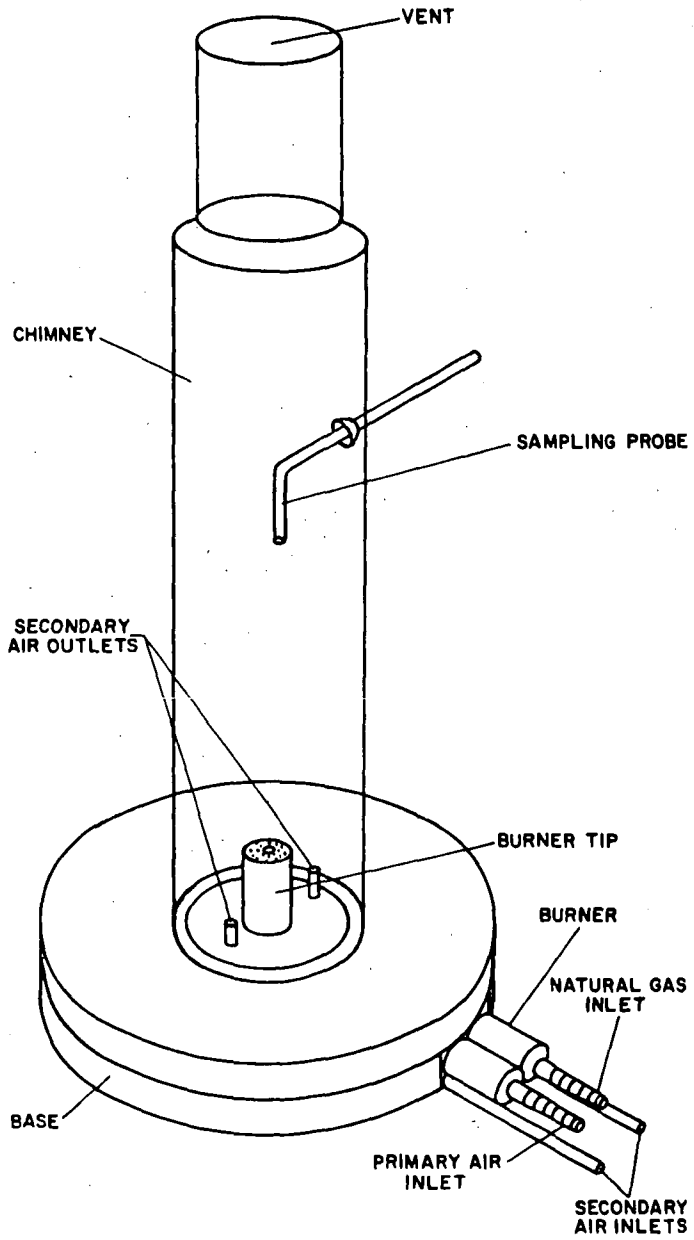


Fig. 1.-CLOSED BURNER SYSTEM FOR COMBUSTION OF NATURAL GAS

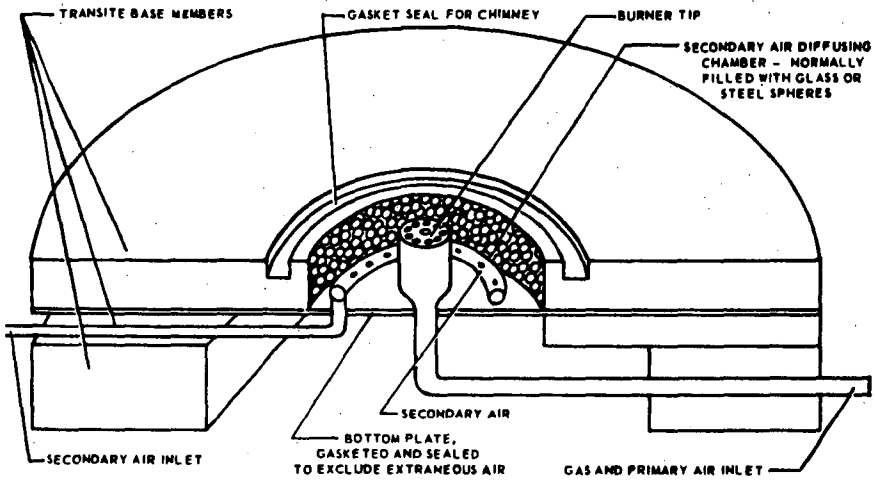


Fig. 2.—MODIFIED BURNER BASE

flue products were normalized to percentages of the total flue products

RESULTS

During this investigation, a large number of saturated and unsaturated aliphatic, polynuclear aromatic, and oxygenated hydrocarbons were identified. Many were determined quantitatively in the ppb (parts per 10^9) concentration range. Table 2 gives a partial list of the organic compounds found in the combustion products under stoichiometric and fuel-rich operating conditions.

Gas chromatography with a flame ionization detector was employed to measure C_1 to C_5 saturated and unsaturated aliphatic hydrocarbons. Under essentially complete combustion conditions, the C_1 to C_5 hydrocarbons were present in the flue products in the ppb range, and several C_4 and C_5 compounds were below limits of detectability, as shown in Tables 3 and 4. When primary air was absent, concentrations of the C_1 to C_5 hydrocarbons varied inversely with the secondary air flow. Total C_5 + hydrocarbons were determined by reversing carrier gas flow in the chromatographic column and backflushing after the emergence of n-butane. Again, the inverse relationship of concentration to secondary air flow was observed, as shown in Table 5.

An alumina column operated at 80°C with argon carrier gas served to separate the C_1 to C_3 fraction. The C_4 to C_5 fraction was separated on a $1/8$ in. x 15 ft column of 28% dimethylsulfolane on Chromasoro P. Separation of total C_5 + hydrocarbons was effected on a $1/8$ in. x 6 ft alumina column operating at 100°C .

Polynuclear aromatic hydrocarbons were collected in a low-temperature trapping system, and separated by means of liquid extractive procedures and column, paper, and gas chromatography. Ultraviolet absorption and fluorescence spectrophotometry were then employed to identify the separated fractions. By these techniques, fifteen polynuclear aromatic compounds were identified; seven of these were determined quantitatively. Quantitative determination was based on separation via column chromatography, and identification and measurement were accomplished by ultraviolet fluorescence spectrophotometry. Table 6 shows that the concentrations ranged from less than 0.1 ppb for o-phenylenepyrene under conditions of essentially complete combustion, to 1040 ppb for pyrene under fuel-rich conditions.

Several classes of oxygenated hydrocarbons were investigated, including aldehydes, phenols, and ketones. Because aldehydes are always produced during incomplete combustion,¹⁸ these compounds were studied in some detail. The spectrophotometric methods used are specific for formaldehyde, acrolein, total aliphatic aldehydes and total aldehydes. Table 7 shows that when only secondary air was present, the concentration of total aldehydes was inversely related to the flow of secondary air. In the absence of secondary air, but with sufficient primary air to ensure essentially complete combustion, aldehydes were produced in only ppb concentrations. Formaldehyde was predominant, and persisted under all but stoichiometric combustion conditions. With increased secondary air, a generally increasing ratio of formaldehyde to other aldehydes was observed. These findings are consistent with the reported stability of formaldehyde.¹⁸

Table 1.—Typical Analysis of Chicago Natural Gas

Component	Mole %	Component	Mole %
Air	3.21	Propane	1.21
Helium	0.08	n-Butane	0.17
Nitrogen	1.79*	i-Butane	0.08
Carbon dioxide	0.63	Pentanes	0.04
Methane	88.21	Hexanes	0.03
Ethane	4.51	Heptanes	0.04
			100.00

Heating Value - 1001 Btu/SCF, Saturated gas at 60°F, 30 in. Hg.

*Nitrogen in excess of that included in air.

Table 2.—TYPES AND QUANTITIES OF ORGANIC COMPOUNDS FOUND IN THE COMBUSTION PRODUCTS OF A NATURAL GAS FLAME

Type of Compound	Concentration Found after	
	Stoichiometric Combustion	Fuel-Rich Combustion
Aldehydes:		
Formaldehyde	< 0.02 ppm	20 ppm
Other Aliphatic Aldehydes	< 0.02	13
Nonaliphatic Aldehydes	< 0.02	6
Total Aldehydes	< 0.02	39
Polynuclear Aromatics:		
Anthanthrene	< 3.0 ppb	275 ppb
Anthracene	< 0.4	46
Benzo [a] pyrene	0.4	89
Fluoranthene	6.0	468
1-Methylpyrene	0.6	78
o-Phenylene-pyrene	0.1	84
Pyrene	14.0	1040
Other Hydrocarbons:		
Methane	0.08 ppm	60,000 ppm
Ethane	0.13	3,500
Propane	0.10	900
i-Butane	< 0.01	50
n-Butane	< 0.01	70
Pentane plus	< 5.00	120
Acetylene	< 0.01	2,500
Ethylene	0.06	4,000
Propylene	< 0.01	260

Table 3.—CONCENTRATION OF SOME C₁ - C₄ HYDROCARBONS AT VARIOUS AERATION LEVELS

Air Input, CF/hr		Concentration ppm									
Primary	Secondary	Alkanes				Alkenes				Acetylene	
		Methane	Ethane	Propane	i-Butane	n-Butane	Ethylene	Propylene	Acetylene		
0	30	0.08*	-	0.02	<0.01	<0.01	0.09	<0.01	<0.01	<0.01	
		0.08*	-	0.11	<0.01	<0.01	0.03	<0.01	<0.01	<0.01	
0	25	3.4	0.16	0.11	<0.01	<0.01	0.84	0.07	0.07	4.6	
		1.6	0.09	0.04	<0.01	<0.01	0.61	<0.02	<0.02	3.3	
		5.2	0.16	0.01	<0.01	<0.01	1.37	0.03	0.03	4.7	
0	20	2800	23.3	0.17	<0.02	<0.02	161	2.3	2.3	240	
		2100	25.0	0.13	<0.02	<0.02	162	2.1	2.1	240	
		1900	22.1	0.16	<0.02	<0.02	182	2.1	2.1	250	
0	17.5	7000	72	1.3	<0.02	<0.02	410	7.8	7.8	910	
		7300	72	1.3	<0.02	<0.02	470	7.7	7.7	850	
		7300	69	1.3	<0.02	<0.02	470	7.9	7.9	880	
0	15	12,500	117	2.3	0.06	0.06	910	17.5	17.5	1400	
		16,300	138	2.2	0.05	0.04	1080	20.2	20.2	1500	
		14,600	-	2.5	0.8	0.06	1030	20.1	20.1	1500	
0	12.5	26,200	343	7.0	-	0.25	1700	68.0	68.0	1900	
		29,200	352	6.9	0.04	0.17	1800	58.5	58.5	2000	
		29,000	441	6.2	0.13	0.20	1800	57.5	57.5	2000	
0	10	58,300	1223	45.4	2.2	3.8	3700	118	118	2600	
		39,100	964	42.1	1.5	2.2	3100	108	108	2600	
		33,200	1048	48.7	0.6	3.9	2700	97	97	2300	
20	0	0.04*	-	<0.01	<0.01	<0.01	<0.01	<0.01	<0.01	<0.01	
		0.04*	-	<0.01	<0.01	<0.01	<0.01	<0.01	<0.01	<0.01	
		0.04*	-	<0.01	<0.01	<0.01	<0.01	<0.01	<0.01	<0.01	
15	0	0.41*	-	<0.01	<0.01	<0.01	<0.01	<0.01	<0.01	<0.01	
		0.37*	-	<0.01	<0.01	<0.01	<0.01	<0.01	<0.01	<0.01	
		0.44*	-	<0.01	<0.01	<0.01	<0.01	<0.01	<0.01	<0.01	
12.5	0	12.8*	-	<0.01	<0.01	<0.01	1.5	<0.01	<0.01	5.2	
		5.4*	-	<0.01	<0.01	<0.01	.5	<0.01	<0.01	2.4	
		15.4*	-	<0.01	<0.01	<0.01	2.4	<0.01	<0.01	9.2	
		19.2*	-	<0.01	<0.01	<0.01	3.2	<0.01	<0.01	-	
10	10	.05*	-	<0.01	<0.01	<0.01	<0.01	<0.01	<0.01	<0.01	
		.05*	-	<0.01	<0.01	<0.01	<0.01	<0.01	<0.01	<0.01	

* Composite methane and ethane peak.

Table 4. - AIR FLOW VS. C₄-C₅ CONCENTRATIONS

Run No.	<u>41b</u>	<u>40a</u>	<u>40b</u>	<u>41a</u>	<u>42a</u>
Flow Rates, CF/hr					
Primary Air	0	0	0	0	17.5
Secondary Air	10	15	20	25	0
Natural Gas	2	2	2	2	2
Concentration, ppm*					
Butene-1	1820	550	165	17	<0.05
<u>i</u> -Butene	<0.05	<0.05	<0.05	<0.05	<0.05
<u>trans</u> -Butene-2	50	8	2	<0.05	<0.05
<u>i</u> -Pentane	<0.05	<0.05	<0.05	<0.05	<0.05
<u>cis</u> -Butene-2	<0.05	<0.05	<0.05	<0.05	<0.05
Pentane	<0.05	<0.05	<0.05	<0.05	<0.05
3-Methylbutene-1	<0.05	<0.05	<0.05	<0.05	<0.05
1,3-Butadiene	40	9	1	<0.05	<0.05
Pentene-1	118	43	7	<0.05	<0.05

* Chromatograph calibrated on basis of response to n-butane

Table 5.-C₅ + HYDROCARBONS

*Air Input, CF/hr,		Total C ₅ + Hydrocarbons,	Air Input, CF/hr		Total C ₅ + Hydrocarbons,
Primary	Secondary	ppm	Primary	Secondary	ppm
5	10	<5	0	25	<5
5	5	30	0	20	<5
			0	15	<5
			0	12.5	80
2.5	10	<5	0	12.5	100
2.5	7.5	20	0	10	90
2.5	7.5	14	0	7.5	110
2.5	5	85	0	7.5	144

* Natural Gas Input, 1 CF/hr

Table 6.-POLYNUCLEAR AROMATIC HYDROCARBONS
DETERMINED IN NATURAL GAS COMBUSTION PRODUCTS

<u>Aeration Conditions</u>	<u>Flow Rate, CF/hr</u>				
	<u>Run No.</u>				
	<u>9</u>	<u>5R</u>	<u>7</u>	<u>8</u>	<u>10</u>
Primary air	0	0	0	0	17.5
Secondary air	10	15	20	25	0
Natural gas	2	2	2	2	2
<u>Component</u>	<u>Concentration, ppb</u>				
Anthanthrene	240	275	11	<3	<3
Anthracene	26	46	6	6	<0.4
Benzo[a] pyrene	89	78	40	11	0.4
Fluoranthene	434	468	256	117	6
1-Methylpyrene	78	48	11	4	0.6
o-Phenylene pyrene	75	75	84	43	<0.1
Pyrene	1040	454	155	103	14

Table 7.-AIR FLOW VS. ALDEHYDE PRODUCTION

<u>Run No.</u>	<u>Flow Rates, CF/hr</u>			<u>Aldehyde Concentration, ppm</u>		
	<u>Primary Air</u>	<u>Secondary Air</u>	<u>Natural Gas</u>	<u>Formaldehyde</u>	<u>Aliphatic Aldehydes</u>	<u>Total Aldehydes</u>
3	0	10	2	19.4	32.9	39.3
4	0	15	2	18.4	25.6	34.6
5	0	20	2	13.4	13.1	18.5
6	0	25	2	2.4	1.9	6.0
8	17.5	0	2	<0.02	<0.01	<0.02

The unsaturated aldehyde acrolein occurs in the exhaust gases from most combustion processes.^{2,7,8,12} Under fuel-rich combustion conditions, acrolein concentrations ranging from less than 0.03 ppm (parts per million) to about 6 ppm (Table 8) were determined by a spectrophotometric method.

Phenols are another group of oxygenated organic derivatives that is known to be present in combustion products from natural gas flames.¹³ Total phenol concentrations varied from 0.007 ppm to about 4 ppm (Table 9).

Several spectrophotometric procedures were investigated for determination of ketones, but interference from water and formaldehyde introduced excessive error. Gas chromatography, however, resulted in accurate determinations of several ketones, as shown in Table 10.

Chromatographic studies gave tentative evidence of the presence of methyl and ethyl alcohols in the flue products. Quantitative measurements were not made, but methyl alcohol peak areas indicated concentrations of about 3 ppm.

DISCUSSION

The experimental data collected in our investigation of the flue products from fuel-rich flames might be interpreted in terms of numerous hypothetical reaction mechanisms that have no real meaning. Instead, let us consider how the formation of trace components produced under poor combustion conditions can be rationalized and qualitatively explained in terms of a few reaction mechanisms which are known to be operative in fuel-rich flames. (Carbenes and perhaps methyne are very likely involved in the formation of flue-gas combustion products; but they are not considered in this treatment.)

Many of the major mechanisms operative in lean flames are reasonably well understood, but the organic chemistry of fuel-rich flames presents a considerably more complex situation.³ The initial reactions in a fuel-rich methane-oxygen flame have been shown to involve formation of methyl radicals, which are probably produced by hydrogen atom abstraction:



The methyl radicals might be called the "key intermediates" in the combustion of methane in fuel-rich systems because their concentration is sufficient to produce other structures by conversion to higher molecular weight intermediates. Subsequent chemical reactions of methyl radicals in fuel-rich flames therefore determine, to a large extent, the structures of the partial combustion products. We should thus be able to relate our experimental results to these methyl radical reactions, especially those that occur with small or essentially zero activation energies.

First, the reaction of methyl radicals with oxygen would not be expected to be the dominant one in an oxygen-deficient flame, but the reaction should occur to some degree with formation of peroxy radicals:

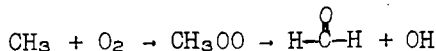


Table 8. -AIR FLOW VS. ACROLEIN PRODUCTION

Run	Natural Gas, CF/hr	Air, CF/hr		Acrolein, ppm
		Primary	Secondary	
21	2	17.5	0	<0.03
22	2	0	10	6.3
23	2	0	15	5.6
24	2	0	20	5.3
25	2	0	25	2.9

Table 9. -AIR FLOW VS. PHENOL PRODUCTION

Run No.	Flow Rates, CF/hr			Phenol Concentration, ppm*
	Primary Air	Secondary Air	Natural Gas	
4	0	10	2	4.0
5	0	15	2	4.1
6	0	20	2	1.0
7	0	25	2	0.5
8	17.5	0	2	0.026
9	25.0	0	2	0.007

* Calibration curves were prepared with phenol solutions as standards.

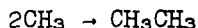
Table 10. -AIR FLOW VS. CARBONYL PRODUCTION

Run	Natural Gas, CF/hr	Air, CF/hr		Carbonyl Production, ppm			
		Primary	Secondary	Acetaldehyde	Acrolein-Acetone	Propionaldehyde	2-Butanone
3637-1	2	0	10	6.2	1.5	0.07	1.6
3637-2	2	0	15	3.4	0.8	0.03	1.0
3637-3	2	0	20	2.9	1.2	0.05	1.8
3637-4	2	0	25	5.0	1.5	0.01	2.8

These radicals are known to decompose rapidly to yield formaldehyde.^{14,17} Further oxidation of formaldehyde would be expected, even in an oxygen-deficient flame, because of the high reactivity of aldehyde groups.

Since the rate of formation of formaldehyde should be greater than the rates of formation of the higher aldehydes from the methyl-radical-derived intermediates that will be discussed later, we would expect formaldehyde to be present in higher concentrations than the other aldehydes in the flue gases. As already shown in Tables 2 and 7, over half of the total aldehydes in almost all of our experiments was formaldehyde when the flue products were produced under oxygen-deficient conditions.

Recombination of excess methyl radicals in oxygen-deficient flames:



would be favored over methyl radical-oxygen reactions, so larger concentrations of ethane relative to formaldehyde would be expected in the flue gases. The formation of ethane in this type of recombination reaction, however, is not as simple as it appears. When the new carbon-to-carbon bond is formed, a large amount of energy is liberated. This energy, along with the original thermal energy carried by the methyl radicals, can dissociate ethane back to methyl radicals, or the resulting vibrationally excited ethane molecules can be deactivated by a three-body collision process. In the presence of a third body, such as another molecule with which the energy-rich ethane molecules collide, the excess energy can be transferred with concurrent formation of substantial amounts of ethane without homolytic dissociation to methyl radicals. However, according to Kistiakowsky,⁴ the energy-rich ethane molecules initially produced do not necessarily require a three-body process to prevent dissociation.

Since methyl radical recombination is a direct one-step path to a stable paraffin, one would expect larger concentrations of ethane than the higher paraffins in the flue gases. This conclusion is supported by the results summarized in Table 2. Significantly higher concentrations of ethane than propane were detected in the flue products under oxygen-deficient conditions. The concentrations of propane were in turn higher than the total C₄+ paraffin concentrations. The natural gases studied in this investigation contained a few percent ethane and propane, but the relative ratios of these hydrocarbons in the flue gases should still be indicative of the combustion mechanism.

The mechanism of formation of ethylene and acetylene in a methane-rich flame has not been fully established, but the general course of the reactions is believed to proceed through C₂ radical intermediates.¹¹ Successive dehydrogenation of ethane yields ethylene and acetylene. The detailed mechanism of the dehydrogenation is not known.⁹ Homolytic C-H bond rupture by unimolecular decomposition or hydrogen atom abstraction should be facilitated in methane-rich flames, because methyl radical recombination affords energy-rich ethane molecules. We therefore expect that stepwise dehydrogenation of ethane proceeds via an ethyl radical intermediate:



to yield substantial amounts of ethylene and acetylene relative to the

other unsaturates. Formation of ethyl radicals subsequently provides direct routes to propane and the butanes, but dehydrogenation should be the preferred reaction path because of the favorable kinetics at high temperatures.⁹

Thus, the formation and relative concentration of the major oxygenated and saturated and unsaturated aliphatic compounds detected as trace components in the flue gases of methane-rich flames have been rationalized on the basis of a few known radical reactions. It should be emphasized that these reactions are by no means the only paths to the observed compounds, but their relationship to the experimental results indicates that they are important.

It is much more difficult to explain the formation of the polynuclear aromatics listed in Table 2. Grossly empirical reaction mechanisms must be postulated because of the complexity of polynuclear aromatic structures.¹⁵ Nevertheless, we believe that a few important conclusions can be drawn from the data collected in our work.

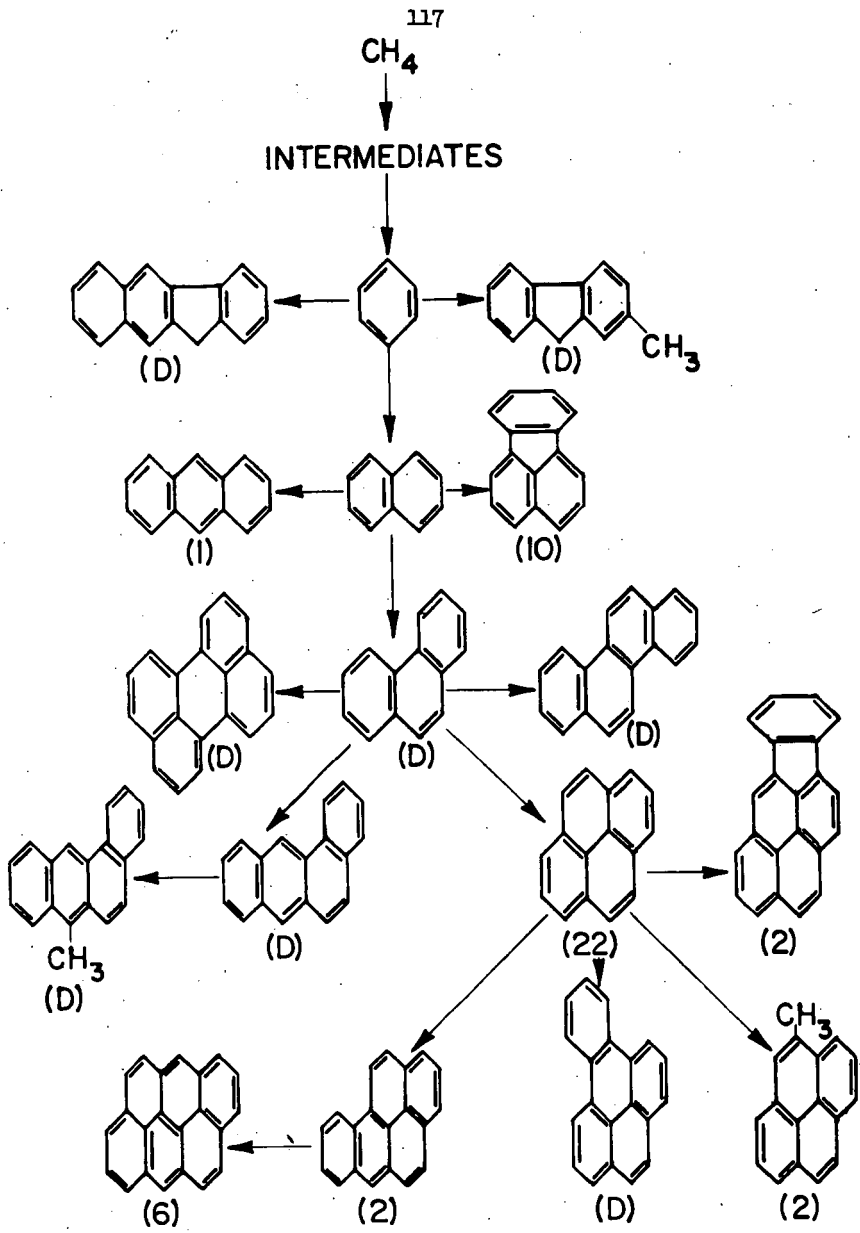
Most investigators who have studied the formation of polynuclear aromatics found that these compounds generally form under fuel-rich conditions.^{6,15} Our data, which include determinations of both aliphatic and aromatic compounds, show that fuel-rich conditions promote polynuclear aromatics formation, but at very low levels relative to the concentrations of the aliphatic compounds. It is therefore difficult to select a particular aliphatic compound, or group of compounds, as key intermediates in the mechanism of formation of the aromatic compounds.

Aliphatic intermediates are, however, clearly the precursors of the aromatic compounds because the natural gases used in our experiments contained zero polynuclear aromatics. Various investigators have suggested that methyne and unsaturates such as ethylene and acetylene play an important role as intermediates.^{6,10,11,15} Empirical reaction paths have also been postulated to account for the formation of polynuclear aromatics from these and other intermediates.¹⁵

In several experiments, our determinations of the polynuclear aromatics formed in fuel-rich flames tend to fall into a particular pattern. The higher molecular weight polynuclear aromatics in the flue gas were consistently present in lower concentrations than those of lower molecular weight. Although other investigators have reported similar results,¹⁰ this information is insufficient for valid conclusions regarding the mechanisms of formation.

However, significant observations can be made. The distribution of the aromatics was about the same in each of our experiments, as shown in Table 6. Furthermore, this distribution corresponds essentially to that reported by others.^{6,10,15} Finally, we observed that the relative concentrations of a few specific polynuclear aromatics are consistently higher than the concentrations of the other aromatics.

These observations suggest that the overall scheme shown in Fig. 3 is a plausible route to the various aromatic compounds identified in our studies. The reactive species and fragments involved in the many reactions required to produce the polynuclear aromatics are, of course, not known. But our results and their apparent relationship to the scheme in Fig. 3 support a stepwise buildup of the higher aromatics through common intermediates. A similar scheme can also be developed with Lindsey's data.¹⁰



A-56493

Fig. 3.—POSSIBLE ROUTES TO POLYNUCLEAR AROMATIC COMPOUNDS

Other interpretations of the distribution of the aromatics (Table 2), such as consideration of their relative stabilities, can be employed to rationalize the results. For example, linearly annelated acenes are known to be more reactive than phenes containing the same number of rings.¹ Thus, one would not expect a large concentration of acenes relative to the angularly annelated phenes in the flue products. Our experimental data show that only one acene, anthracene, was detected. Most of the polynuclear aromatics determined in this investigation contain the phenanthrene nucleus.

Quantitative treatment of the distribution of polynuclear aromatics in terms of electron densities and bond localization energies will be attempted when additional data have been compiled.

REFERENCES CITED

1. Clar, E. J., "Polycyclic Hydrocarbons," Vol. 1. New York: Academic Press, 1964.
2. Cohen, I. R. and Altshuler, A. P., "A New Spectrophotometric Method for the Determination of Acrolein in Combustion Gases and in the Atmosphere," Anal. Chem. **33**, 726-33 (1961) May.
3. Fristrom, R. M. and Westenberg, A. A., "Flame Structure," Chapter XIV. New York: McGraw-Hill Book Company, 1965.
4. Gomer, R. and Kistiakowsky, G. B. The Rate Constant of Ethane Formation From Methyl Radicals," J. Chem. Phys. **19**, 85-91 (1951) January.
5. Griswold, S. S., Chass, R. L., George, R. E. and Holmes, R. G., "An Evaluation of Natural Gas as a Means of Reducing Industrial Air Pollution," J. Air Pollution Control Assoc. **12**, 155-63 (1962) April.
6. Hangebrauck, R. P., Von Lehmden, D. J. and Meeker, J. E., "Emissions of Polynuclear Hydrocarbons and Other Pollutants From Heat-Generation and Incineration Processes," J. Air Pollution Control Assoc. **14**, 267-78 (1964) July.
7. Hughes, K. J. and Hurn, R. W., "A Preliminary Survey of Hydrocarbon-Derived Oxygenated Material in Automobile Exhaust Gases," J. Air Pollution Control Assoc. **10**, 367-73 (1960) October.
8. Kryacos, G., Menapace, H. R. and Boord, C. E., "Gas-Liquid Chromatographic Analysis of Some Oxygenated Products of Cool-Flame Combustion," Anal. Chem. **31**, 222-25 (1959) February.
9. Leroux, P. J. and Mathieu, P. M., "Kinetics of the Pyrolysis of Methane to Acetylene," Chem. Eng. Progr. **59**, 54-59 (1961) November.
10. Lindsey, A. J., "The Formation of Polycyclic Aromatic Hydrocarbons and Carbon Deposits From Normal and Reversed Diffusion Flames," Combust. Flame **4**, 261-64 (1960) September.

11. Miller, S. A. "Acetylene; Its Properties, Manufacture, and Uses," Vol. 1. New York: Academic Press, 1965.
12. Sharma, R. K., McLean, D. R. and Bardwell, J., "An Apparatus for the Analysis of Combustion Products Obtained during the Oxidation of Hydrocarbons," Indian J. Technol. 3, 206-08 (1965) July.
13. Smith, R. G., MacEwen, J. D. and Barrow, R. E., "The Occurrence of Phenols in Air and Combustion Products," Am. Ind. Hyg. Assoc. J. 20 149-52 (1959).
14. Sugden, T. M., "Reactions of Free Radicals in the Gas Phase," Special Publication No. 9. London: The Chemical Society, 1957.
15. Tebbens, B. D., Thomas, J. F. and Mukai, M., "Hydrocarbon Synthesis in Combustion," A.M.A. Arch. Ind. Health 13, 567-73 (1956) June; *ibid.*, "Aromatic Hydrocarbon Production Related to Incomplete Combustion," A.M.A. Arch. Ind. Health 14, 413-25 (1956) November.
16. Thomas, J. F., Sanborn, E. N., Mukai, M. and Tebbens, B. D., "Aldehyde Production Related to Combustion and Polluted Atmospheres," Ind. Eng. Chem. 51, 774-75 (1959) January.
17. Walsh, A. D., "Processes in the Oxidation of Hydrocarbon Fuels - II.," Trans. Faraday Soc. 43, 297-305 (1947).
18. Wilson, K. W., "Fixation of Atmospheric Carbonyl Compounds by Sodium Bisulfite," Anal. Chem. 30, 1127-29 (1958) June.

CHEMICAL COMPOSITION OF PROGRESSIVE PYRIDINE EXTRACTS FROM COAL

R. A. Friedel, J. L. Shultz, and A.G. Sharkey, Jr.

U.S. Department of the Interior, Bureau of Mines,
Pittsburgh Coal Research Center, Pittsburgh, Pa.

SUMMARY

Progressive extraction of coal with pyridine for different periods of time has shown, by mass spectral and other analyses, that certain types of constituents are prominent in the early stages of extraction. Alkylbenzenes and phenols predominate in the first extract; polynuclear aromatics are found to be extracted later. The order of extraction is important in the mechanism of extraction of coals.

INTRODUCTION

Solvent extraction of coal has been used for many years in studying the constitution of coal. With pyridine, one of the best coal solvents, an appreciable fraction of the original can be extracted from high volatile and medium volatile bituminous coals. For these coals the extract is considered fairly representative of the whole coal, and experiments carried out on the extracts are therefore reasonably representative of the whole coal. The pyridine extract itself is generally considered to yield but little more information than does the parent coal; it is qualitatively quite similar to the coal.^{1/} But the extract does present a more tractable sample than the coal and makes possible further processing in solution. And, as shown before, there are quantitative differences between extract and residue.^{1,2/} The principal practice in solvent extraction is exhaustive extraction of the sample in order to obtain the highest yield possible. Dryden has looked closely at the effect of time of extraction on the yield of extract.^{3/}

In extracting coals under various conditions for mass spectrometric investigations, questions arose concerning a possible order of components coming out of the coal. Are all chemical entities extracted simultaneously? Are the following pairs extracted together or in succession: Aliphatics and aromatics, alkylbenzenes and alkyl-naphthalenes, cyclic hydrocarbons and heterocyclics, acids and bases, etc.? Dormans and van Krevelen^{4/} found that molecular weights of the fractions increase with increasing extraction time; van Krevelen^{5/} has used such extraction data and polymer theory to find the interesting result that the extractability of coal solvents can be calculated.

To our knowledge no detailed characterization of the products from successive extractions, a method introduced by Rybicka,^{6/} has been carried out; the comparison of infrared spectra by Brown^{1/} is cited above. We have investigated possible effects of extraction time on composition of the extracts by utilizing progressive extraction, which differs from the successive extraction method of Rybicka^{6/} in that only one solvent is used and extraction times are varied from a few minutes to many hours. Mass spectrometry was used as the principal tool of investigation. Previously we have shown that low ionizing voltage mass spectra of coal extracts can determine quantitatively families of derivatives of various aromatic nuclei that are volatile at 300° C in a vacuum.^{1/} Preliminary experiments on the extraction process quickly showed that after many minutes of extraction there was no longer any difference, detectable by mass spectrometry, in the compositions of the extracts. It was concluded that the effects of progressive extraction would be illustrated best if samples were collected after 5 minutes, after 30 minutes, and after many hours of extraction.

EXPERIMENTAL PROCEDURE

The procedure for progressive extraction was: One gram of Pittsburgh coal of < 200 mesh was combined with 2 cc of pyridine. The mixture was shaken mechanically for 5 minutes, after which time the sample was opened and the solution immediately filtered to remove the extract and solvent from further contact with the coal. The extract solution was immediately centrifuged in order to remove the extract from any minute amounts of coal remaining. The coal thus separated from the extraction process was subjected to a further extraction with a new sample of added pyridine and the extraction was carried out for 30 minutes. At the end of 30 minutes the isolation of the extract was repeated as before. The process was then carried out again after 17 hours of extraction and an extract was again separated.

The mass spectrometer was a Consolidated Electrodynamics Corp. 21-103C with a heated inlet system fabricated in our laboratory and usually operated for this work at 290° C. Data on aromatics were obtained from low-ionizing voltage spectra.

The material analyzed by the mass spectrometer is that material that is sufficiently volatile to be observable. The remainder of each extract is unknown. The significance of the data obtained lies in the comparison of families of aromatics observed for the various extracts. Comparison of weight-average molecular weights with those published is not meaningful. It was determined that 90 percent of the material volatilized at 300° C from Pittsburgh coal is removed from coal by pyridine extraction. For this reason it is believed that the mass spectra of pyridine extracts are representative of the extract and of the coal. Good reproducibility of mass spectra of extracts has been established.^{7/}

RESULTS AND DISCUSSION OF RESULTS

Mass Spectra. The mass spectral analyses and the amounts of extract obtained in terms of percent of the original coal are indicated in table 1. Results of the mass spectral analyses indicate the following: (1) One- and 2-ring aromatics predominate in the 5-minute extract; higher aromatics predominate with longer extraction times. This is expected on the basis that lower molecular weight materials would be present in this extract.^{4,5/} (2) Percentages of benzenes, phenols, and naphthalenes were much greater for the 5-minute extract than for the other two extracts. (3) Yields of phenanthrenes-anthracenes and higher aromatics in the 5-minute extract are all less than those in the longer-time extracts. (4) The largest components found in the 5-minute extract are 4-ring, cata- and peri-condensed aromatics; the 30-minute and 17-hour extracts show components up through 6 rings peri-condensed. (5) The 30-minute extract contains slightly higher concentrations of 3-ring and smaller aromatics; the 17-hour extract contains slightly greater amounts of 4-ring and larger components. (6) Within a family of aromatics (e.g., C₆H₆, C₇H₈, C₈H₁₀, etc.) the distribution maximizes at the lowest molecular weight for the 5-minute extract. This is observed for benzenoids and phenols. Maxima for the other two extracts occur at higher molecular weights.

The larger concentration of phenols in the initial 5-minute extract is a significant finding. It is a direct indication that the basicity of pyridine is an important factor in coal extraction. Van Krevelen has shown that the differences in solubility parameters,⁶ for coals and solvents are apparently of great importance in the extractability of coal solvents; he acknowledged that chemical properties are also likely to be very important.^{5/} Dryden^{3/} and Halleux and Tschamler^{8/} have shown that the availability of free electron pairs in hydrogen bonding solvents such as pyridine is important in interactions with acidic materials.

The beginning of the pyridine extraction process may be the "unlocking" of the coal structure through dissolution of phenolic structures, which are apparently hydrogen bonded (infrared spectra of coals indicate only hydrogen bonded OH, no free OH). However, it has not been established whether the "unlocking" process actually involves the breaking of hydrogen bonded structures.

Infrared Spectra. The spectra of extracts and residues were compared. As described by Brown, there are no qualitative differences, but there are semi-quantitative indications of changes in infrared absorption with extent of extraction.¹ Quantitative differences are appreciable as we found on comparing spectra of extracts and coals.² On the question of "unlocking" of hydrogen bonded structures in coal the infrared spectrum of the 5-minute extract indicates a slightly higher absorption at 1260 cm^{-1} . This absorption is attributable to phenolic structures, so a slightly greater concentration of phenolic structures is indicated for the initial, 5-minute extract. This result is at least some corroboration for the mass spectral indication of a higher phenol concentration in the 5-minute extract. The OH stretching band at 3300 cm^{-1} is not a reliable indication of phenolics in coal.

Aliphatic CH absorption in residues and extracts are compared in table 2. The residue from the 30-minute extract shows an absorbance decrease of 46 percent relative to the extract. Also it is interesting to note that the highest aliphatic C-H concentration occurs in the 30-minute extract; the aliphatic C-H content of the 5-minute extract is somewhat lower.

The CH content of the residues are all smaller than the corresponding extracts. Also, residues show decreasing C-H contents with increase in extraction, which is expected in view of the greater CH absorption bands found in the extracts.^{1,2}

All absorption bands in the residues are slightly weaker and less well-defined than the corresponding bands in the extracts. The spectrum of a coal is most influenced by the sharper absorption spectra of the extract which are attributable to components high in hydrogen, both aromatic and saturated.

Aliphatic/Aromatic Ratios. Determination of the aliphatic/aromatic ratios of the various extracts were attempted by comparison of total ionization from mass spectra at low and high ionizing voltage. This comparison indicated that the 5-minute extract was slightly lower in aliphatic content. This result was considered dubious, but the infrared result apparently confirms it as the aliphatic CH content of the 5-minute extract is indeed slightly lower than that of the 30-minute extract (table 2).

Table 1.- Fractions from the progressive extraction of Pittsburgh seam (hvab) coal with pyridine^{a/}

Extraction time, hours	0.08	0.5	17
Extract, weight percent of coal	2.4	4.6	12.3

Aromatic compound types,
including
alkyl derivatives

Weight percent

Mass spectral analyses:^{b/}

Benzenes	29.2	1.9	1.9
Phenols	10.8	3.1	3.2
Dihydric and/or alkoxyphenols		.5	.5
Naphthalenes	25.4	13.5	12.2
Indenes; naphthols		1.1	.7
Indans		1.5	1.0
Indanols	1.8	2.2	2.1
Acenaphthenes	6.0	6.6	6.2
Acenaphthylenes; fluorenes	10.8	6.8	6.4
Anthracenes; phenanthrenes	3.0	10.6	9.9
Naphthalenes, phenyl substituted	5.5	7.8	7.6
4-ring, cata-condensed	2.5	7.9	8.6
4-ring, peri-condensed	4.5	11.2	11.9
3-ring, phenyl substituted	.5	7.2	7.9
5-ring, cata-condensed		8.0	8.9
5-ring, peri-condensed		7.0	7.6
6-ring, peri-condensed		3.1	3.4

^{a/} One of two complete runs.

^{b/} Compounds containing N, S, and non-phenolic O are probably also present.

Table 2.- Infrared spectra of coal extracts. Absorbance values at 2920 cm⁻¹, aliphatic C-H absorption band

Extraction time, hours	Absorbance at 2920 cm ⁻¹	
	Extract	Residue
0.08	.22	.15
0.5	.26	.14
17.0	.16	.11

References

1. Brown, J. K. Infrared Spectra of Solvent Extracts. Fuel, v. 38, 1959, pp. 55-63.
2. Friedel, R. A. Infrared in Coal Structure Research. Ch. in "Applied Infrared Spectroscopy," ed. D. N. Kendall, Reinhold Publ. Co., New York, pp. 312-343.
3. Dryden, I.G.C. Nature of Specific Solvents for Bituminous Coals. Nature, v. 166, 1950, pp. 561-562.
_____. The Apparent Solubility of Colloidal Materials. Far. Soc. Disc., v. 11, 1951, pp. 28-42.
4. Dormans, H.N.M., and D. W. van Krevelen. Chemical Structure and Properties of Coal. XXVII-Composition and Molecular Weight Distribution of Coal Extracts. Fuel, v. 39, 1960, p. 273.
5. Van Krevelen, D. W. Chemical Structure and Properties of Coal. XXVIII-Coal Constitution and Solvent Extraction. Fuel, v. 44, 1965, pp. 229-241.
6. Rybicka, S. M. The Solvent Extraction of a Low Rank Vitrain. Fuel, v. 38, 1959, pp. 45-54.
7. Sharkey, A. G., J. L. Shultz, and R. A. Friedel. Comparison of the Mass Spectra of Extracts and Vacuum Pyrolysis Products from Coal. Fuel, v. 40, 1961, pp. 423-426.
_____. Application of Low-ionizing Voltage Mass Spectrometry to Oils Derived From Coal. Fuel, v. 41, 1962, pp. 359-371.
8. Halleux, A., and H. Tschamler. Extraction Experiments on Coal with Various Pyridine Bases. Fuel, v. 38, 1959, pp. 291-293.

Presented Before the Division of Fuel Chemistry
American Chemical Society
New York, New York Meeting, September 11-16, 1966

Alterations in Structure and Physical Properties of Green River
Oil Shale by Thermal Treatment

P. R. Tisot

Laramie Petroleum Research Center
Bureau of Mines, U.S. Department of the Interior
Laramie, Wyoming

INTRODUCTION

Oil shale, a major potential source of both liquid fuels and chemicals, is a stratified or varved, highly consolidated, and nearly impervious organic-inorganic complex. The practically insoluble organic matter is distributed within the interstitial pores of the varve's mineral matrix. Each varve representing seasonal deposition consists of two laminae, one of which is richer in organic matter than the other. Bradley (1) reports that the thickness of the varves differs considerably, 0.014 millimeters in the richest oil shale to 9.8 millimeters in the fine-grained sandstone, and that the average thickness of the varves, weighted according to the quantity of each type of rock in the formation, is about 0.18 millimeters. The proportion of organic to mineral matter is not uniform throughout the formation; but the composition of each phase is relatively uniform. The changes in organic matter between varves may be gradual or it may be quite abrupt. When numerous laminae of comparable organic content occur together, they form layers or beds of oil shales, their thickness depends on the number of times these comparable laminae reoccur. Large variations in organic content frequently occur between contiguous beds or those near to each other. Within the Mahogany Zone (5), for example, there exists 1-foot beds which vary in oil yield from about 6 to 77 gallons of oil per ton as shown in figure 1. The Mahogany Marker in this zone is a bed of analcitized tuff approximately 6-inches thick and it is used as a reference bed for correlating oil shales from different locations. Figure 1 also shows how oil yield and weight-percent organic matter are related. In several instances beds of comparable oil yield or organic content occur numerous times, each at a different depth within the formation.

Because the organic matter is not uniformly distributed, the Green River formation, in effect, encompasses many oil-shale beds. Each of these oil-shale beds is characterized with its inherent ratio of organic to inorganic matter, physical structure, and physical properties. The complexity of the oil shales within these beds will impose difficult operational engineering problems in shale-oil production by either in situ or other retorting or conversion methods. Knowledge of the physical and chemical nature of oil shales and of their reaction in a pyrolytic environment should help to resolve these problems.

Research is being directed toward the study of the physical nature and behavior in a thermal environment of the complex organic-inorganic system. Some characteristics of the oil shale's physical structure have been evaluated by Tisot and Murphy (6,7,8) on a 28.6- and a 75.0-gallon-per-ton oil shale. These include particle size and particle-size distribution of the mineral constituents; surface area, pore structure, and pore volume of the raw oil shales and of their respective mineral matrices; and an estimate of the amount of organic matter bonded either chemically or physically to the mineral phase.

The present study evaluates changes in physical properties and alterations in structure which occur when oil shales of widely different organic content are heated

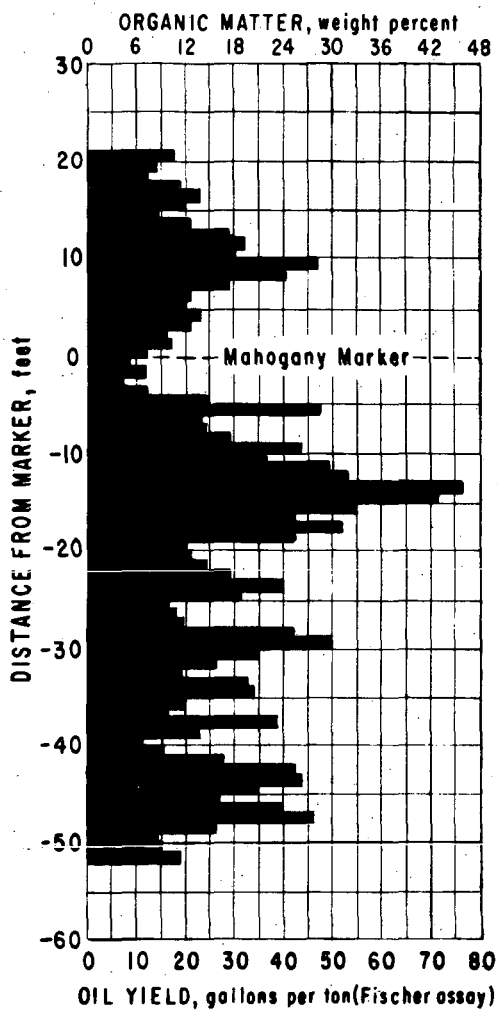


FIGURE 1.-Distribution of Organic Matter Within Mahogany Zone Based on Oil Yield and Content of Organic Matter.

under controlled conditions to 950°F. and to 1,500°F. in a stress-free environment. A stress-free environment was selected because it was envisioned that mass fragmentation to induce permeability in oil shale would likely result in a fragmented mass with a high percentage of stress-free surfaces. Seven oil shales were selected which assayed from 1 to about 60 gallons of oil per ton. This wide spectrum of oil yield approximates the oil shales in the Mahogany Zone. Physical properties evaluated were compressive strength, porosity, permeability, bulk density, weight loss, and structural alteration.

EXPERIMENTAL

Preparation of Samples

Seven oil shales were selected from the Bureau of Mines experimental mine near Rifle, Colorado. Their Fischer assays, to the nearest one-half gallon, were 1.0, 6.5, 13.5, 25.0, 30.0, 39.5, and 58.5 gallons per ton. Each sample, 2-inches thick, was carefully selected to ensure that it was essentially homogenous with respect to distribution of both the organic and mineral phases and that no induced fractures or structural faults were observed at 12X magnification. Small cores, 3/4-inch diameter by 1-1/4-inch long and 3/4-inch diameter by 1-1/2-inch long, were prepared from each oil shale. Some cores were cut with their axes perpendicular to the oil-shale's bedding plane and others with their axes parallel to the bedding plane. Cores were prepared in sufficient number to provide four to six samples for each physical measurement determined on both the raw oil shales and their respective mineral matrices following thermal treatment.

Removal of Organic Matter

Ten to 15 oil-shale cores, dried at 220°F., cooled, weighed, and covered with a porcelain dish, were placed in an electric muffle at room temperature with a thermocouple placed near the center of the group. The temperature was raised in 50-degree increments every 2 hours to 700°F. where degradation of the organic matter became appreciable. Four hours later the temperature was raised to 750°F. and maintained for 12 hours. Degradation of the organic matter appeared complete; however, with most oil shales the cores under these conditions were encrusted with carbonaceous matter. With the cover removed heating was continued by increasing the temperature in 50-degree increments every 2 hours to 950°F. This temperature was maintained for 3 hours. Carbonaceous matter that remained after pyrolysis was oxidized and completely removed throughout the oil-shale cores without significant loss of mineral carbonates. According to Jukkola and others (2) the dolomite in oil shale begins to decompose somewhat below 1,050°F. while the calcite begins to decompose from 1,150° to 1,200°F. The thermal treatment at 950°F. resulted in organic-free cores.

Decomposition of Mineral Carbonates

Some organic-free cores were returned to the electric muffle to thermally decompose the mineral carbonates. They were heated to 1,000°F. in approximately 6 hours and then further heated in 100-degree increments every 3 hours to 1,500°F and maintained at this temperature for 3 hours. This treatment converted the mineral carbonates in the organic-free cores to their respective mineral oxides. Fusion among the mineral particles was not evident.

Chemical Removal of Carbonates

The mineral carbonates were chemically removed from some of the organic-free cores of the 1.0-, 6.5-, and 13.5-gallon-per-ton oil shales heated to 950°F. In these oil shales inorganic cementation between the mineral particles after removing the organic matter was sufficient to prevent significant structural breakdown of the mineral matrices. The organic-free cores were contacted with dilute mineral acid

until the mineral carbonates were completely removed. Permeability, porosity, and weight loss were compared with those of the cores that had the mineral carbonates decomposed at 1,500°F.

Physical Property Measurements

Compressive Strength

Compressive strength, in pounds per square inch, was determined in accordance with ASTM Designation: C170-50. Oil-shale cores 3/4-inch diameter by 1-1/2-inch long were used for this test. Using a Tinus Olsen^{1/} hydraulic compression tester, force was applied to the core at a uniform rate until structural failure occurred.

Bulk Volume

Bulk volume in cubic centimeters was determined by mercury displacement in a U-type pycnometer calibrated to give direct readings (4). Prior to measuring bulk volume, the surface roughness left by the core drill was removed to ensure mercury contact with the core's surface.

Gas Permeability

Permeability was measured across the core with a gas permeameter according to the method of Klinkenberg (3) using helium at a pressure of 3 atmospheres for 1 minute.

Porosity

Sand-grain volume of the core, in cubic centimeters, was measured with a Boyle's-law type porosimeter. The core's porosity was calculated from bulk-volume and sand-grain-volume data.

RESULTS AND DISCUSSION

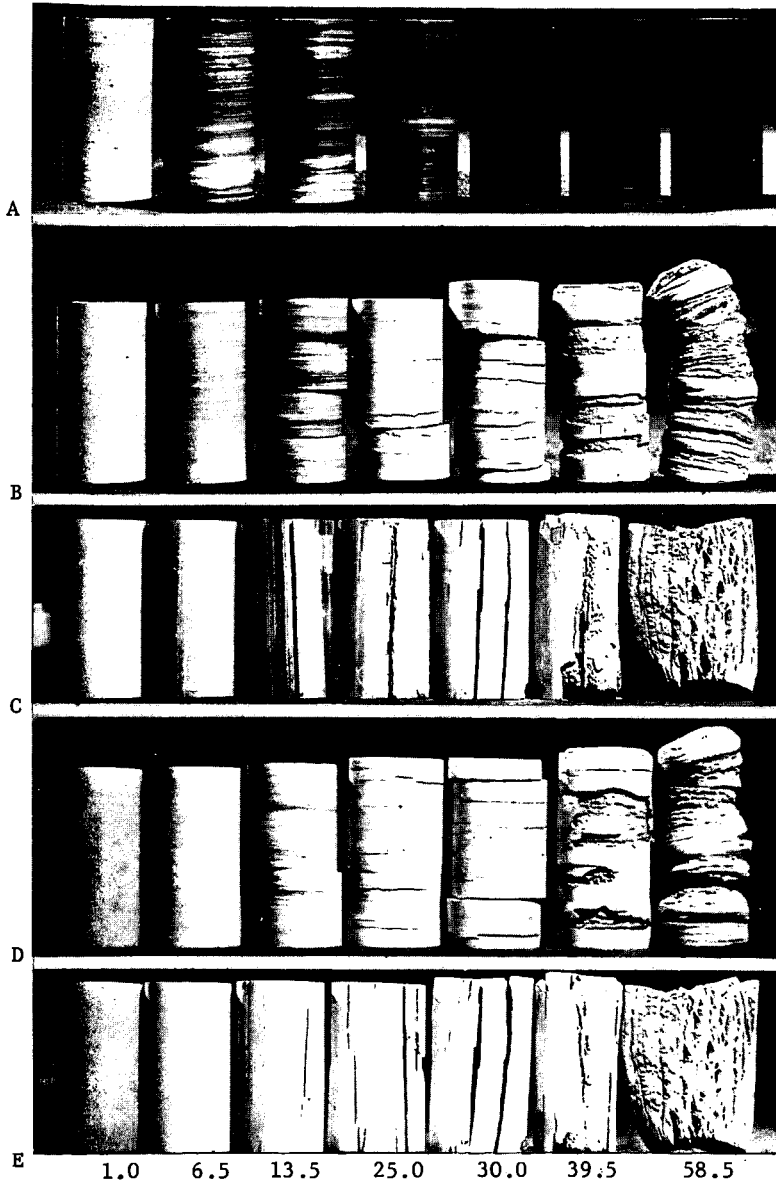
Structural Alterations

Structural alterations incurred by the seven oil shales heated to 950° and 1,500° in a stress-free environment are illustrated in figure 2. Figure 2-A shows the raw oil shales, figures 2-B and 2-C the oil shales heated to 950°F., and figures 2-D and 2-E those heated to 1,500°F.

The mineral matrices from the two low-yield oil shales did not undergo noticeable structural breakdown at either temperature. They were characterized as free of fractures, and they maintained dimensional stability and a high degree of inorganic cementation between both the individual mineral particles and between laminae.

Structural breakdown of the mineral phase began in oil shales of relatively low organic content. A few minute fractures, parallel to the bedding plane, were observed at 400°F. in the 13.5-gallon-per-ton oil shale, a temperature much below that necessary for rapid degradation, 800° to 900°F., of the organic matter. At 950°F. some fractures, all parallel to the bedding plane, completely severed the cores. These were clean separations between laminae indicating that the mineral particles constituting each lamina were more highly cemented to each other than they were to the mineral particles of adjacent laminae. Some of the mineral laminae were less than 100 microns thick. In some sections of the organic-free cores, successive laminae could be cleaved by application of pressure perpendicular to the bedding plane.

^{1/} Reference to specific makes or models of equipment is made to facilitate understanding and does not imply endorsement of such brands by the Bureau of Mines.



OIL YIELD, gallons per ton (Fischer Assay)

FIGURE 2. - Structural alterations of oil shales in a thermally controlled and stress-free environment. A, Raw oil shales; B-C, Oil shales heated to 950°F; D-E, Oil shales heated to 1,500°F.

However, the mineral matrix was still considered as being highly consolidated, and no evidence of friable material was observed.

The cores from the 25.0-gallon-per-ton oil shale developed a few small fractures parallel to the bedding plane at 400° to 450°F. Apparently inorganic cementation between some laminae was insufficient to overcome internal forces probably due to relief of internal stress, swelling, or pressure created by low-molecular-weight materials vaporizing. At 400°F. a pleasant odor was noted indicating escape of organic compounds. With temperature rise, to about 700°F., the existing fractures enlarged and additional ones developed, including some minute fractures perpendicular to the bedding plane. No extensive new fractures developed above 700°F. Low-temperature fracturing permitted access by gases to the core's interior prior to pyrolysis. The organic-free cores contained some friable segments indicating that disintegration of the mineral phase had begun. Decomposition of the mineral carbonates at 1,500°F. did not significantly change the outward appearance of the cores from that at 950°F. though the loss in weight amounted to 21.2 percent.

Behavior of the 30.0-gallon-per-ton oil shale was quite similar to the preceding oil shale under corresponding thermal conditions. Fractures parallel to the bedding plane were observed at 350°F. As temperature increased the fractures became larger and more numerous including some small fractures perpendicular to the bedding plane. Essentially all fractures occurred before any appreciable pyrolysis of the organic matter. Disintegration of the cores was more extensive than the ones from the previous oil shales along with a greater amount of friable material. The extent of fracturing did not noticeably change in heating the cores from 950° to 1,500°F.

Many fractures, predominantly parallel to the bedding plane, were noted at 350° to 450°F. in the 39.5- and 58.5-gallon-per-ton oil shales. The richest oil shale as noted in figure 2 also exhibited extensive swelling. This occurred below 700°F. Some oil shales yielding less than 58.5 gallons per ton will also show considerable swelling if heated rapidly. Because of fracturing and swelling great loss of mechanical strength resulted at preretorting temperatures. A low level of inorganic cementation existed between the mineral particles of these oil shales. Among many of the mineral particles inorganic cementation may have been completely absent as these mineral particles likely were encapsulated by organic matter. The carbonaceous matter that remained after retorting served as a bonding agent for many of the fine mineral particles and it also imparted some mechanical strength to the mineral matrix. However, after the carbonaceous matter was removed by oxidation, the remaining mineral phase was highly friable.

The combination of fracturing and swelling that occurs as preretorting temperatures should be an asset in oil production from an in situ fragmented mass of oil shale. Fracturing and swelling provide easy access for hot gases to the interior of an oil-shale fragment, a more efficient method for heat transfer than conduction. Conversely, fracturing and swelling appear to have undesirable features: (1) Obstruction or blocking of the initial induced permeability of a fractured oil-shale mass, (2) insufficient mechanical strength in the organic-free mineral matrix from rich oil shales to sustain high overburden pressures, (3) filtering action of the porous organic-free mineral matrix to moving solid particles could adversely effect permeability, and (4) entrainment of the fine solid particles in the oil.

Weight Loss

Weight Loss at 950°F.

The loss in weight of each oil shale after heating to 950°F. as a function of its oil yield is shown in figure 3. These losses were due mainly to volatilization of organic matter and subsequent oxidation of the carbonaceous matter that remained after pyrolysis. From Fischer assay analyses, in gallons of oil per ton, the weight

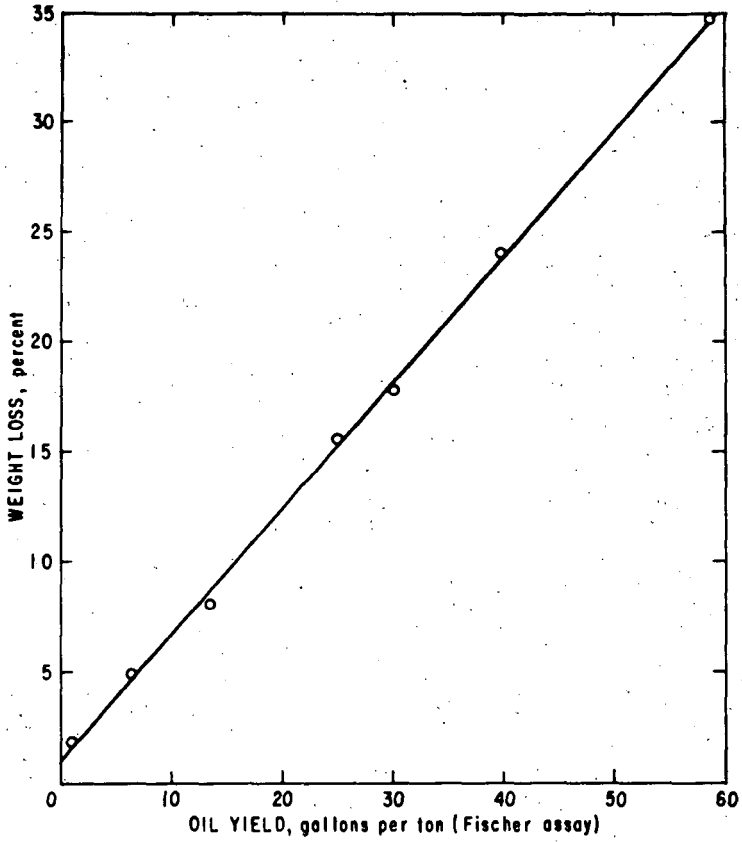


FIGURE 3.-Weight Loss in Oil Shales Heated to 950°F.

loss for oil shales from the Green River formation may be determined from the graph or calculated by the least square equation

$$Y = 0.95 + 0.58X \pm 0.90$$

with an error of estimate of 0.90 weight percent at the 95 percent confidence level.

Weight Loss at 1,500°F.

Weight loss of each oil shale after heating to 1,500°F. is presented in table 1. For purpose of comparison the weight loss at 950°F. is included. At 1,500°F. the

TABLE 1. - Weight loss in oil shales heated to 950° and 1,500°F.

Oil yield, gal/ton	Weight percent loss at 1,500°F.	Weight percent loss at 950°F.
1.0	9.39	1.85
6.5	18.78	4.83
13.5	20.28	8.11
25.0	37.39	15.64
30.0	33.56	17.81
39.5	43.92	24.03
58.5	45.62	34.93

weight loss is attributed mainly to the loss of the organic matter combined with the loss resulting from converting the mineral carbonates to their oxides. As noted in the table, the weight loss at 1,500°F. in oil shales exceeding 13.5 gallons of oil per ton represented a high percentage of each oil shale's initial weight. The weight loss at 1,500°F. did not plot as a straight line because there was no direct correlation in these oil shales between the content of organic matter and that of the mineral carbonates.

Porosity

Porosity of Raw Oil Shales

Measured porosities of the raw oil shales are shown in figure 4. As noted, the two low-yield oil shales had appreciable initial porosity. Assuming that the weight loss after heating to 950°F. was due to organic matter, the volume that this amount of organic matter would occupy was calculated from its specific density. Deducting this volume from the total porosity measured at 950°F. indicated that essentially all of the internal porosity in each of these two oil shales was accessible through interconnecting pores.

In oil shales yielding over 13.5 gallons of oil per ton the porosities were less than 0.03 percent. Previous work (6) on two oil shales has shown the absence of significant micropore volume even though they were finely divided, 44- to 77-microns, to permit exposure of internal pores. Except for the two low-yield oil shales, natural-occurring porosities in the raw oil shales are negligible and thus do not afford accessibility to gases. Porosity may exist to some degree in the oil-shale formation where fractures, faults, or other structural defects occur.

Porosity After Heating to 950°F.

Increase in porosity for each oil shale heated to 950°F. is shown in figure 5. The porosities are plotted as a function of both oil yield and weight percent organic

matter. These porosities which varied from 3 to 61 volume percent of the oil shales' bulk volume represented essentially the volumes occupied by the organic matter. In the first three oil shales structural breakdown of the cores was insignificant and the porosities are those of intact porous structures. However, in the remaining oil shales this is not the case because structural breakdown and disaggregation became so extensive, especially in the richer oil shales, that the mineral matrices no longer remained intact.

From an oil shale's oil yield or weight percent organic matter, its porosity may be read from the graph. Based on oil yield, porosity may be calculated from the least square equation

$$Y = 3.70 + 1.02X \pm 3.74$$

with an error of estimate of 3.74 percent porosity at the 95 percent confidence limit.

Porosity of Acid-Leached Cores

The porosities of the organic-free cores from the 1.0-, 6.5-, and 13.5-gallon-per-ton oil shales were greatly increased after chemically removing the mineral carbonates. The respective porosities were 13.36, 14.70, and 19.09 prior to leaching, and they increased to 30.50, 39.39, and 42.90 percent after leaching. Even after these high increases in porosity their gas permeabilities perpendicular to the oil shale's bedding plane were less than 3 millidarcies. The respective weight losses prior to acid leaching were 1.85, 4.83, and 8.11, and they increased to 24.65, 36.52, and 38.10 percent after leaching. After acid leaching the mineral matrices from the first two oil shales still retained their geometric configuration and considerable mechanical strength. This indicated that other inorganic compounds besides the carbonates contributed to cementation between mineral particles and between laminae. In the 13.5-gallon-per-ton oil shale, acid leaching greatly diminished the degree of cementation between laminae. In many instances complete separation of individual thin mineral laminae occurred; however, the mineral particles constituting each lamina were not considered friable.

Porosity Due to Thermal Decomposition of Mineral Carbonates

Thermal decomposition of the mineral carbonates at 1,500°F. resulted in an increase in porosity as shown in figure 6. The amount of mineral carbonates in the raw oil shales was determined by wet chemical analysis. As noted from the graph an appreciable increase in porosity resulted after decomposing the mineral carbonates. From the mineral carbonate content of an oil shale, the increase in its porosity over that at 950°F. may be read from the graph or calculated by the least square equation

$$Y = 2.21 + 0.65X \pm 1.20$$

with an error of estimate of 1.20 percent porosity at the 95 percent confidence limit.

Porosity After Heating to 1,500°F.

Total increase in porosity after heating the oil shales to 1,500°F. are shown in figure 7. The increases in porosity varied from 2.82 to 70.54 percent of their initial bulk volumes. These porosities constitute essentially the combined void spaces represented by the loss of the organic matter and the decomposition of the mineral carbonates. From weight loss at 1,500°F., the resulting porosity may be read from the graph or calculated from the least square equation

$$Y = - 0.35 + 1.49X \pm 4.88$$

with an error of estimate of 4.88 percent porosity at the 95 percent confidence level.

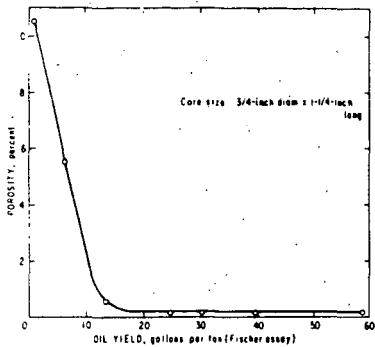


FIGURE 4.-Measurable Porosity in Small Oil-Shale Cores.

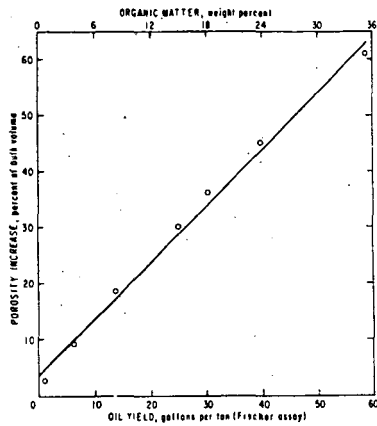


FIGURE 5.-Porosity of Oil Shales After Thermal Treatment of 950°F Based on Oil Yield and Content of Organic Matter.

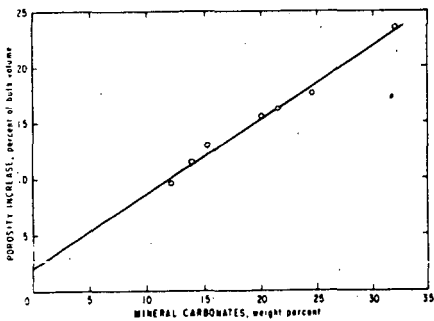


FIGURE 6.-Porosity Increase After Thermal Decomposition of Mineral Carbonates at 1500°F.

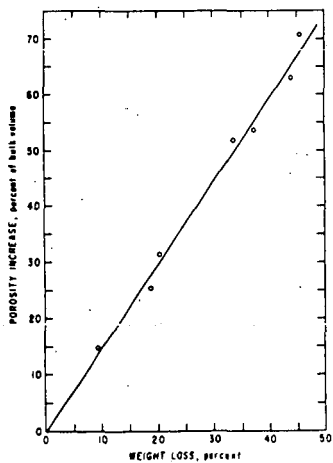


FIGURE 7.-Porosities of Oil Shales After Thermal Treatment to 1500°F.

Compressive Strength

Compressive strengths of the seven oil shales and of their respective mineral matrices heated to 950° and to 1,500°F. are shown in figure 8. Compressive strengths are shown for the cores cut with their axes perpendicular and those with their axes parallel to the oil shale's bedding planes. Each point on the graph represents the average compressive strength of four to six samples.

Compressive Strength of Raw Oil Shales

The raw oil shales had high compressive strengths both perpendicular and parallel to the bedding plane. They varied from 9,000 to 31,000 and 9,000 to 28,400 pounds per square inch in the respective planes. These values were much higher than expected. However, the difference between the two planes in any one oil shale was smaller than expected. The greatest difference between planes was 3,200 pounds per square inch in the 13.5-gallon-per-ton oil shale. Two of the oil shales exhibited higher compressive strength parallel to the bedding plane which was also not expected.

Application of force at a uniform rate on the oil shales yielding less than 30 gallons of oil per ton resulted in corresponding uniform pressure rise without apparent yield until structural failure occurred. This was accompanied by considerable shattering and noise. In contrast, pressure rise in the other oil shales was not uniform throughout the test. It became progressively slower at the higher pressures and completely stopped for some time prior to the core's structural failure. This was indicative of compression or plastic deformation. Most of these cores failed without shattering or significant noise.

Compressive Strength After Heating to 950°F.

The mineral matrices of the three low-yield oil shales heated to 950°F. retained high compressive strength in both planes. They varied from 13,300 to 28,000 pounds per square inch in the perpendicular plane and 6,200 to 26,200 pounds per square inch in the parallel plane. This indicated that a high degree of inorganic cementation existed between both the mineral particles comprising each lamina and between adjacent laminae. With increase in organic matter the compressive strength of the respective organic-free mineral matrices decreases and it becomes very low in those from rich oil shales. As noted in figure 8, the compressive strength of the mineral matrix from the 58.5-gallon-per-ton oil shale was only 20 pounds per square inch in both planes.

Compressive Strength After Heating to 1,500°F.

After thermally decomposing the mineral carbonates at 1,500°F., the three low-yield oil shales still retained high compressive strength. They varied from 10,500 to 15,000 pounds per square inch in the perpendicular plane and 3,700 to 14,900 in the parallel plane. The high compressive strength retained by these mineral matrices indicated that the inorganic cementing material which bonded both the mineral particles within each lamina and between laminae was not greatly effected at this temperature. Except for the two richest oil shales, compressive strengths were lower at 1,500° than at 950°F. Slight fusion may have occurred in the mineral matrices from these two oil shales.

Gas Permeability

Gas permeabilities are presented in table 2 for the three low-yield oil shales and for their respective mineral matrices heated to 950° and 1,500°F. including the mineral matrices that were acid leached after heating to 950°F. Permeability, either perpendicular or parallel to the bedding planes, was not detected in any of the seven raw oil shales at a pressure differential across the cores of 3 atmospheres

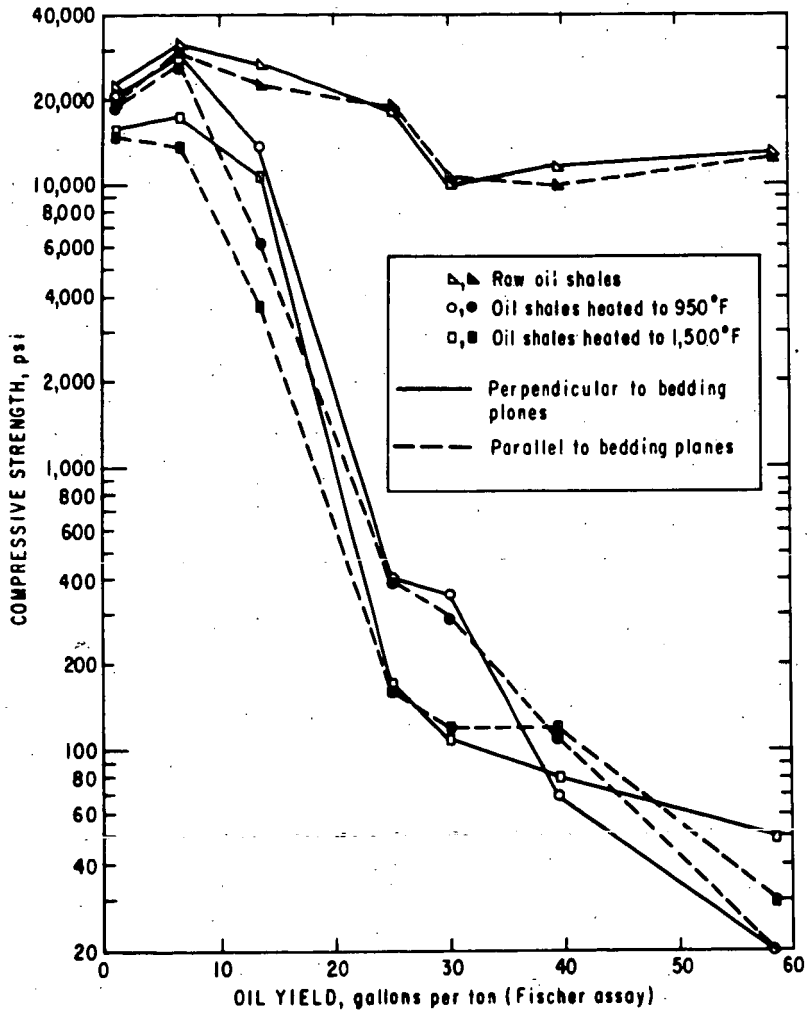


FIGURE 8.-Compressive Strength of Raw Oil Shales And Thermally Treated Oil Shales.

TABLE 2. - Gas permeabilities of raw and treated oil shales^{1/}

Oil yield, gal/ton	Plane	Oil shale			
		Raw	Heated to 950°F.	Heated to 1,500°F.	Heated to 950°F. and acid leached
1.0	A ^{2/}	0	0.10	0.36	0.33
	B ^{3/}	0	0.10	0.56	0.59
6.5	A	0	0.10	0.21	0.39
	B	0	0.10	0.65	1.48
13.5	A	0	0.10	4.53	2.82
	B	0	0.62	8.02	-

1/ Units in millidarcies.

2/ Perpendicular to the bedding plane.

3/ Parallel to the bedding plane.

of helium for 1 minute. Unless fractures, faults, or other structural defects are present, oil shale constitutes a highly impervious system.

Gas permeability was low in both planes of the mineral matrices from the three low-yield oil shales heated to 950° and 1,500°F. The highest permeability measured was 8.02 millidarcies. This was in the mineral matrix from the 13.5-gallon-per-ton oil shale cored parallel to the bedding plane and heated to 1,500°F. Minute fractures may have contributed to its permeability.

Though porosity had more than doubled after acid leaching the mineral matrices from the three low-yield oil shales heated at 950°F., permeability was not greatly increased. In fact, an increase in porosity from 19.09 to 42.90 percent in the 13.5-gallon-per-ton oil shale decreased its permeability from 4.52 to 2.82 millidarcies. This may be attributed to acid-insoluble particles set free during acid leaching. These free particles, in turn, could block interconnecting pores under gas pressure.

Structural breakdown of the mineral matrices in all oil shales that exceeded 13.5 gallons of oil per ton precluded permeability measurements. Extensive structural breakdown that occurs in many oil shales at preretorting temperatures should be an asset in that hot gases are permitted access to the interior of oil-shale fragments.

Bulk Density

The bulk densities of the seven oil shales and of their mineral matrices heated to 950° and 1,500°F. are shown in figure 9. Bulk densities varied from 2.396 to 1.757 in the raw oil shales, 2.277 to 1.142 in the mineral matrices heated to 950°F., and 2.078 to 0.972 in those heated to 1,500°F.

CONCLUSIONS

This study extends our knowledge of changes in physical properties that occur among oil shales of different organic content after controlled heating to 950° and 1,500°F. in a stress-free environment. The physical properties evaluated, compressive strength, porosity, permeability, weight loss, bulk density, and structural deformation, are significant to processing. The wide differences in many of these properties result principally from the oil shales' different organic contents. With increase in organic content, the inorganic cementation between mineral particles decreases yielding organic-free mineral matrices of significantly different physical

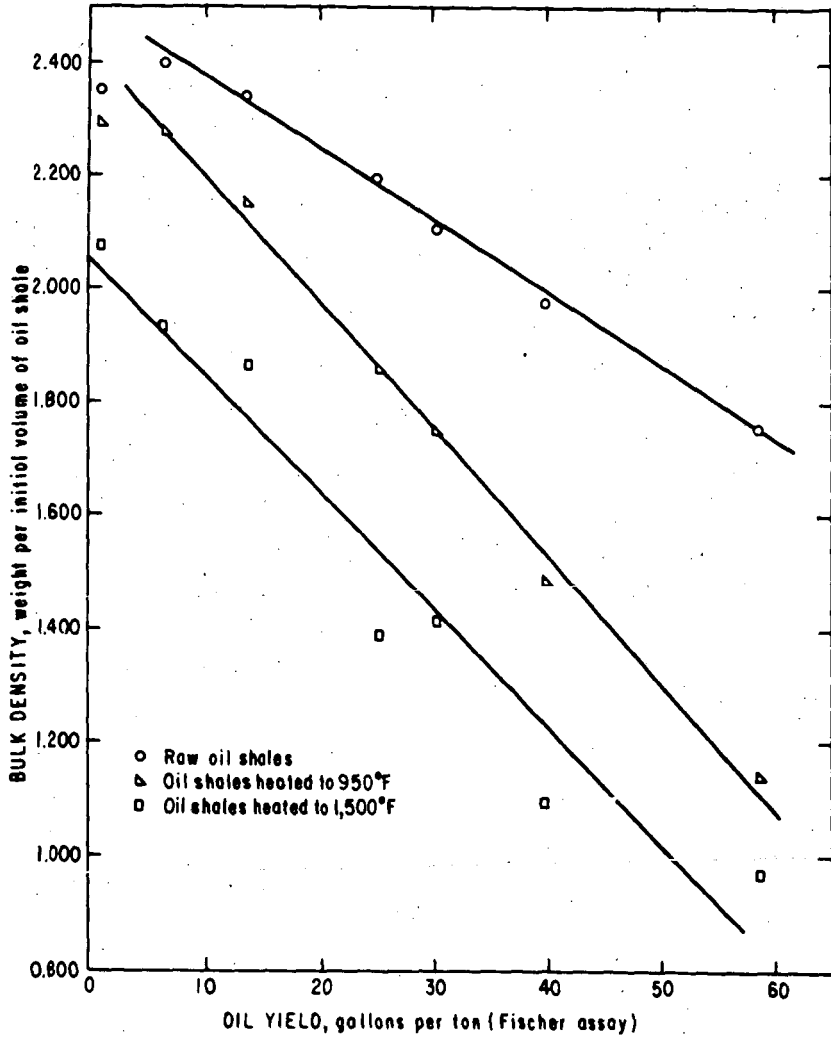


FIGURE 9.-Bulk Densities of Raw And Thermally Treated Oil Shales.

RRS-831

properties and structural deformation. Some physical changes appear to be assets in shale-oil production; however, on the contrary the same changes seem to have undesirable features which will probably impose difficult engineering problems on an in situ operation.

The data presented serve as guidelines permitting a more knowledgeable appraisal of engineering problems associated with in situ processing and permitting a better concept of physical and chemical changes that occur in a mass of fragmented oil shale as it is retorted.

The observations from this investigation are based on small samples of oil shale. Additional information, more nearly representative of actual field conditions, would be desirable to supplement these findings and thus establish more realistic concepts.

ACKNOWLEDGMENT

This work was conducted under a cooperative agreement between the Bureau of Mines, U.S. Department of the Interior, and the University of Wyoming.

REFERENCES

1. Bradley, H. W. Shorter Contributions to General Geology 1929--Geological Survey Professional Paper 158, U.S. Dept. of the Interior, Washington, D.C., 1930, p.87.
2. Jukkola, E. E., A. J. Denilauler, H. B. Jensen, W. I. Barnett, and W.I.R. Murphy. Thermal Decomposition Rates of Carbonates in Oil Shale. *Ind. and Eng. Chem.*, v. 45, No. 12, December 1953, pp. 2711-2714.
3. Pirson, Sylvain J. *Oil Reservoir Engineering*, Second Edition. McGraw-Hill Book Co., Inc., New York, N.Y., 1958, pp. 60-61.
4. Rall, C. G., H. C. Hamontre, and D. B. Teliiferro. Determination of Porosity by a Bureau of Mines Method. *BuMines Rept. of Inv. 5025*, 1954, 24 pp.
5. Stanfield, K. E., I. C. Frost, W. S. McAuley, and H. N. Smith. Properties of Colorado Oil Shale: *BuMines Rept. of Inv. 4825*, 1951, 27 pp.
6. Tisot, P. R. Properties of Green River Oil Shale Determined from Nitrogen Adsorption and Desorption Isotherm. *J. Chem. and Eng. Data*, v. 7, No. 3, July 1962, pp. 405-410.
7. Tisot, P. R., and W.I.R. Murphy. Physical Structure of Green River Oil Shale from Colorado. *BuMines Rept. of Inv. 6184*, 1963, 24 pp.
8. Tisot, P. R., and W.I.R. Murphy. Physical Structure of Green River Oil Shale. *Chem. Eng. Prog. Symposium Series*, v. 61, No. 54, 1965, pp. 25-32.

MEMBERSHIP IN THE DIVISION OF FUEL CHEMISTRY

The Fuel Chemistry Division of the American Chemical Society is an internationally recognized forum for scientists, engineers and technical economists concerned with the conversion of fuels to energy, chemicals, or other forms of fuel. Its interests center on the chemical problems, but definitely include the engineering and economic aspects as well.

Any chemist, chemical engineer, geologist, technical economist, or other scientists concerned with either the conventional fossil fuels, or the new high-energy fuels--whether he be in government, industry or independent professional organizations--would benefit greatly from participation in the program of the Fuel Chemistry Division.

The Fuel Chemistry Division offers at least two annual programs of symposia and general papers, extending over several days, usually at National Meetings of the American Chemical Society. These include the results of research, development, and analysis in the many fields relating to fuels which are so vital in today's energy-dependent economy. Members of the Division have the opportunity to present papers of their own, or participate in discussions with experts in their field. Most important, the Fuel Chemistry Division provides a permanent record of all of this material in the form of complete preprints.

Starting in September 1959, the biennial Fuel Cell Symposia of the Division have been the most important technical meetings for chemists and chemical engineers active in this field. These symposia have all been published in book form. The recent landmark symposium on Advanced Propellant Chemistry is to be published in book form also. Further, the Division is strengthening its coverage of areas of air and water pollution, gasification, and related areas.

In addition to receiving several volumes of preprints, each year, as well as regular news of Division activities, benefits of membership include: (1) Reduced subscription rates for "Fuel" and "Combustion and Flame," (2) Reduced rates for volumes in the "Advances in Chemistry Series" based on Division symposia, and (3) The receipt card sent in acknowledgment of Division dues is good for \$1.00 toward a complete set of abstracts of all papers presented at each of the National Meetings.

To join the Fuel Chemistry Division as a regular member, one must also be or become a member of the American Chemical Society. Those not eligible for ACS membership because they are not practicing scientists, engineers or technical economists in areas related to chemistry, can become Division Affiliates. They receive all benefits of a regular member except that they cannot vote, hold office or present other than invited papers. Affiliate membership is of particular value to those in the informational and library sciences who must maintain awareness of the fuel area. Non ACS scientists active in the fuel area and living outside of the United States are invited also to become Division Affiliates.

Membership in the Fuel Chemistry Division costs only \$4 per year, or \$11 for three years, in addition to ACS membership. The cost for a Division Affiliate, without joining ACS, is \$10 per year. For further information, write to:

Dr. Frank Rusinko, Jr., Secretary-Treasurer
ACS Division of Fuel Chemistry
c/o Speer Carbon Company
St. Marys, Pennsylvania 15857
Telephone: 814-834-2801

RECENT FUEL DIVISION SYMPOSIA

Volume	Title	Presented At
Vol. 8, No. 1	Symposium on Gas Generation General Papers	Philadelphia, Pa. April, 1964
Vol. 8, No. 2	Symposium on Chemical Phenomena in Plasmas Symposium on Kinetics and Mechanisms of High Temperature Reactions	Philadelphia, Pa. April, 1964
Vol. 8, No. 3	Symposium on Pyrolysis and Carbonization of Coal Symposium on Mineral Matter in Coal	Chicago, Illinois August, 1964
Vol. 9, No. 1	Symposium on Advanced Propellant Chemistry*	Detroit, Michigan April, 1965
Vol. 9, No. 2	Symposium on Fuel and Energy Economics General Papers	Detroit, Michigan April, 1965
Vol. 9, No. 3 (Parts 1 & 2)	Symposium on Hydrocarbon-Air Fuel Cells**	Atlantic City, N. J. September, 1965
Vol. 9, No. 4	Symposium on Coatings Based on Bituminous Materials General Papers	Atlantic City, N. J. September, 1965
Vol. 10, No. 1	Symposium on Fossil Fuels and Environmental Pollution Joint with the Division of Water, Air, and Waste Chemistry	Pittsburgh, Pa. March, 1966
Vol. 10, No. 2	Symposium on Pyrolysis Reactions of Fossil Fuels Joint with the Division of Petroleum Chemistry	Pittsburgh, Pa. March, 1966

* To be published by Advances in Chemistry.

** Published by Academic Press, Inc.

PROJECTED PROGRAMS

Symposium on Chemical Reactions in Electrical Discharges Joint with Division of Physical Chemistry Bernard D. Blaustein, Chairman	Miami Beach, Fla. April, 1967
Symposium on Electrochemical Reactions in Solution General Papers Joint with Divisions of Physical Chemistry and Analytical Chemistry and in cooperation with Electrochemical Society Ernest Yeager, Chairman	Miami Beach, Fla. April, 1967
Symposium on Detonations and Reactions in Shock Waves Joint with Division of Physical Chemistry R. W. Van Dolah, Chairman	Chicago, Illinois September, 1967
Symposium on Advances in Spectrometry of Fuels and Related Materials Joint with Division of Analytical Chemistry R. A. Friedel, Chairman	Chicago, Illinois September, 1967
Symposium on Fuel Cell Technology B. S. Baker, Chairman	Chicago, Illinois September, 1967
Symposium on Oil Shale James H. Gary, Chairman (Tentative; may be Spring 1968)	Chicago, Illinois September, 1967
General Papers Irving Wender, Program Chairman	Chicago, Illinois September, 1967